Quantification of Grass Erosion Due to Wave Overtopping at the Afsluitdijk

Martijn Kriebel
July 2019

Witteveen + Bos

UNIVERSITY OF TWENTE.

Cover photo: the Afsluitdijk in the direction of Friesland, as seen from Den Oever (Ministerie van Economische Zaken, 2015).

Quantification of Grass Erosion Due to Wave Overtopping at the Afsluitdijk

Thesis submitted in partial fulfillment of the requirements for the degree of Master of Science in Water Engineering and Management at the University of Twente.

To be publicly defended on 12 July 2019.

Author:
Martijn Kriebel
m.kriebel@alumnus.utwente.nl

Graduation committee:

Prof. dr. S.J.M.H. Hulscher	University of Twente *Marine and Fluvial Systems*
Dr. J.J. Warmink	University of Twente *Marine and Fluvial Systems*
V.M. van Bergeijk MSc.	University of Twente *Marine and Fluvial Systems*
Ing. C. Kuiper	Witteveen+Bos *Coasts, Rivers and Land Reclamation*
Ir. H. Trul	Witteveen+Bos *Flood Protection and Land Development*

Witteveen + Bos

UNIVERSITY OF TWENTE.

SUMMARY

Grass erosion on the crest and inner slope due to wave overtopping is one of the mechanisms that can cause a flood defense to fail according to the Dutch WBI 2017 safety standards. The probability of failure of the grass cover layer for a certain grass quality is determined based on the combination of significant wave height and average overtopping discharge. However, this relationship is only established for wave heights up to 3 meter. At the time of writing, a new design is being finalized for the Afsluitdijk, which is one of the primary flood defenses in the Netherlands. The normative significant wave height for this new design is 3.38 meter, thus exceeding the maximum wave height for which the probability of failure due to grass erosion is defined in the WBI 2017. Previous studies have used the cumulative overload method to quantify the combinations of wave height and critical overtopping discharge for wave heights up to 4 meter, but the effects of the geometrical and cover material transitions present on the Afsluitdijk have not been studied in detail.

The goal of this study is to find the relationship between the significant wave height and the critical average overtopping discharge for wave heights larger than 3 meter. This is done using two approaches: (1) the cumulative overload method (COM) and (2) a combination of the coupled crest-inner slope velocity equations (VE) and the transition model (TM). However, the basic modelling approach that is used in this study could be applied to other models that can predict the amount of erosion due to wave overtopping. Simulations are carried out with significant wave heights up to 4 meter for the new design of dike section 17a of the Afsluitdijk. Several different cross-sectional locations are included in order to study the effects of transitions. Additionally, sensitivity analyses are performed to study towards which parameters the COM and the VE-TM are most sensitive and which could cause the largest variation in the found relationships.

Both the COM and the VE-TM predict an increasing critical average overtopping discharge for a decreasing significant wave height for all cross-sectional locations. In all simulations the inner toe is predicted as the weakest cross-sectional location, with a minimum critical average overtopping discharge of $q_{crit.}$ = 3.4 L/s/m (COM) and $q_{crit.}$ = 1.4 L/s/m (VE-TM) for a significant wave height of approximately 4 meter. For locations on the crest, both modelling approaches predict a similar development of the flow velocity for a changing wave height, resulting in approximately equal relationships between the critical discharge and the wave height. For the other cross-sectional locations the predicted relationships are not the same, as the effects of a changing inner slope length on the hydraulic load at these locations are predicted differently in the two approaches. Furthermore, the COM predicts that a grass-to-asphalt transition is able to withstand a larger average overtopping discharge than an asphalt-to-grass transition. However, the VE-TM results show the opposite. This can be attributed to the fact that the local turbulence at these transitions is not accurately calculated in the VE-TM.

Based on the findings in this study, it is recommended to carry out (scaled) wave overtopping experiments for wave heights larger than 3 meter that focus on finding the critical average overtopping discharges for the inner slope and the inner berm. The obtained data from these experiments can be used to validate the simulation results of this study. Additionally, this data may result in a better estimation of the flow velocity on the crest, which is subject to large uncertainties and towards which the COM and the VE-TM are sensitive. Furthermore, it is recommended to apply a more detailed turbulence model in the VE-TM in order to obtain more realistic critical discharges for cover material transitions. Finally, in order for the simulation results to be included in the WBI 2017, the modelling approach in this study should be modified so that a distribution for the probability of failure can be found for waves larger than 3 meter.

PREFACE

In front of you lies my master thesis *"Quantification of Grass Erosion Due to Wave Overtopping at the Afsluitdijk",* which is the final result of the research that I carried out in the last five months at Witteveen+Bos and marks the completion of my study Water Engineering and Management at the University of Twente.

I would like to thank Hizkia Trul for his daily guidance and for giving me the opportunity to write my thesis at Witteveen+Bos, and Coen Kuiper for providing me with new knowledge and information regarding the Afsluitdijk. Furthermore, I grateful to thank Suzanne Hulscher, Jord Warmink and Vera van Bergeijk for their valuable feedback and their supervision throughout my graduation period. Finally, I want to thank my family and friends who have supported me throughout my study.

Martijn Kriebel

Enschede, July 5, 2019

TABLE OF CONTENTS

1. INTRODUCTION

1.1 PROBLEM CONTEXT

The Netherlands has experienced many floods throughout its existence due to its low-lying land and an abundance of water resources. As a result of a storm, the flood of 1916 caused devastation in areas adjacent to the former Southern Sea (*Zuiderzee*). This led to the decision of the Dutch government to close off the Southern Sea by building a large dam. Not only would this decrease the chances of flooding, but it would also create the possibility of land reclamation. Although such a plan was not new, it was the design of hydraulic engineer Cornelis Lely that would eventually be used as a basis for the construction of the dam: the Afsluitdijk (literally: Closure Dike). With the construction of this primary flood defense, which was finished in 1933, the Southern Sea was no longer part of the sea and the newly created freshwater body was named Lake IJssel (*IJsselmeer*). An overview of the area is given in Figure 1.

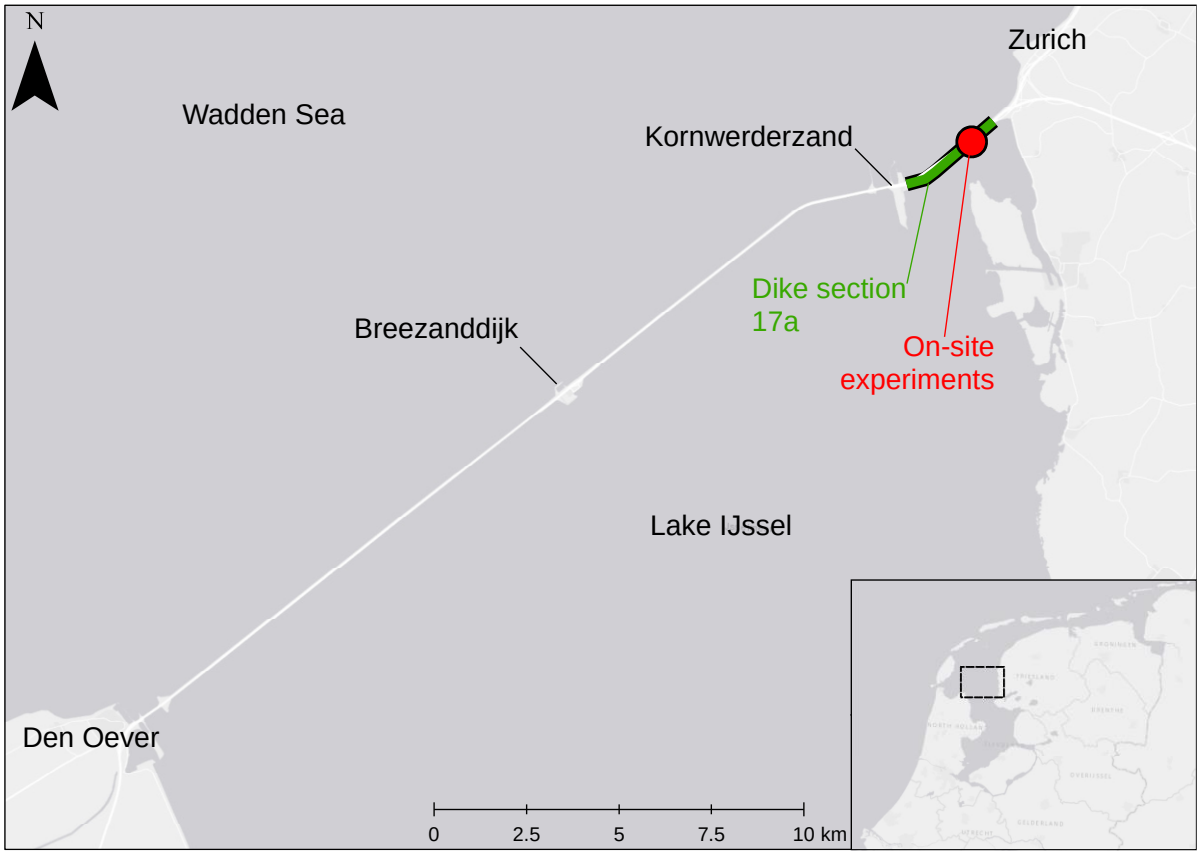

Figure 1: Location of the Afsluitdijk. Dike section 17a is marked green, the location of the on-site experiments (Bakker et al., 2009) *is marked red.*

Over 70 years later, safety assessments carried out by the Inspectie Verkeer en Waterstaat (2006, 2011) have shown that the Afsluitdijk does not meet the legal safety requirements anymore. According to Witteveen+Bos (2013) the dam is not high enough to withstand the waves that approach from the Wadden Sea-side in the case of a normative storm, meaning that more wave overtopping can occur than is allowed. Furthermore, the grass cover on the crest and the inner slope (the Lake IJssel-side) is not strong enough to withstand the hydraulic load of the overtopping waves, making these locations susceptible to erosion. Rijkswaterstaat (the Dutch Directorate-General for Public Works and Water Management) decided that both problems should be addressed to make the dam "overtopping-resistant", meaning that wave overtopping is allowed in the case of severe storms, but only if the inner slope is strong enough to withstand this hydraulic load.

At the time of writing a new design for the Afsluitdijk is being finalized by the consortium "Levvel". A main uncertainty in creating this design is the strength of the grass cover on the crest, inner slope and inner berm (Witteveen+Bos, 2013). The required strength of this grass cover depends on the hydraulic load that it experiences as a result of the overtopping waves. According to the EurOtop Manual (Van der Meer et al., 2018) the severity of wave overtopping is not only determined by the average overtopping discharge, but also by the height of the waves that cause the overtopping. On average, higher waves cause a larger volume to overtop per wave than lower waves, which results in a larger hydraulic load on the cover layer. This can be explained by the fact that the overtopping water has a larger flow velocity in the case of a large overtopping volume than when the overtopping volume is low. This results in a large shear stress on the soil surface, which can damage the cover layer. This is supported by Van der Meer et al. (2010b) who concluded that a low number of overtopping waves with a large overtopping volume are more damaging than a high number of overtopping waves with a low overtopping volume, even though the average overtopping discharge is the same. This shows that using only the average overtopping discharge as indicator of cover layer failure is inadequate, and that a relationship between the average overtopping discharge and the significant wave height should be used instead.

To study the strength of the grass cover on the Afsluitdijk, wave overtopping experiments at dike section 17a (Figure 1) were carried out with a significant wave height of 2 meter (Bakker et al., 2009). Furthermore, a new assessment method for grass erosion on the crest and inner slope (*GEKB, Graserosie Kruin en Binnentalud*) can be used, which is prescribed in the WBI 2017 (*Wettelijk Beoordelingsinstrumentarium 2017*). This method indicates the probability of failure of a grass cover layer based on the combination of significant wave height, average overtopping discharge and grass quality. This can be carried out for wave heights up to 3 meter using a lognormal distribution, for which the parameters are presented in Table 1.

Table 1: Lognormal probability distribution parameters μ and σ for the probability of failure of the grass cover layer based on the critical overtopping discharge, wave height category and grass quality (Rijkswaterstaat, 2018).

	Closed sod		**Open sod**	
Wave height category	**μ [m³/s/m]**	**σ [m³/s/m]**	**μ [m³/s/m]**	**σ [m³/s/m]**
0 m – 1 m	0.225	0.250	0.100	0.120
1 m – 2 m	0.100	0.120	0.070	0.080
2 m – 3 m	0.070	0.080	0.040	0.050

However, the results of these methods cannot be used to determine the resistance against erosion in the new design of the dam. The document *Hydraulische Randvoorwaarden Afsluitdijk* (Rijkswaterstaat, 2017) prescribes the hydraulic boundary conditions that must be used for the new design of the Afsluitdijk. In Appendix D of this report several important hydraulic boundary conditions concerning wave overtopping are given. For the new design of the Afsluitdijk the hydraulic boundary conditions that are calculated for the year 2024 are considered to be normative, which corresponds to a significant wave height of 3.38 meter for dike section 17a. This is higher than the waves that were simulated during the on-site wave overtopping experiments, and it exceeds the WBI 2017 GEKB wave height categories.

At the time of writing, experiments are being carried out in the Delta Flume of Deltares with a modelled version of the outer slope of the Afsluitdijk. These experiments are carried out for scaled incident waves that represent significant wave heights larger than 3 meter. Although this will provide useful data regarding hydraulic parameters at the crest (average wave overtopping discharges and wave overtopping volume per wave for several different wave characteristics), they are only focused on studying the effects of the outer slope design of the Afsluitdijk. Because the inner slope and inner berm are not modelled in the Delta Flume, the experiments do not provide information on the erosion resistance of these locations.

Van Hoven (2015) and Van Hoven and Van der Meer (2017) used a method based on the cumulative overload method (COM) to calculate the probability of failure for combinations of average overtopping discharges and significant wave heights up to 4 meter. They compared the found relationships to the distributions from Table 1 and concluded that the WBI 2017 distributions are very conservative. However, Van Hoven (2015) did not include acceleration, load or strength factors which account for the effects of transitions and objects on the dike cover in the COM. As there are various transitions and objects present on the Afsluitdijk, the results are not valid for the grass cover layer of the dam. Van Hoven and Van der Meer (2017) included three combinations of these factors: for the transition from inner slope to berm, a worst case scenario with the most extreme possible values and average values that lie between the used values for the other two combinations. However, these values are not representative for the Afsluitdijk because there are many other types of transitions and objects on the dam. Van Hoven and Van der Meer (2017) concluded that, when transitions and/or objects are included, the calculated probability of failure can exceed the probability given by the WBI 2017 parameters. They therefore recommended further research into the effects of these transitions and objects on grass erosion due to wave overtopping.

Besides the COM, other erosion models exist that can determine when failure of the grass cover layer occurs. An overview of these models is given by Trung (2014). One of the most realistic models is the transition model (TM) that is proposed by Valk (2009), which is also applied by Bomers et al. (2018) and is based on models described by Van den Bos (2006) and Hoffmans et al. (2009). The TM is able to calculate the erosion depth caused by each overtopping wave at each cross-dike location. Additionally, it takes the depth-dependency of several grass cover strength variables into account. One of the main input parameters of the TM is the bed shear stress caused by the overtopping wave, which depends on the flow velocity. This velocity can be obtained using the coupled velocity equations (VE) presented by Van Bergeijk et al. (2019b), which describe the change in the maximum flow velocity along the cross-section. These velocity equations include the effects of flow acceleration on the inner slope as well as the effects of a changing bottom roughness at cover material transitions.

In conclusion, there is no reliable relationship between the significant wave height and the critical average overtopping discharge currently available for the grass cover of the new design of the Afsluitdijk, because the dam contains many transitions/objects and a normative significant wave height larger than the current upper limit of 3 meter needs to be considered. It is therefore unknown what combination of crest height and grass cover strength is required in order to ensure the safety of the flood defense. This can be studied using state-of-the-art modelling approaches such as the cumulative overload method or a combination of the coupled velocity equations and the transition model.

1.2 Study Objective

The aim of this thesis is to quantify the relationship between the significant wave height and the critical average overtopping discharge for the grass cover layer of the new design of the Afsluitdijk, including the effects of the transitions that are present on the dam. In line with previous studies, the focus lies on dike section 17a. Because there are several transitions present at every location in this dike section and only a limited number of objects that are large enough to influence the grass erosion process (Van der Meer and Van Hoven, 2014), only the effects of transitions are included in this study. Furthermore, because the normative significant wave height for this dike section is 3.38 meter, significant wave heights up to 4 meter are considered.

A first approach for finding the relationship follows the efforts made by Van Hoven (2015) and Van Hoven and Van der Meer (2017) using the cumulative overload method (COM). As a second approach the coupled velocity equations (VE, Van Bergeijk et al. (2019b)) are combined with the transition model (TM, Valk (2009)). The results of the COM approach and the VE-TM approach are compared to

see to what extent this yields different results, and especially to see what critical average overtopping discharges are calculated for wave heights larger than 3 meter. Furthermore, the sensitivity of both the COM and VE-TM towards their input parameters is studied, as these often rely on coefficients which are not well established in the literature or because assumptions are required for their calculations. By ranging these input values, the parameters that have the largest effect on the calculated critical average overtopping discharges are found. If (a part of) the cross-section of the Afsluitdijk requires reinforcement, this information can be used to see what type of reinforcement could be the most effective. Additionally, more resources can then be used in field surveys or future research for finding accurate values for these parameters. These results can eventually decrease the uncertainty in the relationships between the significant wave heights and critical average overtopping discharges that are found with the COM and the VE-TM. In the end, the reduction of uncertainty can contribute to an optimal decision in the trade-off between raising the crest height versus strengthening the cover layer on the crest, inner slope and berm of the Afsluitdijk.

Based on this objective, the following main research question is formulated:

What is the relationship between the significant wave height and critical average overtopping discharge for wave heights up to 4 meter for the new design of the Afsluitdijk, and towards which parameters is this relationship most sensitive?

To answer this, the following research questions are defined:

1. What is the relationship between the significant wave height and the critical average overtopping discharge that is found using the COM?
2. What is the relationship between the significant wave height and the critical average overtopping discharge that is found using the VE-TM?
3. How does the relationship between the significant wave height and the critical average overtopping discharge differ between the COM and VE-TM?
4. Towards which parameters in the COM and the VE-TM are the found relationships between the significant wave height and the critical average overtopping discharge most sensitive?

1.3 Study Area

The Afsluitdijk, with a total length of 32 kilometers, is located between Den Oever in the province of North-Holland and Zurich in the province of Friesland (see Figure 1). Besides being a primary flood defense, the Afsluitdijk also fulfills other functions. It separates the saline water in the Wadden Sea from the fresh water in the Lake IJssel, which is the largest freshwater buffer in the Netherlands (Ministerie van I&M and Ministerie van EZ, 2015). Furthermore, the A7/E22 highway and a bicycle path are located on top of the dike, creating a direct connection between the provinces of North-Holland and Friesland.

The Afsluitdijk is not a uniform dam and is therefore divided into 17 dike sections (*dijkvakken*) in which the hydraulic load and dam strength are more or less constant. For dike section 17a, the cross-sectional design is schematized in Figure 2. This figure is based on Rijkswaterstaat (2009) and shows the current design. The implementation of the new design, mentioned in Section 1.1, is discussed in Section 3.3.2. The study area extends from the outer toe up to the end of the inner berm and can be divided into two parts. The first part starts at the outer toe and ends at the start of the crest. This part of the cross-section is used to calculate the hydraulic boundary conditions at the start of the crest, which serves as input for the COM and the VE-TM. The second part starts at the start of the crest and extends until the end of the inner berm. For this part the critical average overtopping discharges are calculated.

The full crest and inner slope, as well as large part of the inner berm are covered with grass and are erodible. Furthermore, parts of the inner berm are covered with asphalt due to the highway and two parallel roads on either side. Modern dikes in the Netherlands generally have a core of sand which is covered by a layer of grass on clay. The clay, which is poorly permeable and erosion resistant, and the grass, which increases the overall strength of the cover layer, protect the sandy core (TAW, 1999). The Afsluitdijk also follows this structure, as can be seen in Figure 2. This shows that the crest, inner slope and a small part of the inner berm, which all have a grass cover layer, are located on a layer of boulder clay (*keileem*). Furthermore, the major part of the inner berm, where most of the grass cover layer is located, is built of sand. Soil survey results for several locations within dike section 17 show that the boulder clay has an average sand content of 51% and a plasticity index of 16, which is classified as "erosion-prone clay" (Rijkswaterstaat, 2012). Additionally, the grass cover quality was assessed as average or good, depending on the exact location.

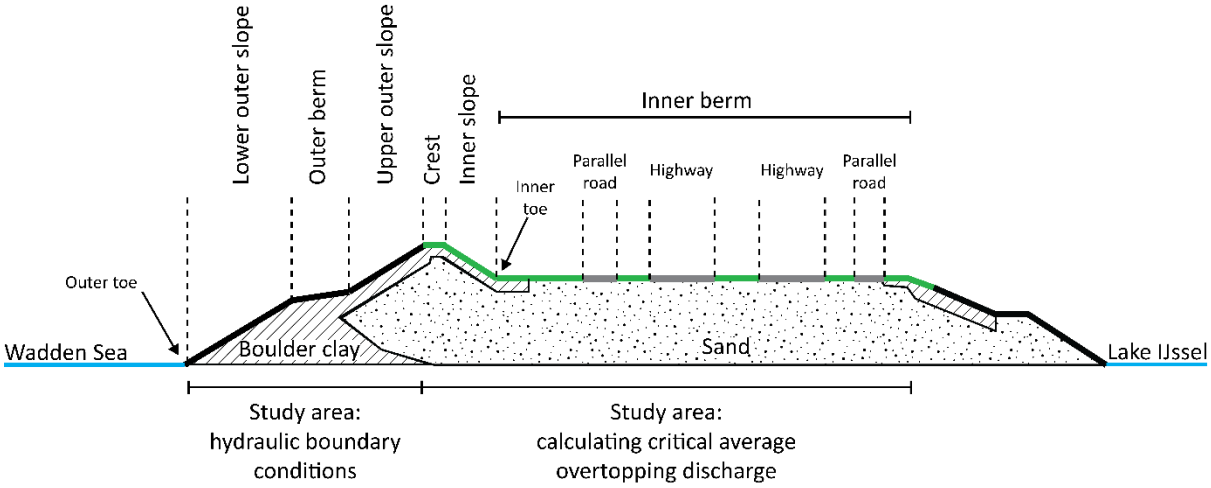

Figure 2: Cross-sectional schematization of the Afsluitdijk at dike section 17a, showing the surfaces covered with asphalt (grey), other non-erodible material (black) and grass (green), as well as the structure of the core. Figure based on Rijkswaterstaat (2009)*. Note: figure is not to scale.*

1.4 Thesis Outline

This thesis starts by giving background information about the subject in Chapter 2. Then, the methodology that is used to answer the research questions is presented in Chapter 3. The results of the study are presented in Chapter 4, followed by a discussion in Chapter 5. Lastly, the conclusions of this study are stated in Chapter 6, and recommendations for future research are given in Chapter 7.

2. THEORETICAL BACKGROUND

2.1 WAVE OVERTOPPING

A schematization of the wave overtopping process is shown in Figure 3. When waves propagate towards a dike or dam (1), they initially approach the structure undisturbed. When the waves enter the wave impact zone (2), they start to shoal and break due to a decreasing water depth near the structure. The waves then enter the wave run-up zone (3) in which the waves run up and down the outer dike slope. Wave overtopping occurs when the maximum wave run-up level exceeds the crest level, allowing water to flow over the crest (4) and towards the inner slope (5) and inner berm (Schüttrumpf and Oumeraci, 2005; Van der Meer et al., 2018).

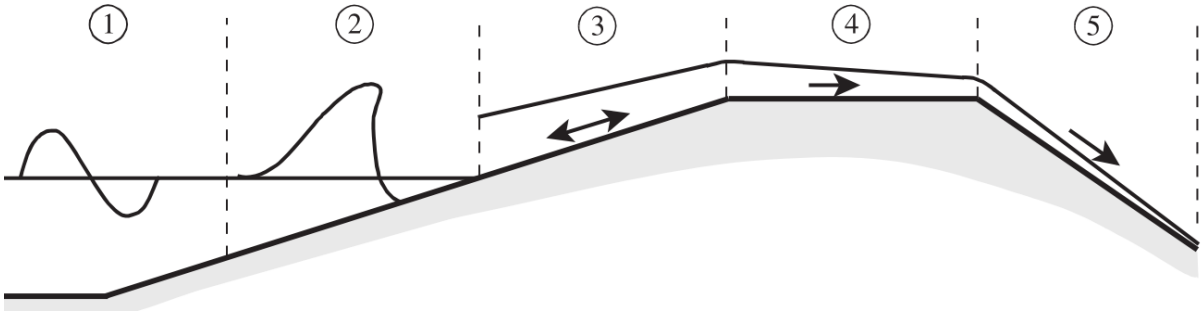

Figure 3: Process of wave overtopping. (1) undisturbed waves propagate to the dike, (2) wave impact zone in which waves start to shoal and break, (3) wave run-up zone in which waves run up/down the outer dike slope, (4) wave overtopping zone in which water flows over the dike crest, (5) water flows down the inner dike slope (Schüttrumpf and Oumeraci, 2005).

Schüttrumpf and Oumeraci (2005) concluded that failure of the inner slope is often initiated by individual overtopping waves and that, besides the average overtopping discharge, the flow velocities and layer thicknesses of these waves are required as hydraulic boundary conditions in order to predict erosion. This is supported by Van der Meer et al. (2018) who state that wave overtopping experiments have shown that the front velocity (i.e. the flow velocity of the overtopping wave front) of the overtopping water is the dominant parameter in initiating damage to a grass cover layer. Because an overtopping wave does not cause a steady, uniform layer of water to flow over the crest and inner slope, these variables depend on both cross-sectional location and moment in time. According to Van der Meer et al. (2010b) and Hughes et al. (2012) the layer thickness, flow velocity and overtopping discharge at a certain cross-sectional location all follow a sawtooth-like pattern, as shown in Figure 4. The parameters quickly increase to a maximum when the front of the overtopping wave arrives, after which they all non-linearly decrease to zero once the wave has passed.

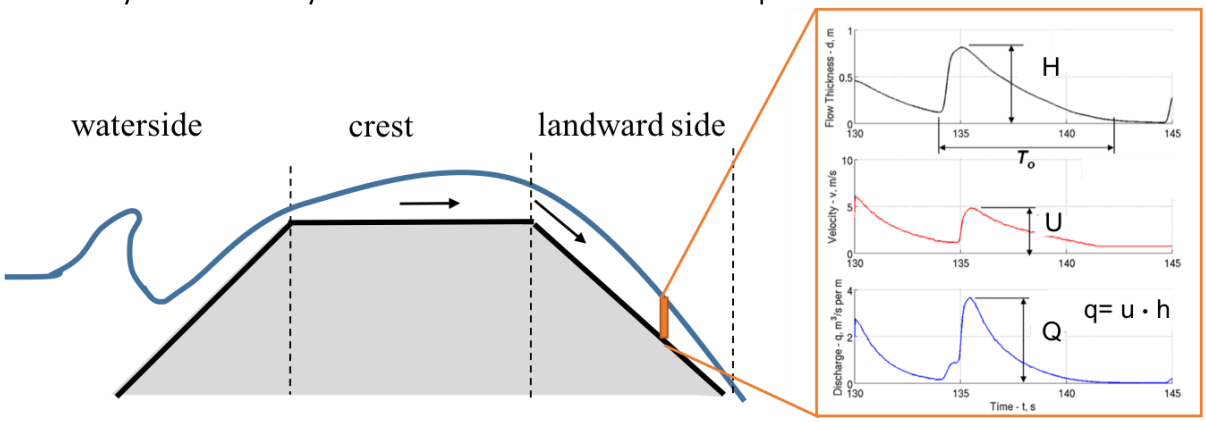

Figure 4: Schematization of wave overtopping at a dike. The graphs, originating from measurements by Hughes et al. (2012), *show the layer thickness H, flow velocity U and overtopping discharge Q as a function of time on the inner slope. Note that the values at the start of the graph (t = 130 s) belong to a previous overtopping wave. Figure adapted from Van Bergeijk et al.* (2019b).

2.2 Grass Erosion

The grass cover consists of two main layers: the topsoil, which is approximately 0.2 meter in depth, and the subsoil (Hoffmans et al., 2009; Morris et al., 2012). According to the WBI 2017, the grass cover layer of a flood defense fails when water breaks through the topsoil and starts eroding the subsoil (’t Hart et al., 2016). Within the topsoil, a sod layer (also known as turf) can be distinguished, which is generally assumed to be approximately 150 mm in depth. These layers are shown in Figure 5. Large pores and clay clumps are generally present in the topsoil due to biological activity and cracking as a result of shrinking and swelling of the soil due to a lack or abundance of moisture respectively (Hoffmans, 2012). The TAW (1997) describe the theoretical vertical structure of a well-rooted sod layer as follows:

- 1 – 35 mm: loose clay particles and plant remains which are washed away easily.
- 5 – 50 mm: loosely packed clay particles but with a large number of roots. Erosion of this layer only occurs slowly.
- 50 – 150 mm: more closely packed clay particles but with a lower number of roots. This layer is only susceptible to erosion in a situation with a very long period of wave loading.

The structure of the grass cover at a depth of more than 150 mm consists of more densely packed clay particles (sometimes sand) and a further decrease in the number of roots. Research by Sprangers (1999) shows that the density of the grass roots decreases exponentially with depth. This indicates that the subsoil layer has a relatively low grass root density. The strength of this part of the grass cover layer is therefore mainly determined by the cohesion and the internal friction angle of the soil (Hoffmans et al., 2009).

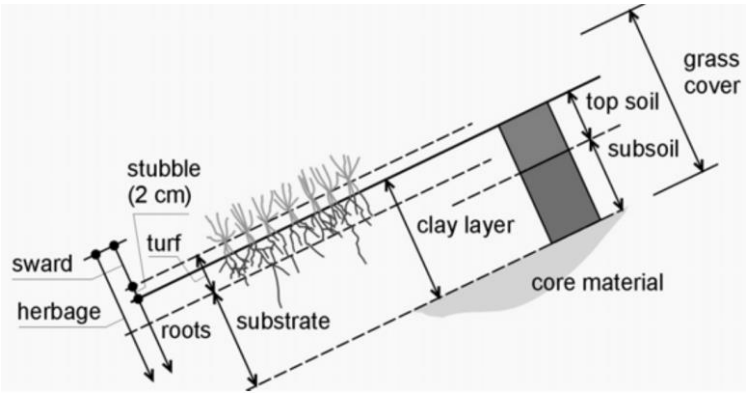

Figure 5: Structure of a grass cover layer (Hoffmans et al., 2009).

According to the Ministerie van Verkeer en Waterstaat (2007) and Hoffmans (2012) the resistance against erosion of a grass cover layer as a whole can mainly be attributed to the structure of the root layer, and not necessarily to the grass leaves above the ground surface. Chemical processes in the area around the roots are important for the cohesivity of soil particles, causing them to be “cemented” together. Additionally, fine root hairs keep small soil aggregates and soil particles together because they are anchored within the substrate, while the network of coarse roots also trap larger aggregates.

The importance of the grass roots is confirmed by several experiments which are discussed by Steendam et al. (2011), and specifically for the Afsluitdijk by Bakker et al. (2009). Failure of the top layer did not follow immediately after failure of the sod layer during these experiments, even though the soil was determined to be erosion-prone. Steendam et al. (2011) argue that the soil below the sod layer may still contain roots which can keep the soil together, even when the sod layer itself fails. The roots that extend below the sod layer may also have changed the soil properties due to the chemical cementing process. This shows that the topsoil and subsoil layers have distinct characteristics, which needs to be taken into account when modelling grass erosion.

2.3 TRANSITIONS

Erosion as a result of wave overtopping is often observed at locations on the water retaining structure where a certain transition takes place (Van der Meer et al., 2010a). This is because these affect the severity and extent to which grass erosion occurs, either because they influence the hydraulic load or because of a reduction of grass cover strength. Van der Meer and Van Hoven (2014) present an overview of both transitions and objects that are present on the Afsluitdijk (Appendix B). It must be noted that this overview is not completely representative for dike section 17a as this dike section does not include, for example, a small slope between the berm and the highway. Furthermore, no bicycle path is present but a parallel road. However, the table still gives a good overview of most of the transitions and objects present at dike section 17a. Additionally, values for the load factor α_m and strength factor α_s are given. These factors are used in the COM and indicate the effect of a transition or object on the hydraulic load and on the strength of the grass cover respectively. This is discussed in more detail in Section 3.3.1.

Common transitions on dikes and dams are cover material transitions from grass to asphalt and from asphalt to grass. When water flows over a smooth surface (e.g. asphalt) it experiences only little friction, causing a higher flow velocity than when it flows over a relatively rough surface (e.g. grass). Consequently, the load at a transition from asphalt to grass is high, because the flow velocity is high when the water arrives at the erodible grass layer. When there is a transition from grass to asphalt, the load and therefore the erosion will be less due to the lower flow velocity at this transition (Hoffmans et al., 2014). Furthermore, there will be more erosion at the asphalt to grass transition than at the transition from grass to asphalt due to an increase in turbulence (Bomers et al., 2018). For abrupt height differences between the grass and asphalt cover, the concentration and impact of the hydraulic load causes erosion. In the case of an abrupt transition where the highest layer is upslope and the lower layer is downslope, the hydraulic load on the downslope layer will be higher due to the impact of the free-falling water. If the downslope layer is erodible, this may lead to erosion (Figure 6a). In the case of an abrupt transition at which the highest layer is downslope and the lowest layer is upslope, the downslope layer will block the water. If the downslope layer is erodible (Figure 6b), the impact force can cause erosion. If the upslope layer is erodible and the downslope layer is non-erodible (Figure 6c), the turbulence that occurs as a result from the water splitting upon arriving at the higher layer can cause erosion of the erodible upslope layer. Additionally, if the non-erodible downslope layer is located on an erodible layer, this may eventually lead to undermining and destabilization of the layer.

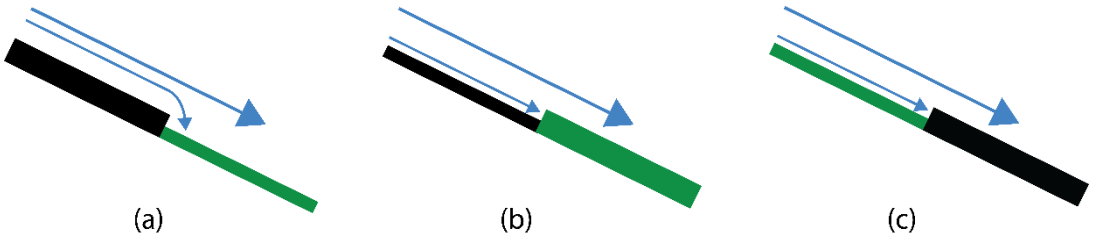

Figure 6: Three examples of cover material transitions with abrupt height differences, a) water flows from a higher non-erodible layer to a lower erodible layer, b) water flows from a lower non-erodible layer to a higher erodible layer, c) water flows from a lower erodible layer to a higher non-erodible layer.

A transition that is present on all dikes and dams is a change in inclination. At the transition from the crest to the inner slope of the dike (i.e. a convex change of inclination), the centripetal force acting on the water particles is directed upwards, causing a decrease in normal force at the dike surface. The opposite happens at the transition from the inner slope to the horizontal inner berm (i.e. a concave change of inclination), where the centripetal force is directed downwards, causing an increase in normal force at the dike surface (Hoffmans et al., 2014). Therefore, erosion is more likely to occur at the transition from inner slope to inner berm. This is supported by experiments with the Wave

Overtopping Simulator, which showed that erosion first occurred at the concave transition because the load at this location is relatively high. Furthermore, it was found that a more gradual concave transition from the slope to the berm experienced little to no erosion, while a more abrupt transition did. This can be explained by the fact that the total force that the soil needs to exert in the normal direction to curve the water flow can be distributed over a relatively long distance, while the same amount of force needs to be exerted over a much shorter distance in the case of an abrupt height difference (Van Steeg and Van Hoven, 2013).

In conclusion, it is important to include the effects of transitions at the Afsluitdijk when studying grass erosion. They can locally decrease the strength of the grass cover or increase the hydraulic load, which makes it likely for grass erosion and possibly failure of the grass cover layer to occur quicker here than at other cross-sectional locations.

3. METHODOLOGY

This chapter presents the methodology which is followed to answer the research questions from Section 1.2. First, the general approach is described for all research questions, which is also shown in Figure 7. Next, the approaches are presented for the COM and VE-TM individually. This is followed by a description of how the results are compared to each other as well as information regarding the sensitivity analysis which is carried out for several parameters in the COM and VE-TM approaches.

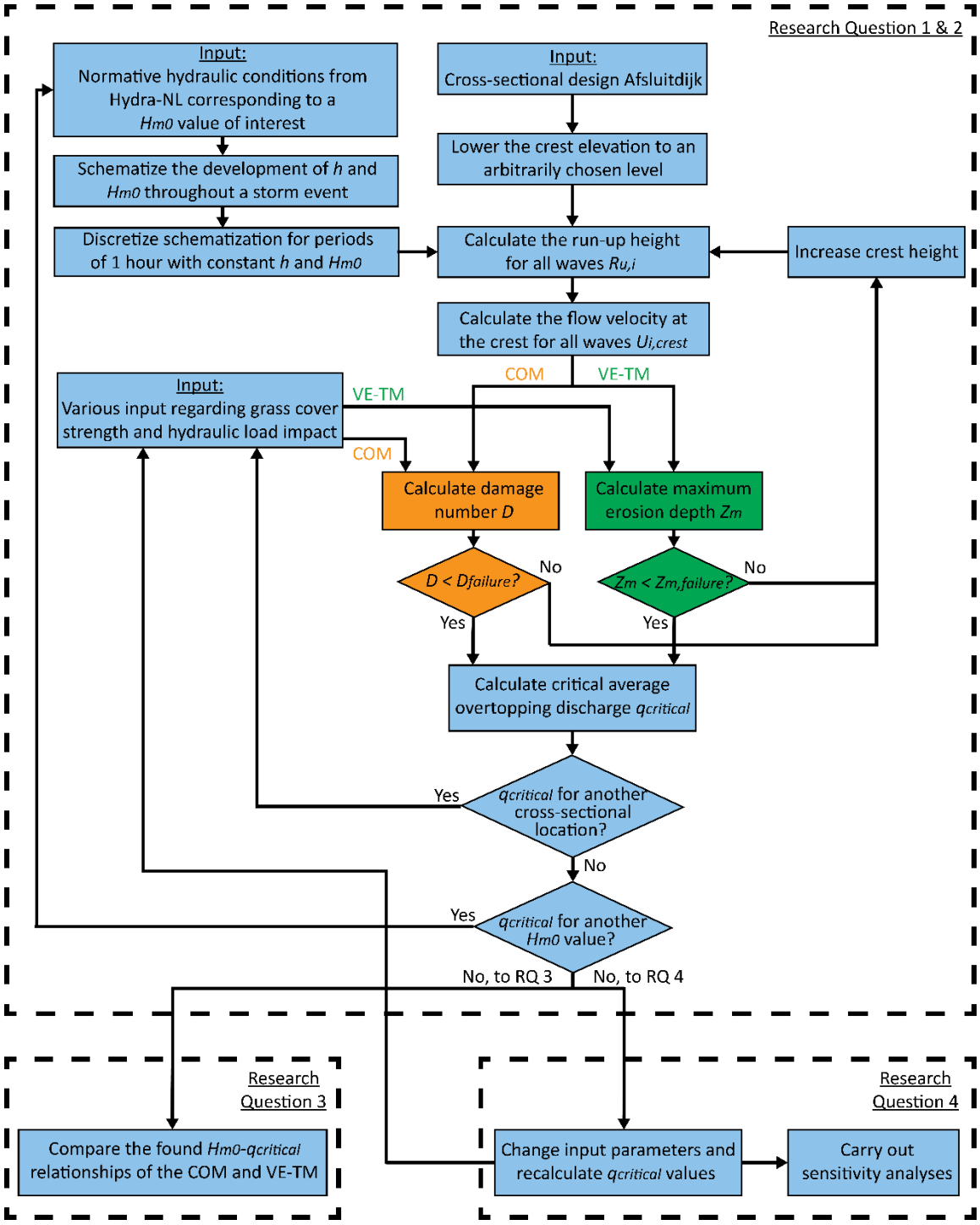

Figure 7: Overview of the methodology that is followed for the different research questions. The orange and green components are only followed for the COM and the VE-TM respectively, the blue components are followed for both models. The variables $D_{failure}$ and $z_{m,failure}$ are respectively the damage number and maximum erosion depth at which failure occurs, h the normative water level and H_{m0} the normative significant wave height.

3.1 General Approach

Figure 7 presents an overview of the methodology that is followed for each research question. The components that are marked orange are only followed in the COM approach (Section 3.3), while the green components are only followed in the VE-TM approach (Section 3.4). The components that are marked blue are shared by both the COM and the VE-TM approach. The calculations and methods that are used for each step are discussed more thoroughly in the following sections of this chapter.

A large part of the methodology for Research Question 1 and 2 is the same, as the COM and the VE-TM partly require the same input and eventually result in the same type of output: critical average overtopping discharges. First, the number of waves that approach the Afsluitdijk and their magnitude needs to be known. This data is extracted from the WBI 2017 Hydra-NL software. However, this only describes the normative hydraulic conditions at the peak of the storm event. In reality the storm conditions would build up until the peak of the storm event is reached, followed by a decrease until the end of the event. Based on the normative values found with Hydra-NL, the water level h and the wave height H_{m0} are schematized for a normative storm event to reflect this behaviour. The equations to calculate the flow velocity are only valid under constant hydraulic conditions, thus the schematized water level and wave height are discretized for periods of 1 hour. During these periods the water level and wave height are kept constant.

Besides the hydraulic conditions, the new design of the Afsluitdijk is required as input as well. The crest elevation of this design is initially lowered to an arbitrary level at which failure is expected to occur. Then, using the discretized water level and wave height and the new design of the Afsluitdijk a run-up height for each incident wave is found. This run-up height is then used to calculate the flow velocity at the start of the crest, which serves as input for both models.

The COM and the VE-TM require several input parameters regarding the strenght of the grass cover and the impact of the hydraulic load. Combined with the flow velocity at the start of the crest, the damage that is caused by the overtopping waves can be calculated for a certain cross-sectional location. Using the COM, this damage is expressed as a damage number. The calculated damage number is compared with the damage number for failure, which is found from literature (see Section 3.3.1). If the calculated damage number is higher than the damage number for failure, the geometry is changed so that the elevation of the crest increases. Then, the corresponding run-up height is determined and the calculation process is repeated until the calculated damage number is lower than the damage number for failure. This is the first iteration in which the geometrical characteristics do not cause failure of the cover layer, and the average overtopping discharge that is calculated using these characteristics is therefore the critical average overtopping discharge. This discharge can be considered as the maximum overtopping discharge that is allowed under the given hydraulic conditions without failure of the cover layer. After this, the calculations can be carried out again for a different cross-sectional location or for a different normative significant wave height.

A similar method is used for the VE-TM, except for the fact that a maximum erosion depth is calculated instead of a damage number. As long as the calculated erosion depth is larger than the erosion depth at which failure occurs, which is found from literature (see Section 3.4.1), the geometrical characteristics of the Afsluitdijk are changed so that the crest elevation increases. The calculations are then repeated until the calculated erosion depth is lower than the erosion depth of failure, and the corresponding critical average overtopping discharge is calculated.

The $H_{m0} - q_{critical}$ relationships are found separately for the COM and the VE-TM. The results of these two modelling approaches are compared to each other in Research Question 3. Besides comparing the magnitude of the found critical average overtopping discharges, the general behaviour of the

cross-sectional locations for the two modelling approaches is studied as well as the behaviour of the individual locations for the different significant wave heights.

Lastly, in Research Question 4 the values of several parameter are changed and simulations are carried out again with these new values. The new simulation results are then compared to the original results from Research Questions 1 and 2 to see the sensitivity of the COM and the VE-TM towards these parameters. This is done because the parameter values are often calculated based on assumptions or coefficients from literature which are not well established. By carrying out sensitivity analyses, the effects of these uncertainties in the calculations of the parameters on the resulting critical average overtopping discharges can be studied.

It is interesting to note that this modelling approach, as schematized in Figure 7, is not limited to the COM and the VE-TM but can theoretically be used in combination with any modelling approach that is able to calculate the damage on the cover layer caused by overtopping waves.

3.2 Hydraulic Boundary Conditions

3.2.1 Normative Storm Event

In order to find how many waves will overtop and what their flow velocity at the crest will be, the number of waves and their magnitude for a normative storm event need to be determined. Van Hoven (2015) and Van Hoven and Van der Meer (2017) used stationary storm conditions for their COM modelling approaches. This means that throughout the simulated storm event, the storm water level and the significant wave height were kept at a constant value. Van Hoven (2015) compared this approach (using a storm duration of six hours) to a more realistic approach in which both the storm water level and the wave height would develop throughout the storm event, with the peaks located in the middle of the event. It was concluded that for storm-driven water systems these stationary storm conditions yield a damage number that is approximately twice the damage number that would result from an approach in which the water level and water height would develop over time. Van Hoven and Van der Meer (2017) therefore used a storm duration of three hours instead of six hours to compensate for this. However, it is expected that the approach in which the water level and wave height develop over time yields the most realistic result. This is therefore the approach that is used to determine the number of incident waves and their characteristics. The differences in the simulation results that are obtained using the three-hour storm approach of Van Hoven and Van der Meer (2017) and the storm development approach are discussed in Section 5.1.

Rijkswaterstaat (2017) presents the combination of water level h, spectral wave height H_{m0} (also referred to as significant wave height), peak wave period T_p and angle of wave attack θ with a corresponding return period of 43 500 years for the year 2024 at the Afsluitdijk. These storm conditions, which are underlined in Table 2, are considered to be normative for the new design. In order to obtain correct values for other storm events, an attempt was made to reproduce the given values using the WBI 2017 software Hydra-NL and the procedure described by Rijkswaterstaat (2017). The found differences between these values are small (< 1%), and this approach is therefore used to find combinations of hydraulic conditions for waves that are lower and higher than the normative design wave height (with a minimum significant wave height of H_{m0} = 1.92 meter and a maximum of H_{m0} = 4.02 meter). These are presented in Table 2.

Table 2: Normative hydraulic parameters for dike section 17 of the Afsluitdijk. The underlined hydraulic conditions are normative for the new design and are given by Rijkswaterstaat (2017). All other values are obtained using Hydra-NL version 2.0.0 in combination with the database "WTI2011_Waddenzee_v01" and procedure described by Rijkswaterstaat (2017).

Water level h [m+NAP]	**Significant wave height H_{m0} [m]**	**Peak wave period T_p [s]**	**Angle of wave attack θ [°N]**	**Return period [years]**
3.38	1.92	5.57	286.4	5
3.78	2.22	5.95	285.5	20
4.21	2.52	6.33	284.8	100
4.59	2.86	6.66	283.9	500
4.74	2.98	6.80	283.9	1 000
5.08	3.22	7.08	318.3	5 000
5.32	3.38	7.03	319.0	43 500
5.65	3.72	7.52	319.3	100 000
5.93	4.02	7.74	320.8	500 000

Each set (i.e. a combination of h, H_{m0}, T_p and θ) describes a storm event with a certain return period. However, as these values serve as input for studying the effect of a changing significant wave height on the critical average overtopping discharge, all hydraulic conditions should be kept constant except for the wave height. To see how the other hydraulic conditions influence this result, the significant wave height is varied for three scenarios:

- Low h and θ conditions: h = 3.38 m+NAP, θ = 286.4 °N.
- Medium h and θ conditions: h = 4.74 m+NAP, θ = 283.9 °N.
- High h and θ conditions: h = 5.93 m+NAP, θ = 320.8 °N.

The wave period is not kept constant but varies along with the wave height, as these are directly related. Under the assumption that the steepness of the incoming waves stays constant, regardless of the storm event, the wavelength will increase when the significant wave height increase, in turn increasing the wave period.

The normative water level of a storm is the sum of the storm surge and the astronomical tide. The development of the normative water level can be extracted from the WBI 2017 software *Waterstandsverloop* version 3.0.1. However, another possible approach is to program this schematization based on descriptions from the literature and the values presented in Table 2. In this way, new hydraulic conditions can easily be implemented and does not require manual exporting and importing of data. The tidal curve can be extracted from the *Waterstandsverloop* software at dike section 17a. It should be noted that this is the average astronomical tide, and that events such as spring and neap tide are not considered. Furthermore, according to Chbab and De Waal (2017) and Botterhuis et al. (2017) the development of the storm surge water level in de Wadden Sea can be described by a trapezium (dashed red line in Figure 8) with the following characteristics:

- Base duration: the schematized trapezium has a base duration (i.e. storm duration) of 45 hours (Chbab, 2015; Chbab and De Waal, 2017).
- Top duration: the duration of the top of the trapezium is 2 hours.
- Top water level: both one hour before and after the peak, the storm surge water level is 0.1 meter lower than the peak storm surge water level.
- Phase difference: the storm surge peak occurs +5.5 hours before the tidal peak (Chbab, 2015; Chbab and De Waal, 2017). Following the literature, this is denoted as a positive phase difference. According to Chbab (2015) the phase difference is, in theory, randomly and uniformly distributed. However, analyses of historical data have shown that this is not the case, most likely due to the interaction between the storm surge and the astronomical tide.

Because all of the trapezium characteristics are known as well as the average tidal curve, the development of the water level during a storm can be schematized by scaling up the storm surge curve until the sum of the storm surge water level and the tidal water level equals the desired normative water level. An example of this is given as Figure 8. The normative water level curve was compared with the curve from *Waterstandsverloop* version 3.0.1, which showed that the two are identical. This indicates that the normative water level can be correctly schematized based on the WBI 2017 using the information provided in this chapter.

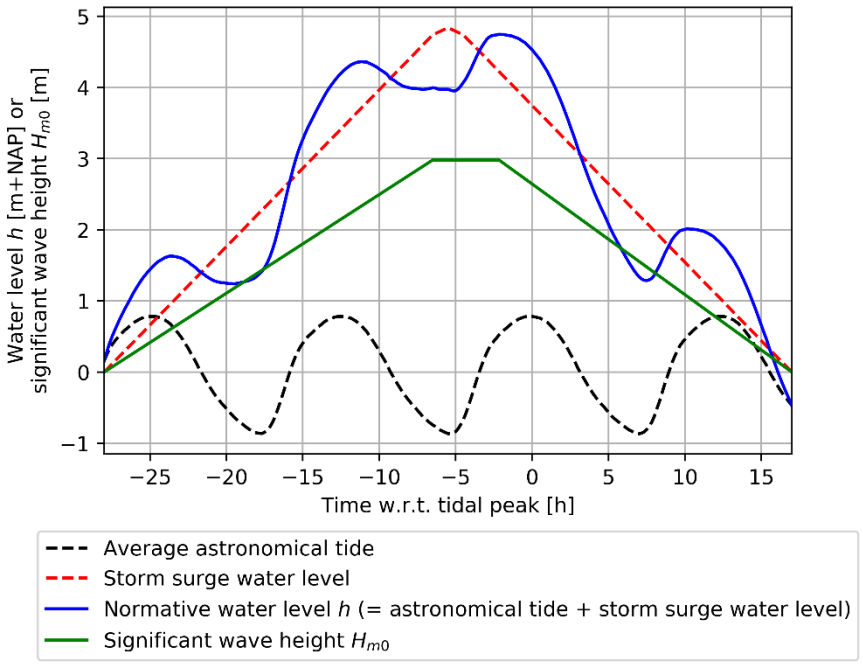

Figure 8: Schematization of a storm event with a normative water level of h = 4.74 m+NAP and a normative significant wave height of H_{m0} = 2.98 m.

A similar approach is used for the development of the significant wave height throughout the storm. Following Van Hoven (2015) the development of $\mathrm{H_{m0}}$ follows the normative water level curve. The top period during which the maximum $\mathrm{H_{m0}}$ occurs starts at the same time as the top period of the storm surge, but its duration can be longer or shorter than two hours in order to make sure the maximum $\mathrm{H_{m0}}$ also occurs when the maximum h takes place. In the case of Figure 8 the top period duration of $\mathrm{H_{m0}}$ is extended by approximately two hours, resulting in a total duration of the maximum $\mathrm{H_{m0}}$ of circa 4 hours. Lastly, it is assumed that the angle of wave attack θ stays constant throughout the storm event. This is a realistic assumption as the waves in a storm event are generally scattered around one main direction (Van der Meer et al., 2018).

This schematization of the hydraulic conditions is eventually used to calculate the hydraulic load on the cover layer. However, according to Van der Meer et al. (2018) the average overtopping discharge should be calculated for a constant water level and stationary wave conditions, which is not the case for this study. It is therefore necessary to discretize both the water level and wave height development so that the storm event is schematized by a number of periods in which the hydraulic conditions are constant. Following Van Hoven (2015) this is done for periods with a duration of one hour, resulting in a total of 45 periods as presented in Figure 9. For all further calculations the discretized water levels and wave heights values are used. These vary depending on the normative values that occur at the peak of the storm event (Table 2).

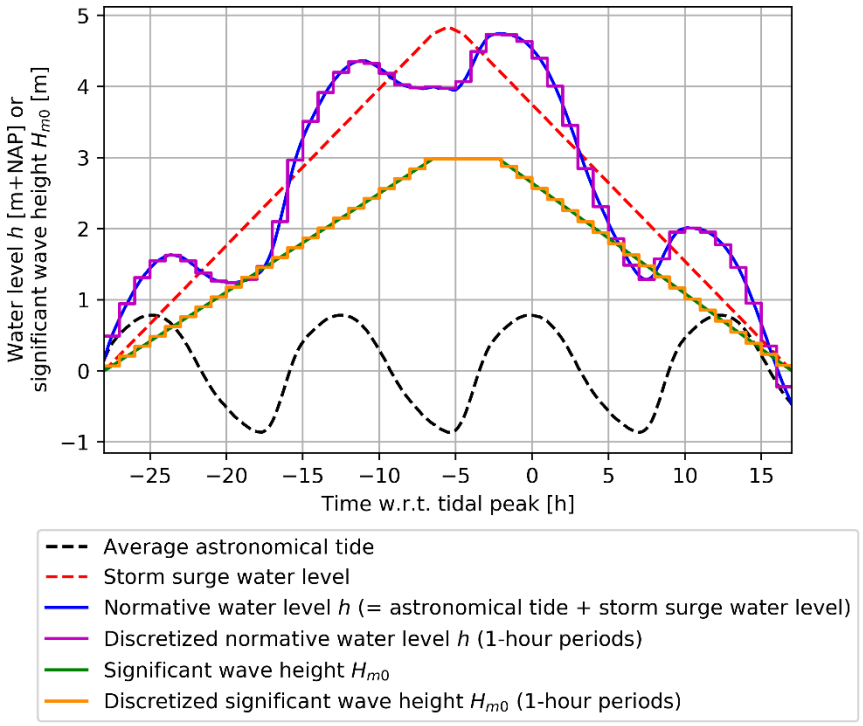

Figure 9: Schematization of a storm event with a normative water level of h = 4.74 m+NAP and a normative significant wave height of H_{m0} = 2.98 m, including the discretization periods with a duration of 1 hour.

3.2.2 Wave Run-Up Height

Whether a wave will overtop depends on its run-up height. According to the EurOtop Manual (Van der Meer et al., 2018), the following equations can be used under constant hydraulic conditions to calculate the run-up height that is exceeded by 2% of the incident waves:

$$R_{u2\%} = H_{m0}\left(1.75 * \gamma_b * \gamma_f * \gamma_\beta * \xi_{m-1,0}\right) \quad \text{(Eq. 1a)}$$

With a maximum value of:

$$R_{u2\%} = H_{m0}\left(1.07 * \gamma_f * \gamma_\beta\left(4 - \frac{1.5}{\sqrt{\gamma_b * \xi_{m-1,0}}}\right)\right) \quad \text{(Eq. 1b)}$$

And:

$$\xi_{m-1,0} = \frac{\tan\alpha_{outer,char.}}{\sqrt{s_{m-1,0}}} \quad \text{(Eq. 2)}$$

$$s_{m-1,0} = \frac{H_{m0}}{L_{m-1,0}} \quad \text{(Eq. 3)}$$

$$L_{m-1,0} = \frac{gT_{m-1,0}^2}{2\pi} \quad \text{(Eq. 4)}$$

Where:

H_{m0}:	Significant wave height	[m]
$L_{m-1,0}$:	Spectral wavelength in deep water	[m]
$R_{u2\%}$:	Run-up height above the still water level that is exceeded by 2% of the incident waves (i.e. the 2% run-up height)	[m]
$s_{m-1,0}$:	Wave steepness	[-]
$T_{m-1,0}$:	Spectral wave period	[s]
$\alpha_{outer,char.}$:	Characteristic outer slope angle	[°]
γ_b:	Influence factor for a berm	[-]
γ_f:	Influence factor for the roughness of the outer slope	[-]
γ_β:	Influence factor for oblique wave attack	[-]
$\xi_{m-1,0}$:	Breaker parameter (/surf similarity parameter/Iribarren number)	[-]

The calculation methods for the influence factors γ_β, γ_b, γ_f as well as the breaker parameter $\xi_{m-1,0}$ are presented in the paragraphs below. Furthermore, it is assumed that the spectral wave period and consequently the spectral wavelength develop similarly to the significant wave height, meaning that the wave steepness stays constant throughout the storm event.

The presented equations for the (maximum) 2% run-up height are used for a so-called "design or assessment approach", which includes a partial safety factor of one standard deviation compared to the "mean value approach". By including this partial safety factor, the hydraulic load is increased, which decreases the critical average overtopping discharge. In other words: the resulting critical discharges will be lower than when using the mean value approach and can therefore be considered as conservative. Additionally, it should be noted that the equation calculates the 2% run-up height using one H_{m0} value for which the discretized hydraulic conditions from Section 3.2.1 can be used. This means that the 2% run-up height that is calculated should be seen as the run-up height that is exceeded by 2% of the incoming waves within the considered discretization period, and not by all incoming waves throughout the storm.

Breaker Parameter $\xi_{m-1,0}$

In order to calculate the breaker parameter, the angle of the outer slope needs to be known. However, as the outer design of the Afsluitdijk consists of a composite profile (two slopes connected with a berm), a characteristic slope angle for the outer slope $\alpha_{outer,char.}$ should be used. This is an iterative process that is described by Van der Meer et al. (2018) and which results in a first and a second estimate of the slope angle. It is the second estimate that is used as the characteristic slope angle in further calculations (i.e. $\alpha_{outer,char.} = \alpha_{outer,char\ 2nd\ estimate}$).

For both the first and second estimate, the point of wave breaking is used as the start of the characteristic slope. This point is the location on the outer design of the dam that is located at $1.5*H_{m0}$ below the still water line. As an end point for the first estimate, the location on the outer design that is located $1.5*H_{m0}$ above the still water line is recommended. Using this first estimate of the characteristic slope angle, a first estimation of the wave run-up height can be calculated with Eq. 1a and Eq. 1b. This wave run-up height is then used in Eq. 5b as end point for the second estimation. Furthermore, if the end points in the first and second estimates are located above the crest level, the crest level should be taken as end point. Illustrations that clarify this calculation process can be found in Van der Meer et al. (2018). Lastly, it should be noted that when the composite profile contains a non-horizontal berm (which is the case for the Afsluitdijk), the horizontal berm width B should be calculated by extending the lower and upper slope until a horizontal berm is created.

$$\tan\alpha_{outer,char\ 1st\ esimate} = \frac{3H_{m0}}{L_{slope} - B} \text{ for } 1.5H_{m0} < R_c$$
$$\tan\alpha_{outer,char1st\ esimate} = \frac{1.5H_{m0} + R_c}{L_{slope} - B} \text{ for } 1.5H_{m0} > R_c \quad \text{(Eq. 5a)}$$

$$\tan\alpha_{outer,char\ 2nd\ esimate} = \frac{(1.5H_{m0} + R_{u2\%\ from\ 1st\ estimate})}{L_{slope} - B} \text{ for } R_{u2\%\ from\ 1st\ estimate} < R_c$$
$$\tan\alpha_{outer,char\ 2nd\ esimate} = \frac{(1.5H_{m0} + R_c)}{L_{slope} - B} \text{ for } R_{u2\%\ from\ 1st\ estimate} > R_c \quad \text{(Eq. 5b)}$$

Where:

B:	Width of the horizontal outer berm	[m]
L_{slope}:	Horizontal length between the start and end point of the estimated characteristic slope	[m]
R_c:	Crest freeboard, i.e. the vertical distance between the crest and the still water level	[m]

Influence Factor for Oblique Wave Attack γ_β

Van der Meer et al. (2018) present the equations below for the influence factor for oblique wave attack γ_β.

$$\gamma_\beta = 1 - 0.0033|\beta| \quad \text{for } 0° \leq |\beta| \leq 80°$$
$$\gamma_\beta = 0.736 \quad \text{for } |\beta| > 80° \qquad \text{(Eq. 6)}$$

Where:

β: Angle of wave attack [°]

This equation is valid for short-crested waves, which are waves with crests that have a finite width, are not parallel to each other and have individual directions that are scattered around the main direction. During storms these criteria are generally met (Van der Meer et al., 2018). The angle of wave attack used in the equation is the angle between the direction of the wave and the perpendicular line to the long axis of the dike, after refraction and diffraction transformations. It is assumed that these effects are already included in the angles of wave attack presented in Table 2. In order to transform these angles of wave attack, which are given in °N, to angles relative to the line that is perpendicular to the dam, the orientation of the long axis of the Afsluitdijk with respect to 0 °N needs to be known. From satellite imagery this is found to be approximately 47 °N.

Influence Factor for a Berm γ_b

For the influence factor for a berm γ_b, Van der Meer et al. (2018) suggests an equation based on the geometry of the outer slope. However, Sigurdarson and Van der Meer (2012) found that the berm influence also depends on the wave steepness. Chen et al. (2019, subm.) present the equation below based on experiments with physical models, which includes the wave steepness as well.

$$\gamma_b = 1 - \left(\frac{b_0}{\sqrt{s_{m-1,0}}}\right) r_B (1 - r_{dh}) \qquad \text{(Eq. 7)}$$

$$s_{m-1,0} = \frac{H_{m0}}{L_{m-1,0}} \qquad \text{(Eq. 8)}$$

$$r_B = \frac{B}{L_{berm}} \qquad \text{(Eq. 9)}$$

For a berm inside the influence area and above the still water line (SWL):

$$r_{dh} = 0.5 - 0.5 \cos\left(\pi \frac{d_b}{R_{u2\%}}\right) \qquad \text{(Eq. 10a)}$$

For a berm inside the influence area and below the still water line (SWL):

$$r_{dh} = 0.5 - 0.5 \cos\left(\pi \frac{d_b}{2H_{m0}}\right) \qquad \text{(Eq. 10b)}$$

For a berm outside the influence area:

$$r_{dh} = 1 \qquad \text{(Eq. 10c)}$$

Where:

b_0:	Empirical coefficient (= 0.21 for an impermeable outer berm (Chen et al., 2019, subm.), see Appendix A)	[-]
d_b:	Vertical distance between the middle of the outer berm and the still water line (SWL)	[m]
L_{berm}:	Characteristic berm length	[m]
r_B:	Influence of the outer berm width	[-]
r_{dh}:	Influence of the berm level	[-]
$s_{m-1,0}$:	Wave steepness	[-]

The influence area for the value of r_{dh} is defined by Van der Meer et al. (2018) as $\text{SWL} - 2H_{m0} < \text{outer berm elevation} < \text{SWL} + R_{u2\%}$. When a berm lies outside of this area, it has no influence on wave run-up and wave overtopping. It should be noted that when a berm is located inside the

influence area and below the SWL, the equation for $R_{u2\%}$ needs to be solved iteratively as r_{dh} becomes dependent on $R_{u2\%}$.

Influence Factor for Roughness γ_f

Studies by Capel (2015) and Van Steeg et al. (2018) have shown that the influence factor for the roughness γ_f is not a fixed value, but depends on wave conditions and the configurations of the dike. These considerations are included in the following equation given by Chen et al. (2019, subm.):

$$\gamma_f = 1 - \frac{c_0 R_c}{H_{m0} \xi_{m-1,0}} \quad \text{(Eq. 11)}$$

Where:

c_0: Empirical coefficient (= 0.36 (Chen et al., 2019, subm.) for protruding blocks on the upper outer slope (Appendix A)) [-]

The value of c_0 needs to be determined by means of calibration. The new design of the Afsluitdijk (Appendix A) shows that the lower outer slope is covered by Basalton (Holcim Basalton Quattroblocks) and the outer berm by asphalt concrete. Chen et al. (2019, subm.) do not present c_0 values for these situations, and constant roughness influence factors of γ_f = 0.9 (Basalton) and γ_f = 1.0 (asphalt concrete) are therefore used. These are material-specific values that are suggested by Van der Meer et al. (2018). For protruding elements, which are present on the upper outer slope, Chen et al. (2019, subm.) found c_0 = 0.36. Although the new design uses a different pattern, it is assumed that the value of Chen et al. (2019, subm.) can also be applied here as both situation concern protruding elements on an impermeable slope.

At the start and end of the storm event the significant wave height H_{m0} is low and the crest freeboard R_c high as a result of low water levels. This can lead to unrealistically low γ_f values for the upper outer slope when using Eq. 11. Therefore, this calculation method should only be used in the ranges $0.90 \leq R_c/H_{m0} \leq 1.33$ and $1.50 \leq \xi_{m-1,0} \leq 2.03$, which are the validation ranges that were used by Chen et al. (2019, subm.). For higher or lower hydraulic conditions outside these ranges the upper or lower limit is used instead, depending on which limit is closest to the actual value. For example, if $\xi_{m-1,0}$ = 1.40 the corresponding γ_f value in this situation is calculated using the closest limit value of the validation range, which is $\xi_{m-1,0}$ = 1.50. This approach likely results in over- or underestimation of γ_f at the start and end of the storm event, but as these relatively low hydraulic conditions contribute least to the total amount of erosion it is expected that the influence on the final critical average overtopping discharge is minimal.

This influence factor for roughness of the upper outer slope should be combined with the values for the lower outer slope and outer berm in order to get one overall influence factor. Van der Meer et al. (2018) use a weighted average based on the values for γ_f and the length of the sections at which they are valid. According to Chen et al. (2019, subm.) this weighted average method for a composite slope has not been validated, and its accuracy is therefore unknown. Based on experimental results, the following equations for γ_f on a uniform slope and $\gamma_{f,composite}$ calculation method for composite slopes were derived:

$$\gamma_{f,composite} = \frac{\alpha_1 \gamma_{f,1} L_1 + \alpha_2 \gamma_{f,2} L_2 + \alpha_3 \gamma_{f,3} L_3}{\alpha_1 L_1 + \alpha_2 L_2 + \alpha_3 L_3} \quad \text{(Eq. 12)}$$

Where:

L_1, L_2, L_3: Coverage length of the roughness elements on the upper outer slope, outer berm and lower outer slope [m]

$\alpha_1, \alpha_2, \alpha_3$: Location-weighting factor for the upper outer slope (= 0.65), outer berm (= 0.22) and lower outer slope (= 0.13) respectively (Chen et al., 2019, subm.) [-]

$\gamma_{f,1}, \gamma_{f,2}, \gamma_{f,3}$: Roughness influence factors for the upper slope, berm and inner slope respectively [-]

3.2.3 Crest Flow Velocity

The flow velocity at the start of the crest, which is required as input for both the COM and the VE-TM, can be calculated using the 2% run-up height from the previous section. According to the EurOtop Manual (Van der Meer et al., 2018) the flow velocity at the start of the crest which is exceeded by 2% of the incident waves can be calculated as:

$$U_{2\%,crest} = c_{U,2\%}\sqrt{g(R_{u2\%} - R_c)} \quad \text{for } R_{u2\%} > R_c \qquad \text{(Eq. 13)}$$

Where:

$c_{U,2\%}$:	Coefficient	[-]
$R_{u2\%}$:	Run-up height above the still water level that is exceeded by 2% of the incident waves (i.e. the 2% run-up height)	[m]
R_c:	Freeboard of the crest above the still water line	[m]
$U_{2\%,crest}$:	Flow velocity at the start of the crest exceeded by 2% of the incident waves	[m/s]

According to Van der Meer et al. (2015) the $c_{U,2\%}$ coefficient is not well established, and lies between 1.4 and 1.5 for slopes between 1:3 and 1:6. Therefore, the $c_{U,2\%}$ value for a slope with characteristic slope angle $\alpha_{outer,char.}$ is calculated using linear interpolation within this given range. As mentioned in Section 3.2.2 the 2% run-up height should be calculated for each discretized period during which the hydraulic conditions are constant. Because the run-up height is used as input in the calculation above, the same is true for $U_{2\%,crest}$. However, Eq. 13 only results in a value for the flow velocity at the start of the crest that is exceeded by 2% of the incoming waves within the discretized period, and not in an exact flow velocity value at the crest for each incoming wave. To obtain this flow velocity for each wave, an approach described by Van der Meer et al. (2015), Van Hoven (2015) and Van Hoven and Van der Meer (2017) can be used. Under the constant hydraulic conditions within a discretization period and by assuming a Rayleigh distribution for the wave run-up, the exceedance probability of an individual wave within a discretization period can be calculated as:

$$P_{i,discr.} = \frac{r_{i,discr.}}{N_{discr.} + 1} \qquad \text{(Eq. 14)}$$

Where:

$N_{discr.}$:	Total number of incident waves within the discretization period	[-]
$P_{i,discr.}$:	Probability of exceedance of wave i within the discretization period	[-]
$r_{i,discr.}$:	Rank of wave i within the discretization period, with $r_{i,discr.}$ = 1 for the highest wave and $r_{i,discr.}$ = $N_{discr.}$ for the lowest wave	[-]

Because the hydraulic conditions are constant within the discretization period, the ranking of the waves occurs randomly. The total number of incident waves can be calculated by dividing the total storm event duration (45 hours) by the mean wave period T_m of the incident waves.

$$N_{discr.} = \frac{t_{s,discr.}}{T_m} \qquad \text{(Eq. 15)}$$

Where:

$t_{s,discr.}$:	Duration of discretization period	[s]
T_m:	Mean wave period	[s]

From Table 2 only the peak wave period T_p is known, which would likely result in an underestimation of the number of waves. According to Van der Meer et al. (2018) the relation T_p/T_m lies between 1.1 and 1.25, so when using an average value $T_m = T_p/1.175$. Using this, a probability of exceedance for each wave within each discretization period $P_{i,discr.}$ can be calculated. Based on this probability, the run-up level of each wave can be calculated as:

$$R_{u,i,discr.} = R_{u2\%,discr.}\sqrt{\frac{\ln(P_{i,discr.})}{\ln(0.02)}} \quad \text{(Eq. 16)}$$

Where:

$R_{u2\%,discr.}$: Run-up height above the still water level that is exceeded by 2% of the incident waves within the discretization period [m]

$R_{u,i,discr.}$: Run-up height above the still water line for wave i within the discretization period [m]

Finally, the flow velocity can be calculated with the following equation, which is similar to Eq. 13:

$$U_{i,crest} = c_{U,2\%}\sqrt{g(R_{u,i,discr.} - R_c)} \quad \text{for } R_{u,i,discr.} > R_c \quad \text{(Eq. 17)}$$

Where:

$U_{i,crest}$: Maximum flow velocity at the start of the crest for overtopping wave i [m/s]

Originally, Eq. 13 calculates the flow velocity which is exceeded by 2% of the incident waves, which are all characterized by certain constant hydraulic parameters. However, because the probability of exceedance of each wave is taken into account, the flow velocity $U_{i.,crest}$ in Eq. 17 can be seen as the maximum flow velocity of overtopping wave i.

3.3 COM Modelling Approach

3.3.1 COM

The cumulative overload method (COM) is given by Hoffmans et al. (2018) as:

Cumulative overload method (COM)

$$D = \sum_{i=1}^{N}(\alpha_m(\alpha_a U_i)^2 - \alpha_s U_c^2) \quad \text{for } \alpha_m(\alpha_a U_i)^2 > \alpha_s U_c^2 \quad \text{(Eq. 18)}$$

Where:

D: Cumulative hydraulic overload (also known as damage number) [m^2/s^2]

N: Total number of overtopping waves for which $\alpha_m(\alpha_a U_i)^2 > \alpha_s U_c^2$ [-]

U_c: Critical flow velocity of the grass cover [m/s]

U_i: Front velocity of the overtopping wave at the start of the crest of the flood defense [m/s]

α_a: Acceleration factor due to increase of flow velocity on slope [-]

α_m: Load factor indicating the influence of an obstacle/transition on the flow velocity U_i [-]

α_s: Strength factor indicating the influence of an obstacle/transition on the critical flow velocity U_c [-]

In order to determine when the cover layer fails, the damage number at which failure occurs $D_{failure}$ needs to be known. Based on the analysis of Wave Overtopping Simulator results at several dikes in the Netherlands, $D_{failure}$ = 7000 m^2/s^2 was found by Van der Meer et al. (2015). Van Hoven and Van der Meer (2017) use the same value in their calculations, and mention a standard deviation of 700 m^2/s^2. However, in their analysis Van der Meer et al. (2015) also mention that the damage number at which failure occurs is larger than 7000 m^2/s^2 when only considering the Afsluitdijk-results. Because no exact value is given, a (conservative) value of $D_{failure}$ = 7000 m^2/s^2 is used in the COM simulations.

The presented equation uses the flow velocity of the overtopping wave front (i.e. front velocity) as input. Van der Meer et al. (2010b) concluded that the front velocity can be considered equal to the maximum (depth-averaged) flow velocity. While this variable indicates the hydraulic load on the cover layer, the critical flow velocity indicates the strength of the grass cover. Van der Meer and Van Hoven (2014) found that the critical flow velocity for the Afsluitdijk lies in the range 5 – 8 m/s. On average, stripping of the grass cover layer occurred at 6.5 m/s whereas failing of the topsoil layer occurred at 8 m/s. The fact that two critical flow velocities were found shows that it is a depth-dependent variable. However, Van der Meer and Van Hoven (2014) suggest to use a critical flow velocity of 6.5 m/s when carrying out tests regarding failure of the grass cover layer, which is approximately equal to the value estimated by Van Hoven (2015). This value is therefore used in the COM simulations, but the fact that a large safety margin is included and that the critical flow velocity is a depth-dependent variable in reality should be kept in mind.

Besides the (critical) flow velocity, the COM is characterized by three additional factors. First of all, the load factor α_m indicates the influence of a transition or an obstacle on the flow velocity. This factor has a minimum value of 1.0 (when there are no transitions or objects) and a theoretical maximum value of 2.0. Hoffmans et al. (2018) give an overview of calculation methods for this factor for revetment transitions, geometrical transitions and flow blocking objects. Secondly, the strength factor α_s indicates the influence of a transition or an obstacle on the critical flow velocity of the grass cover. It has a theoretical minimum of 0.8 (for relatively weak grass at a transition) and a maximum of 1.0 (for locations where the grass is at its maximum strength). Values for both the load and strength factor for transitions and objects on the Afsluitdijk are given by Van der Meer and Van Hoven (2014), see Appendix B. Lastly, the acceleration factor α_a indicates the increase in flow velocity when water flows down the inner slope. Its value depends on the slope angle, the flow velocity on the crest and the distance of the studied location from the crest (i.e. the location on the slope) but lies in the range of 1.0 (no acceleration) up to 1.6 (maximum acceleration). However, from experiments Van Hoven and Van der Meer (2017) found a constant acceleration factor of α_a = 1.4 for slopes between 1:2.3 and 1:4.5. As the new design of the Afsluitdijk has an inner slope of 1:2.5 (see Appendix A), this acceleration factor is used.

3.3.2 Schematization of Cross-Sectional Design

Appendix A shows the new design for dike section 17a from the outer toe to the inner toe. Besides different geometric characteristics compared to the current design (see Figure 2), the cover material of the outer slope differs as well. Both the lower outer slope and upper outer slope are covered with Holcim Quattroblocks, which are a type of Basalton, while the outer berm is covered with asphalt concrete. Additionally, the upper outer slope contains a rib pattern of protruding elements, which reduces the amount of wave run-up and overtopping. Because no detailed new design of the inner part of the Afsluitdijk (i.e. crest, inner slope and inner berm) is available yet, the current design is used for these sections (see Figure 2). Detailed technical drawings of this design are given by Rijkswaterstaat (2009).

As shown in Figure 7 there are two main types of input required in order to calculate the critical average overtopping discharge: the hydraulic conditions and the cross-sectional design of the Afsluitdijk. As the goal of the modelling is to find the critical discharge for several normative significant wave heights, the hydraulic conditions should be kept constant within each calculation and the critical discharge should be found by changing the cross-sectional design. The most logical approach for this is to start with a very low crest which is likely to lead to failure of the cover layer. Then, the geometry of the cross-section is changed so that the crest elevation increases, after which the calculations are carried out again. This iterative process can be seen in Figure 7. However, design choices need to be made in order to implement this variable crest elevation.

First of all, the lowest crest elevation (i.e. the crest height during the first iteration) needs to be determined. For this an arbitrarily chosen elevation level could be chosen. However, as mentioned earlier, the new outer profile of the Afsluitdijk is a composite, consisting of a lower outer slope, berm and upper outer slope. If a low first crest elevation is chosen, the consequence is that in some iterations the effects of a berm are not included (because the crest elevation at which the critical discharge is found is lower than the berm elevation), whereas in other iterations these effect must be included (when the crest elevation is above the berm elevation). Because this would be unrealistic, the crest elevation is defined as one centimeter above the highest point of the outer berm as a starting point.

Several characteristics of the cross-sectional design should be considered for the COM approach. If the crest elevation is increased while the crest width is kept constant, the slope angles should increase, leading to steeper slopes. For some simulations this may lead to unrealistic steep or gentle slopes that could never be implemented in reality due to macro-stability considerations. On the other hand, if the crest width is variable and the slope angles are kept constant, the model could simulate very narrow or negative crest widths for high crest elevations. This is unrealistic and can lead to computational problems as well. Therefore, an approach is preferred which ensures a constant crest width as well as constant slope angles, which is possible by shifting the inner slope as a whole. A crest width of 2.50 meter is used for this, which is the width that is specified in the new design (Appendix A). Although this approach increases the inner slope length, it does not influence the COM calculations as the acceleration factor α_a is mainly dependent on the slope angle (Van Hoven and Van der Meer, 2017). Because this angle is kept constant for all iterations, a constant α_a value is used for the inner slope regardless of its length.

Another aspect that should be considered is the parallel road that is located next to the inner toe. If the inner slope is shifted, the distance between the inner toe and the parallel road becomes smaller. It is therefore possible that the parallel road becomes covered by the inner slope in a certain iteration. To prevent this, the parallel road is shifted at the same rate as the inner slope. There are also other roads located on the inner berm, but only the parallel road next to the inner toe is considered in the simulations because it experiences the highest hydraulic load due to the high flow velocity at the end of the inner slope.

This approach is illustrated in Figure 10. In the first iteration, the crest elevation equals the berm elevation plus the set crest elevation accuracy (one centimeter in this case). In this situation, the upper outer slope is very short but characterized by the same angle as defined in the new design (see Appendix A). While the critical average overtopping discharge is not found, the crest elevation is increased by N*accuracy where N is the number of the iteration. To keep the slope angles and crest width constant, the inner slope is shifted to the right (Lake IJssel-side) relative to the location of the slope in the first iteration. The parallel road is shifted accordingly to make sure it is always located behind the inner toe. This process is repeated until the crest elevation is found that results in the critical average overtopping discharge.

A limitation of this approach is the width of the inner berm, which restricts the available shifting distance of the inner slope and the parallel road. Under the assumption that both parallel roads and the highway (see Figure 2) all need to be present on the inner berm, the maximum available distance equals the berm width minus the width occupied by the parallel roads and highway. Furthermore, because the parallel road that is closest to the inner toe is shifted at the same rate as the inner slope, the distance between the inner toe and this parallel road also needs to be subtracted from the available shifting distance. Under these design conditions the maximum crest elevation that the model is able to simulate is +10.57 m+NAP.

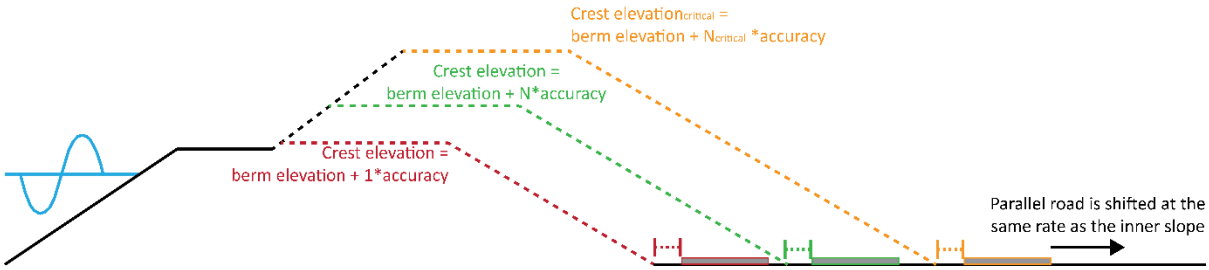

*Figure 10: Schematization of the iterative crest elevation increase process. In the first iteration the crest elevation is set at 1*accuracy above the berm elevation (where accuracy = 1 cm). When the critical average overtopping discharge is not found in iteration number N, the crest elevation is increased and the inner slope is shifted. The parallel road is shifted at the same rate as the inner slope, resulting in a constant distance between the inner toe and parallel road. This is repeated until the critical discharge is found in iteration number $N_{critical}$ with a corresponding crest elevation of $elevation_{critical}$. Note that the figure is not to scale.*

3.3.3 Studied Locations

The selection of locations that are studied in the COM approach, presented in Table 3 and Figure 11, can partly be based on the overview in Appendix B, which gives the load and strength factors α_m and α_s of the transitions on the Afsluitdijk. For the crest the transition from hard cover material on the upper outer slope to the grass cover on the crest (location 1) as well as the transition from crest to inner slope (location 2) are considered to be the most critical points on the crest. The flow velocity then increases on the inner slope (location 3), after which it arrives at the inner toe (i.e. the transition from inner slope to inner berm, location 4).

Several asphalt to grass and grass to asphalt transitions are present on the berm as can be seen in Section 1.3. When looking at the α_m and α_s values in Appendix B these are considered to be equally strong as the transition from hard cover material on the outer to the crest. Adding these in the COM simulations would therefore not provide additional information because they result in the same critical discharge values. However, it can be expected that the parallel road that is closest to the inner toe experiences additional hydraulic load due to the flow acceleration on the inner slope. The transitions from grass to asphalt and asphalt to grass at this road are therefore included in the analysis as location 5 and 6 respectively. Values for α_m and α_s for this specific location are not given in Appendix B, but it can be considered similar to the transitions from grass to the bicycle path and vice versa. Van der Meer and Van Hoven (2014) apply the same acceleration factor for this locations as for the inner slope. However, this seems to be an overestimation as the parallel road is not located immediately next to the inner toe. An arbitrarily chosen acceleration factor of $\alpha_a = 1.2$ is therefore estimated to be more suitable. As the effect of the acceleration is lower for locations further away from the end of the inner slope, it is assumed that this acceleration factor is only valid for the transition from grass to the asphalt of the parallel road, and not for the asphalt to grass transition because erosion at this location is too far away from the inner slope to be influenced by the flow acceleration.

These considerations result in the locations of interest for the COM presented in Table 3 along with the corresponding load, strength and acceleration factors. A schematized overview of the studied locations on the cross-section of the Afsluitdijk is presented in Figure 11.

Table 3: Overview of the load, strength and acceleration factors of the studied locations in the COM approach (Figure 11).

Location	Description	Load factor α_m	Strength factor α_s	Acceleration factor α_a
1	Transition from the hard cover material on the outer slope to the grass cover on the crest	1.0	0.9	1.0
2	Transition from the crest to the inner slope	1.0	1.0	1.0
3	Inner slope	1.0	1.0	1.4
4	Inner toe; transition from the inner slope to the inner berm	1.2	1.0	1.4
5	Transition from the inner berm grass to the asphalt of the parallel road	1.0	0.9	1.2
6	Transition from the asphalt of the parallel road to the inner berm grass	1.7	0.9	1.0

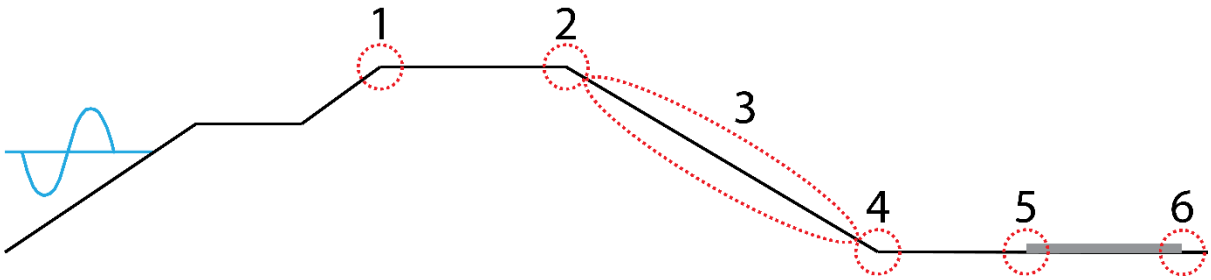

Figure 11: Schematized overview of the cross-section of the Afsluitdijk and the studied locations in the COM approach, see also Table 3. Note that the figure is not to scale.

3.3.4 Critical Average Overtopping Discharge

The methods presented in the previous sections are used to calculate the damage number. The geometrical characteristics of the cross-section are then changed for each iteration until the damage number reaches a value below the damage number of failure, as can be seen in the methodology overview given in Figure 7. It is at this point that the limit state for failure of the grass cover layer under the given hydraulic conditions is reached, and the corresponding average overtopping discharge needs to be calculated. This is done for the discretization period at the peak of the storm event which is in line with the approaches of Van Hoven (2015) and Van Hoven and Van der Meer (2017). The calculated discharge can therefore be regarded as the maximum average overtopping discharge that is allowed within a storm event before failure of the grass cover at the studied locations occurs.

Chen et al. (2019, subm.) present a calibrated version of the overtopping discharge equation for breaking waves that originates from the TAW (2002). Because the influence factors for the berm and roughness in Section 3.2.2 are also calculated with calibrated equations from the same study, this overtopping discharge equations is used as well in order to stay consistent.

Breaking waves

$$q_{crit.} = \sqrt{gH_{m0}^3}\left(\frac{0.067}{\sqrt{\tan\alpha_{outer,char.}}}\gamma_b\xi_{m-1,0}\exp\left[-4.90\frac{R_c}{H_{m0}\xi_{m-1,0}\gamma_b\gamma_f\gamma_\beta\gamma_v}\right]\right) \quad \text{(Eq. 19a)}$$

Where:
γ_v: Influence factor for a wall at the end of the outer slope (= 1, because there is no wall present) [-]

For non-breaking waves, the original equation by TAW (2002) is used. This equation indicates the maximum overtopping discharge, and a check must therefore be made whether $q_{crit.} < q_{crit.,max}$.

Non-breaking waves (max. $q_{crit.}$)

$$q_{crit.,max} = \sqrt{gH_{m0}^3}\left(0.2 * \exp\left[-2.6\frac{R_c}{H_{m0}\gamma_f\gamma_\beta}\right]\right) \quad \text{(Eq. 19b)}$$

3.4 VE-TM Modelling Approach

3.4.1 VE-TM

The coupled crest-inner slope velocity equations (VE) presented by Van Bergeijk et al. (2019b) consist of two equations: an equation for horizontal surfaces such as the crest and the inner berm, and an equation for the inner slope.

Velocity equation for horizontal surfaces

$$U_{max(x)} = \frac{1}{\frac{fx}{2q} + \frac{1}{U_0}} \quad \text{(Eq. 20a)}$$

Velocity equation for the inner slope

$$U_{max(s)} = \frac{\alpha}{\beta} + \mu \exp(-3\alpha\beta^2 s) \quad \text{(Eq. 20b)}$$

Where:

f:	Bottom friction coefficient	[-]
q:	Discharge of the overtopping wave	[$m^3/s/m$]
s:	Along-slope coordinate	[m]
$U_{max(s)}$:	Maximum depth-averaged flow velocity of the wave at along-slope location s	[m/s]
$U_{max(x)}$:	Maximum depth-averaged flow velocity of the wave at cross-sectional location x	[m/s]
U_0:	Maximum depth-averaged flow velocity at the start of the horizontal surface	[m/s]
x:	Cross-dike coordinate	[m]
α:	Parameter	[$m^{1/3}/s^{2/3}$]
β:	Parameter	[$s^{1/3}/m^{2/3}$]
μ:	Parameter	[m/s]

The equation for the inner slope uses an along-slope coordinate s which can be calculated from the horizontal cross-dike coordinate x as follows:

$$s = \frac{x - B_c}{\cos(\phi)} \quad \text{for } x \geq B_c \quad \text{(Eq. 21)}$$

Where:

B_c:	Crest width	[m]
ϕ:	Angle of the inner slope	[°]

Furthermore, parameters α, β and μ can be calculated using:

$$\alpha = \sqrt[3]{g \sin\phi} \quad \text{(Eq. 22a)}$$

$$\beta = \sqrt[3]{\frac{f}{2q}} \quad \text{(Eq. 22b)}$$

$$\mu = U_{s,0} - \frac{\alpha}{\beta} \quad \text{(Eq. 22c)}$$

Where:

$U_{s,0}$: Maximum depth-averaged flow velocity at the start of the slope [m/s]

The bottom friction coefficient can be calculated as:

$$f = \frac{2gn^2}{h_U(x)^{1/3}} \quad \text{(Eq. 23a)}$$

With a lower limit of:

$$f_{lim} = \frac{gq \sin(\phi)}{4U_{s,0}^3} \quad \text{(Eq. 23b)}$$

Where:

g:	Gravitational acceleration (= 9.81)	[m/s^2]
$h_U(x)$:	Location-dependent layer thickness at the moment of maximum flow velocity	[m]
n:	Manning's roughness coefficient	[s/m$^{1/3}$]

The maximum flow velocity at the start of the crest can be calculated using the approach that is discussed in Section 3.2.3. For the flow velocity at the start of the inner slope and inner berm the flow velocities at the end of the crest and the end of the inner slope can be used respectively. Furthermore, Van Bergeijk et al. (2019b) assumed that the discharge q of the overtopping wave is constant, indicating that no infiltration of water into the cover layer occurs. Under this assumption, the value for q only needs to be calculated once. This can be done by multiplying the flow velocity of the overtopping water with the layer thickness at the start of the crest. Van der Meer et al. (2018) gives the following equation for the layer thickness at the start of the crest that is exceeded by 2% of the incident waves:

$$h_{2\%,crest} = c_{h,2\%}(R_{u2\%} - R_c) \quad \text{for } R_{u2\%} > R_c \qquad \text{(Eq. 24)}$$

When using a similar approach as for the maximum flow velocity at the start of the crest (Section 3.2.3) the maximum layer thickness can be calculated as:

$$h_{i,discr.,crest} = c_{h,2\%}(R_{u,i,discr.} - R_c) \quad \text{for } R_{u,i,discr.} > R_c \qquad \text{(Eq. 25)}$$

Where:

$c_{h,2\%}$:	Coefficient	[-]
$h_{i,discr.,crest}$:	Maximum layer thickness at the start of the crest for wave i within the discretization period	[m]
$R_{u,i,discr.}$:	Run-up height above the still water line for wave i within the discretization period	[-]
R_c:	Freeboard of the crest above the still water line	[m]

Van der Meer et al. (2018) concluded that the value of the coefficient $c_{h,2\%}$ should lie in the range 0.20 – 0.30 for slopes in the range 1:4 – 1:6. Similar to the calculation of the value for $c_{U,2\%}$ in Section 3.2.3 a value for $c_{h,2\%}$ can be found for the characteristic outer slope $\alpha_{outer,char.}$ by linearly interpolate within this given range. By multiplying the found maximum layer thickness with the earlier found maximum flow velocity at the start of the crest a maximum discharge is found. Note that, because the maximum layer thickness is used instead of the actual layer thickness at the moment of maximum flow velocity, a maximum discharge is found instead of an average discharge. This assumption is discussed in Section 5.4.2.

For the bottom friction f Eq. 32a is given by Van Bergeijk et al. (2019b). As only the maximum layer thickness is known, calculating the bottom friction with this equation would result in an overestimated friction value. A more realistic value is given by Steendam et al. (2012), who used data from overtopping experiments to find a bottom friction value for grass of f_{grass} = 0.01. This is also the friction value that Van Bergeijk et al. (2019b) used for validation of their flow velocity equations. However, no validated friction value for asphalt $f_{asphalt}$ can be found from the literature. This value needs to be estimated using Eq. 32a, for which a Manning's roughness coefficient for asphalt of n = 0.0145 is used. Furthermore, the layer thickness just upstream of the location at which the friction should be calculated is used in the equation, as this is the most accurate estimation of the layer thickness for the considered location. It is calculated by dividing the discharge of the overtopping wave by the flow velocity just upstream of the considered location.

The transition model (TM) is given by Valk (2009) as:

Transition model (TM)

$$z_m = T_{ovt.}\left(\frac{\omega^2\tau_0(d) - \tau_c(d)}{E_{soil}(d)}\right) \quad \text{for } \omega^2\tau_0(d) > \tau_c(d) \qquad \text{(Eq. 26)}$$

Where:

$E_{soil}(d)$:	Depth-dependent soil erosion parameter	[m/s]
$T_{ovt.}$:	Overtopping duration at the studied cross-sectional location	[s]
z_m:	Maximum erosion depth	[m]
$\tau_0(d)$:	Depth-dependent bed shear stress caused by the overtopping wave	[N/m^2]
$\tau_c(d)$:	Critical depth-dependent bed shear stress	[N/m^2]
ω:	Turbulence coefficient	[-]

In this equation the bed shear stress $\tau_0(d)$, which describes the load on the grass cover, is based on studies that looked at the load caused by a water jet that hits the grass cover under an angle, as only the transition from the inner slope to the inner berm was considered (hence the name "transition model"). In this definition of the bed shear stress, it is assumed that the formed erosion hole retains water, which dampens the impact of the shear stress from a new overtopping wave. However, this equation contains a coefficient which was specifically calibrated by Valk (2009) for the transition from inner slope to inner berm. As this is not generally applicable for the whole cross-section of the Afsluitdijk, it is assumed that bed shear stress is constant regardless of the erosion depth. This depth-independent bed shear stress can be calculated using the following definition stated by Van Bergeijk et al. (2019b):

$$\tau_0 = \frac{1}{2}\rho_w f U^2 \qquad \text{(Eq. 27)}$$

Where:

f:	Bottom friction coefficient for overtopping wave i	[-]
U:	Flow velocity of overtopping wave i	[m/s]
ρ_w:	Mass density of water (= 1030 (Verheij et al., 2010))	[kg/m^3]

Here, the flow velocity U becomes the maximum depth-averaged flow velocity U_{max} when the resulting flow velocities from the VE are used as input. The calculated bed shear stress therefore also becomes the maximum bed shear stress. Then, when summing the erosion caused by each overtopping wave for the whole storm event, the TM-equation that is used in the VE-TM approach becomes:

$$z_{m,sum} = \sum_{i=1}^{N}\left(T_{ovt,i}\left(\frac{\omega^2\tau_{0,i} - \tau_c(d)}{E_{soil}(d)}\right)\right) \quad \text{for } \omega^2\tau_{0,i} > \tau_c(d) \qquad \text{(Eq. 28)}$$

Where:

N:	Total number of overtopping waves for which $\omega^2\tau_{0,i} > \tau_c(d)$	[-]
$T_{ovt,i}$:	Overtopping duration of wave i at the studied cross-sectional location	[s]
$z_{m,sum}$:	Summed maximum erosion depth for all overtopping waves N	[m]
$\tau_{0,i}$:	Bed shear stress caused by overtopping wave i	[N/m^2]

Valk (2009) studied two different methods for implementation of the overtopping duration $T_{ovt.}$: characteristic overtopping durations at the inner slope as a function of wave volume and an equation of Bosman et al. (2008) which describes the duration at the crest as a function of wave period, run-up height and crest height. Valk (2009) concluded that the method with the equation of Bosman et al. (2008) results in four times larger erosion depths than the method with the characteristic values.

However, because the overtopping duration was not the only variable that was varied in the comparison, this larger erosion depth cannot be completely attributed to the difference in overtopping duration. Nevertheless, the equation of Bosman et al. (2008) is likely to still result in larger erosion depths as it describes the duration at the crest, which is expected to be longer than on the inner slope due to a lower flow velocity. Because the predicted duration Bosman et al. (2008) shows good agreement with physical model experiments and because it is expected to lead to more conservative critical average overtopping discharges, this equation is used for the overtopping duration in the TM. It is given as the 2% exceedance overtopping duration at the start of the crest:

$$T_{ovt.,2\%\,@\,x=0} = 1.15 * T_{m-1,0} \sqrt{\frac{R_{u2\%} - R_c}{2g}} \quad \text{(Eq. 29)}$$

A similar approach as for the flow velocity at the crest (Section 3.2.3) can be used to calculate the overtopping duration for each individual wave at the start of the crest:

$$T_{ovt.,i,@\,x=0} = 1.15 * T_{m-1,0,discr.} \sqrt{\frac{R_{u,i,discr.} - R_c}{2g}} \quad \text{(Eq. 30)}$$

Where:

$R_{u2\%}$: Run-up height above the still water level that is exceeded by 2% of the incident waves [m]

$R_{u,i,discr.}$: Run-up height above the still water line for wave i within the discretization period [m]

$T_{ovt.,2\%\,@\,x=0}$: Overtopping duration that is exceeded by 2% of the incident waves at the start of the crest [s]

$T_{ovt.,i,@\,x=0}$: Overtopping duration for overtopping wave i at the start of the crest [s]

$T_{m-1,0}$: Spectral wave period [s]

$T_{m-1,0,discr.}$: Spectral wave period within the discretization period (= constant due to constant hydraulic conditions) [s]

As mentioned in Section 3.2.2, it is assumed that the wave steepness stays constant throughout the storm event, and that therefore the spectral wave period develops similarly to the significant wave height as these two variables are interdependent (see Section 3.2.1 for the discretization of the significant wave height). When the water flows over the dike, it is slowed down because of the friction it experiences. This means that the overtopping duration increases for locations farther away from the start of the crest. Bosman et al. (2008) also present an equation for other locations that include this effect, but as this is only valid for the crest it cannot be applied to the complete cross-section of the Afsluitdijk. Additionally, Van Bergeijk et al. (2019b) derived the velocity equation based on the assumption that the overtopping duration is constant for all cross-sectional locations. Therefore, for all locations $T_{ovt.,i} = T_{ovt.,I,@\,x=0}$.

According to Hoffmans et al. (2009) the turbulence coefficient can be calculated as:

$$\omega = 1.5 + 5r_0 \quad \text{(Eq. 31)}$$

Where:

r_0: Relative turbulence intensity [-]

Hoffmans (2012) gives the following equations for the relative turbulence intensity on horizontal surfaces and on the slope:

r_0 on horizontal surfaces
$$r_0 = 0.85\sqrt{f} \quad \text{(Eq. 32a)}$$

r_0 on a slope
$$r_0 = \sqrt{\frac{gq \sin\phi}{U_{max}^3}} \quad \text{(Eq. 32b)}$$

Following the approach of Hoffmans et al. (2009), Valk (2009) expressed the depth-dependent soil erosion parameter in terms of the depth-dependent overall strength parameter:

$$E_{soil}(d) = \frac{\alpha_{soil}}{C_E(d)} \quad \text{(Eq. 33)}$$

$$C_E(d) = \alpha_E \frac{g^2 d_a}{\nu U_c^2} \quad \text{(Eq. 34)}$$

Where:

$C_E(d)$:	Depth-dependent overall strength parameter	[$m^{-1}s^{-1}$]
d_a:	Diameter of the detaching aggregates (= 0.004 (Mirtskhoulava, 1991))	[m]
U_c:	Critical flow velocity	[m/s]
α_E:	Coefficient (= 10^{-10} (Hoffmans et al., 2009))	[-]
α_{soil}:	Coefficient (= 1 (Valk, 2009))	[m^2]
ν:	Kinematic viscosity (= 10^{-6} (Hoffmans, 2009))	[m^2/s]

The definition for d_a originates from Mirtskhoulava (1991) who looked at cohesive soils (such as the clay at the Afsluitdijk) and assumed that the aggregates are spherical. A diameter of d_a = 0.004 m is suggested, which is also used by Hoffmans et al. (2009). Furthermore, a critical flow velocity of U_c = 6.5 m/s is used in the calculation of C_E based on the range $5 \leq U_c \leq 8$ m/s that is given by Van der Meer and Van Hoven (2014) for the Afsluitdijk. This is the same critical flow that is used in the COM approach (Section 3.3.1).

The definition for the critical depth-dependent shear stress $\tau_c(d)$ was derived by Valk (2009) based on the turf-element model (Hoffmans et al., 2009; Hoffmans, 2012) and indicates the strength of the cover layer. This critical shear stress is the sum of the cover layer strength originating from the weight of the soil (left term in Eq. 35), the grass root tensile stress (left term in Eq. 36) and the cohesion of the clay (right term in Eq. 36).

$$\tau_c(d) = \alpha_\tau\left((\rho_s - \rho_w)g d_a + \tau_{total}(d)\right) \quad \text{(Eq. 35)}$$

$$\tau_{total}(d) = 0.7 t_r * RAR(d) + f\left(\tau_{clay,0}(1 + \alpha_{cs} * d)\right) \quad \text{(Eq. 36)}$$

Where:

d:	Erosion depth (due to previously overtopping waves that caused erosion)	[m]
f:	Clay inhomogeneousity factor (= 0.21 (Valk, 2009))	[-]
$RAR(d)$:	Depth-dependent root area ratio	[-]
t_r:	Root tensile strength (= $45*10^6$ (Valk, 2009))	[N/m^2]
α_{cs}:	Factor for clay cohesion increase over the depth (= 20 (Valk, 2009))	[m^{-1}]
α_τ:	Pressure fluctuation (= 1/18 (Hoffmans et al., 2009))	[-]
ρ_s:	Mass density of the soil (= 1850 (Van Etten, 2009))	[kg/m^3]
$\tau_{clay,0}$:	Cohesion of clay (= $15.78*10^3$ (Van Etten, 2009))	[N/m^2]
$\tau_{total}(d)$:	Depth-dependent total shear stress caused by the grass root tensile stress and clay cohesion	[N/m^2]

Van Etten (2009) presents the results from five consolidated undrained (CU) triaxial tests that have been carried out on the Afsluitdijk, which include values for the undrained cohesion. Verruijt (2012) argues that the undrained cohesion can be considered as a representative cohesion parameter for the soil when the load that act on it only occurs for a short period of time. This is the case for overtopping waves, which cause a relatively short period of load on the dike cover layer. In this period, it can be assumed that little to no drainage occurs. Therefore, under this assumption the undrained cohesion values from Van Etten (2009) can be used, resulting in an estimated average value of $\tau_{clay,0}$ = 15.78*10^3 N/m^2.

Both Hoffmans et al. (2009) and Hoffmans (2012) use a value for the clay inhomogeneousity factor of f = 0.021. However, as the TM overestimated erosion rates, Valk (2009) adjusted this value to f = 0.21. Furthermore, both the root tensile strength value of t_r = 45*10^6 N/m^2 and the value for the factor for increase of clay cohesion over the depth α_{cs} = 20 m^{-1} were found by calibrating the overall strength parameter C_E to match known values.

The mass density of the soil of the Afsluitdijk can be found from data presented by Van Etten (2009). As these values range depending on location and depth, a representative average value is estimated to be ρ_s = 1850 kg/m^3. Furthermore, values for the root area ratio RAR at Dutch dike grassland, which indicates the ratio of a cross-sectional area that is occupied by grass roots, are given by Hoffmans (2012). However, these values are only valid "near the surface. Therefore, the following equation which is suggested by Valk (2009) and based on research of Sprangers (1999) is used:

$$RAR(d) = 7.46 * 10^{-4} * e^{-22.32d} \quad \text{(Eq. 37)}$$

Where:
d: Depth [m]

The VE are able to calculate the flow velocities for any cross-sectional location. This means that a certain horizontal accuracy Δx (i.e. the value of the spatial step of the VE-TM along the cross-section) needs to be specified. Because the WBI 2017 does not specify a minimum required size of the erosion hole, an arbitrary size of 10 cm is chosen (i.e. Δx = 0.1 meter).

In order to determine when the grass cover layer fails, the depth at which failure occurs should be known. According to the WBI 2017 the grass cover layer fails when an erosion depth of 20 centimeter is reached, i.e. $z_{m,sum,failure}$ = 0.20 meter ('t Hart et al., 2016). As shown in the methodology overview in Figure 7 the crest elevation is increased until the calculated erosion depth in the iteration is less than $z_{m,sum,failure}$. Using the geometrical characteristics of that iteration and the hydraulic conditions that were given as input, the critical average overtopping discharge can be calculated as described in Section 3.3.4.

3.4.2 Schematization of Cross-Sectional Design

The cross-sectional schematization for the VE-TM is the same as that for the COM approach, which is presented in Figure 10. However, the implications of some design choices are different for the VE-TM. When the crest elevation is increased, the inner slope is shifted and the crest width is kept constant. Because the VE-TM includes the effects of bottom roughness on the flow velocity, this means that the total resistance caused by this roughness on the crest is constant for all iterations. Furthermore, this approach causes the inner slope length to increase, which would also be the case in reality when the crest height is increased. A longer inner slope means that the total resistance on the flow caused by the bottom roughness increases, but also that the water can accelerate for a longer period of time. These effects should be kept in mind when analyzing the simulation results.

3.4.3 Studied Locations

To enable a good comparison between the VE-TM and the COM simulations results, the locations in the COM approach (Section 3.3.3) are also studied in the VE-TM approach. Furthermore, two extra locations are included so that all erodible parts of the cross-sectional are considered: the part of the crest between the transitions at the start and at the end of the crest (location A) as well as the part of the inner berm between the inner toe and the parallel road (location B). These are labeled with letters instead of numbers to distinguish the additional locations in the VE-TM approach from the locations that are used in both the COM and VE-TM approach. All locations that are studied in the VE-TM approach are presented in Table 4 and Figure 12.

Table 4: Overview of the studied locations along the cross-section in the VE-TM approach, see also Figure 12.

Location	Description
1	Transition from the outer slope to the crest
A	Crest
2	Transition from the crest to the inner slope
3	Inner slope
4	Inner toe; transition from the inner slope to the inner berm
B	Part of the inner berm between the inner toe and the parallel road
5	Transition from the inner berm grass to the asphalt of the parallel road
6	Transition from the asphalt of the parallel road to the inner berm grass

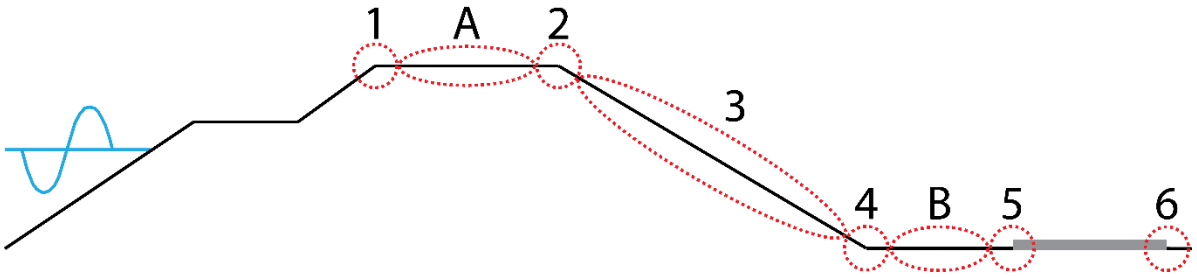

Figure 12: Schematized overview of the cross-section of the Afsluitdijk and the studied locations in the VE-TM approach, see also Table 4. Note that the figure is not to scale.

3.5 Comparison of Modelling Results

Because the COM and the VE-TM are two distinct modelling approaches that incorporate the aspects of the wave overtopping and grass erosion process in different ways, they are expected to result in different relationships between the significant wave height and the critical average overtopping discharges. The simulation results are compared to see in what ways these relationships vary, and to study what the underlying reasons could be for these differences. The results are studied for all simulated significant wave heights, but extra attention is paid to the critical discharges that are predicted for the wave heights that are larger than 3 meter. Furthermore, the simulation results of the cross-sectional location that is characterized by the lowest critical discharge are discussed in more detail, as this can be considered the "weakest" location. During a storm event, failure is expected to occur here first, making it an important point for the safety of the cross-section as a whole. It is checked whether this location is the same in the COM and the VE-TM approach, and to what extent the predicted H_{m0}–$q_{crit.}$ relationship differs.

3.6 Sensitivity Analyses

Sensitivity analyses are carried out for several parameters in the COM and the VE-TM, because these often rely on assumptions or coefficients that are not well established in the literature. The analyses can be used as a basis for future research, which can focus on improving the accuracy of the parameters that cause the largest variation in the calculated critical average overtopping discharges.

Furthermore, these sensitivity analyses results are useful if reinforcement of a cross-sectional location of the Afsluitdijk is required based on the simulation results from the previous sections. The effectiveness of the different possible reinforcements can be estimated based on the results of the sensitivity analyses, as for some parameters a relatively small change in parameter value may result in a large increase in critical discharge.

Sensitivity analyses are performed for the following parameters:

- Critical flow velocity U_c (COM & VE-TM).
- Flow velocity at the start of the crest $U_{i,crest}$ (COM & VE-TM).
- Factors for the load α_m, strength α_s and acceleration α_a (COM).
- Relative turbulence intensity r_0 (VE-TM).
- Overall strength parameter C_E (VE-TM).

The following paragraphs describe the sensitivity analysis approach for each of these parameters in further detail. The analyses are carried out for the "medium" combination of normative water level h and angle of wave attack θ (Section 3.2.1). Similar to the comparison of the COM and VE-TM modelling results in Section 3.5, special attention is paid to the weakest cross-sectional location.

3.6.1 Critical Flow Velocity (COM & VE-TM)

According to Van der Meer and Van Hoven (2014) the critical flow velocity of the grass cover on the Afsluitdijk lies in the range of 5 m/s ≤ U_c ≤ 8 m/s. Furthermore, analysis has shown that the topsoil of the grass cover layer on the Afsluitdijk is characterized better by a critical flow velocity of U_c = 6.5 m/s, while the lower part is characterized by U_c = 8 m/s. For this reason, it is interesting to vary the U_c value and see the effects on the critical average overtopping discharge. The results of the following scenarios are compared to each other:

- Default: U_c = 6.5 m/s in both the COM and the VE-TM approach.
- Scenario "default -12%":
  - $U_{c,COM}$ = 5.8 m/s for the whole cover layer.
  - $U_{c,VE-TM,upper}$ = 5 m/s for the upper 10 cm of the grass cover layer,
    $U_{c,VE-TM,lower}$ = 6.5 m/s for the lower 10 cm of the grass cover layer.
- Scenario "default +12%":
  - $U_{c,COM}$ = 7.3 m/s for the whole cover layer.
  - $U_{c,VE-TM,upper}$ = 6.5 m/s for the upper 10 cm of the grass cover layer
    $U_{c,VE-TM,lower}$ = 8 m/s for the lower 10 cm of the grass cover layer.

These scenarios are based on implementation of the two-layered behavior of the grass cover in the VE-TM approach. In both scenarios the critical flow velocity of the lower 10 cm of the cover layer is larger than the critical velocity in the upper 10 cm, based on the lower and upper limits of the U_c range given by Van der Meer and Van Hoven (2014). These values result in a change in average critical flow velocity of -12% and +12% (hence the scenario names). It should be noted that the division of the cover layer into two parts of 10 cm thickness is done arbitrarily, as Van der Meer and Van Hoven (2014) did not specify the exact depths for which the two critical flow velocities were valid. Furthermore, because depth-dependent values cannot be implemented in the COM, the value of U_c in this approach is varied for the cover layer as a whole by applying the same percentual changes.

3.6.2 Flow Velocity at the Start of the Crest (COM & VE-TM)

Both the COM and the VE-TM calculate the damage caused by overtopping waves based on the flow velocity at the start of the crest $U_{i,crest}$, which is determined using the 2% wave run-up height $R_{u2\%}$ and the probability of exceedance of each wave $P_{i,discr.}$ (Section 3.2.3). These calculations rely on several assumptions that introduce uncertainties in the calculated damage.

For example, the probability of exceedance per wave depends on the assumed development of water level and wave height during the storm event, the chosen number of discretization periods and the assumption that the incident waves follow a Rayleigh distribution. The influence factor for roughness γ_f, which is required for the run-up height, is calculated using an equation of Chen et al. (2019, subm.). Because this equation is only validated within certain R_c/H_{m0} and $\xi_{m-1,0}$ ranges, a value for γ_f needed to be assumed for situations which do not lie within these ranges. Furthermore, the equation for $U_{i,crest}$ includes a coefficient $c_{U,2\%}$. The value for this coefficient is not well established according to Van der Meer et al. (2015). Also, in Section 3.2.3 it is assumed that the value of this coefficient can be obtained by linear interpolating the range of values given by Van der Meer et al. (2018) for the characteristic outer slope angle.

To evaluate the impact of these assumptions on the calculated critical average overtopping discharge, the results of the scenarios below are compared to each other for both the COM and the VE-TM:

- Default: $U_{i,crest}$ according to Section 3.2.3
- Scenario "default -20%": a 20% decrease of $U_{i,crest}$.
- Scenario "default +20%": a 20% increase of $U_{i,crest}$.

The 20% variation in both scenarios is arbitrarily chosen, as it is difficult to estimate an accurate range of possible $U_{i,crest}$ values due to the many coefficients and variables. Variation in the $c_{U,2\%}$ coefficient only results in ±7% change due to its narrow range of values for conventional slope angles (Section 3.2.3). On the other hand, variations in the run-up height $R_{u2\%}$ have larger effects, which depend on the absolute value of $R_{u2\%}$ itself and on the value of the crest freeboard R_c. When using $R_{u2\%}$ = 3 m and R_c = 2 m as an example, an increase of 5% for each of the influence factor values in the run-up height calculation (γ_b, γ_f and γ_β, see Section 3.2.2) results in a 20% increase of flow velocity at the start of the crest. These are realistic values, and it is therefore reasonable to expect a 20% change in $U_{i,crest}$ values.

3.6.3 Load, Strength and Acceleration Factors (COM)

In the COM the effects of transitions are incorporated using influence factors for the load α_m, strength α_s and acceleration α_a. The values for the load factor given by Van der Meer and Van Hoven (2014) (see Appendix B) are estimated using theoretical models, while the strength factor is based on experiments. Furthermore, the acceleration factor is not a constant but depends on the distance from the crest and the flow velocity at the crest, although Van Hoven and Van der Meer (2017) argue that the flow velocity at the crest can be multiplied with a constant acceleration factor. These methods introduce uncertainties in the influence factors and therefore in the critical average overtopping discharges that are found using the COM.

The possible ranges of these factors are given by Hoffmans et al. (2018) as $1.0 \leq \alpha_m \leq 2.0$, $0.8 \leq \alpha_s \leq 1.0$ and $1.0 \leq \alpha_a \leq 1.6$. Influence factors with a value of 1.0 that are used in the COM simulations (see Table 3) indicate that for the corresponding location no additional load or reduction in strength is expected. It can therefore be assumed that these values do not change. However, the magnitude of factor values that are not 1.0 may change as a result of inaccuracies in the methods that are used to derive them. These values are therefore varied within the given ranges of Hoffmans et al. (2018) to

study the sensitivity of the COM towards the influence factors. The simulation results of the following scenarios are compared to each other:

- Default: α_m, α_a and α_s values according to Section 3.3.3.
- Scenario "low impact of overtopping waves": lower α_m and α_a values, higher α_s values.
- Scenario "high impact of overtopping waves": higher α_m and α_a values, lower α_s values.

Table 5 shown an overview of the influence factor values for these two scenarios, as well as the "default" values that are described in Section 3.3.3.

Table 5: Overview of the values that are used for the influence factors for the load α_m , strength α_s and acceleration α_a in the low and high impact scenario. The values that are changed compared to the "default" influence factor values are underlined.

Location	Location description	Low			Default (Section 3.3.3)			High		
		α_m	α_s	α_a	α_m	α_s	α_a	α_m	α_s	α_a
1	Transition from the hard cover material on the outer slope to the grass cover on the crest	1.0	*1.0*	1.0	1.0	0.9	1.0	1.0	*0.8*	1.0
2	Transition from the crest to the inner slope	1.0	1.0	1.0	1.0	1.0	1.0	1.0	1.0	1.0
3	Inner slope	1.0	1.0	*1.2*	1.0	1.0	1.4	1.0	1.0	*1.6*
4	Inner toe; transition from the inner slope to the inner berm	*1.0*	1.0	*1.2*	1.2	1.0	1.4	*1.4*	1.0	*1.6*
5	Transition from the inner berm grass to the asphalt of the parallel road	1.0	*1.0*	*1.0*	1.0	0.9	1.2	1.0	*0.8*	*1.4*
6	Transition from the asphalt of the parallel road to the inner berm grass	*1.5*	*1.0*	1.0	1.7	0.9	1.0	*1.9*	*0.8*	1.0

3.6.4 Relative Turbulence Intensity (VE-TM)

The relative turbulence intensity is implemented in the VE-TM equations based on the equations given by Hoffmans (2012), which are presented in Section 3.4.1. Van Bergeijk et al. (2019a, subm.) state that the intensity of the turbulence has a large influence on the modelled erosion depth, which makes it an interesting parameter to study in the sensitivity analysis.

Valk (2009) uses a constant value of r_0 = 0.20 for the transition from the inner slope to the inner berm. However, it is stated that this value is applicable for the whole inner slope of a dike and that r_0 = 0.15 can be used for horizontal surfaces. Bomers et al. (2018) used relative turbulence intensities of r_0 = 0.10 for the inner slope and r_0 = 0.17 for the crest, which origin from measurements during field experiments at a river dike. No value is given for the inner berm, but because the water at both the start of the crest and at the start of the inner berm is highly turbulent (Yuan et al., 2014; Van der Meer et al., 2018) it can be assumed that a value of r_0 = 0.17 also applies to the inner berm. Using this information, the results of the following scenarios are carried out to study the sensitivity of the VE-TM towards the relative turbulence intensities:

- Default: $r_{0,slope}$ and $r_{0,hor.}$ based on equations of Hoffmans (2012).
- Scenario Valk (2009): $r_{0,slope}$ = 0.20 (inner slope), $r_{0,hor.}$ = 0.15 (crest and inner berm).
- Scenario Bomers et al. (2018): $r_{0,slope}$ = 0.10 (inner slope), $r_{0,hor.}$ = 0.17 (crest and inner berm).

3.6.5 Overall Strength Parameter (VE-TM)

The overall strength parameter C_E is a parameter in the VE-TM that is initially calculated using the critical flow velocity U_c (Section 3.4.1). However, the values for the critical flow velocity are uncertain, so the used overall strength parameter values are uncertain as well. Whether the VE-TM simulation results are sensitive towards changes in this parameter can be studied by carrying out simulations with varying C_E values. It is possible to implement this parameter as a constant using values found in literature. Verheij et al. (1995) and Hoffmans et al. (2009) present similar C_E values for grass layers, as can be seen in Table 6. The grass cover layer on the Afsluitdijk was classified as "good" according to Bakker et al. (2009) based on the classification prescribed in the *Voorschrift Toetsen op Veiligheid Primaire Waterkeringen 2006* (VTV 2006). As this classification is also used for the data given by Hoffmans et al. (2009), their C_E values are considered for the sensitivity analysis. The simulation results of the following scenarios are compared to each other:

- Default: calculation of C_E based on U_c following Valk (2009). $C_E = 0.009 * 10^{-4}\ m^{-1}s^{-1}$ for U_c = 6.5 m/s.
- Good: $C_E = 0.016 * 10^{-4}\ m^{-1}s^{-1}$ (VTV 2006 grass type "good") for the complete grass cover layer. A 78% increase compared to the default C_E value.
- Average: $C_E = 0.022 * 10^{-4}\ m^{-1}s^{-1}$ (VTV 2006 grass type "average") for the complete grass cover layer. A 144% increase compared to the default C_E value.
- Combined (a 111% increase compared to the default C_E value):
  - $C_{E,upper} = 0.022 * 10^{-4}\ m^{-1}s^{-1}$ (VTV 2006 grass type "average") for the upper 10 cm of the grass cover layer
  - $C_{E,lower} = 0.016 * 10^{-4}\ m^{-1}s^{-1}$ (VTV 2006 grass type "good") for the lower 10 cm of the grass cover layer.

The latter implementation of the C_E values, a combination of two grass types, is chosen because of the grass cover characteristics on the Afsluitdijk described by Van der Meer and Van Hoven (2014). According to their findings, the lower part of the cover layer is characterized by a higher critical flow velocity than the upper part. This can be simulated by using two different C_E values for the cover layer. It should be noted that the depth of 10 cm at which the grass type changes is chosen arbitrarily.

Table 6: Overall strength parameter C_E values for different categories of grass (Verheij et al., 1995; Hoffmans et al., 2009).

Verheij et al. (1995)		**Hoffmans et al. (2009)**	
Grass type	**C_E [$m^{-1}s^{-1}$]**	**Grass type (VTV 2006)**	**C_E [$m^{-1}s^{-1}$]**
Good	$0.01 * 10^{-4}$	Good	$0.016 * 10^{-4}$
Average	$0.02 * 10^{-4}$	Average	$0.022 * 10^{-4}$
Poor	$0.03 * 10^{-4}$	Poor	$0.033 * 10^{-4}$
Very poor	$< 0.5 * 10^{-4}$	Very poor	$0.062 * 10^{-4}$

4. RESULTS

In this chapter the results are presented that follow from the methodology, as described in the previous chapter. First, the results from the COM and VE-TM simulations are presented individually. After this, the results of both modelling approaches are compared, and sensitivity analyses are carried out.

4.1 COM

Figure 13 shows the relationships between the critical average overtopping discharge $q_{crit.}$ and the significant wave height H_{m0} that are calculated with the COM for the studied cross-sectional locations (Section 3.3.3). These relationships are found for the low, medium and high conditions of normative water level h and angle of wave attack θ (Section 3.2.1).

For all significant wave heights and all three $h-\theta$ combinations the order of the cross-sectional locations in terms of critical average overtopping discharge is the same. The inner toe (location 4) is the weakest location, with a minimum value of $q_{crit.}$ = 3.4 L/s/m for H_{m0} = 4.02 m and a low h–θ combination. Therefore, it is likely that this location would fail first as a result of grass erosion caused by the overtopping waves. Other weak spots are, in order of increasing critical average overtopping discharge, the inner slope (location 3) and the transitions from asphalt to grass (location 6) and grass to asphalt (location 5). Furthermore, the simulation results show that locations 1 and 2 on the crest are able to withstand significantly higher average overtopping discharges, which are a factor 4 – 8 larger than the values for the inner toe. The maximum critical average overtopping discharge that is predicted from the simulations is $q_{crit.}$ = 103.8 L/s/m for H_{m0} = 1.92 m and a high h–θ combination

The general behavior of all curves in Figure 13 can be described as an increasing critical average overtopping discharge for a decreasing significant wave height. This effect is larger for the locations that are able to withstand higher discharges, such as the locations on the crest, than for locations with lower critical discharges. Figure 14 shows this in more detail for significant wave heights above 2.98 m. Here, the changes in critical discharges relative to the $q_{crit.}$ value at H_{m0} = 4.02 m are shown. Besides showing the lowest absolute $q_{crit.}$ values in Figure 13, location 4 is also characterized by the lowest relative increase in $q_{crit.}$ for a decreasing H_{m0}. On the other hand, location 2 shows a significantly larger relative increase in $q_{crit.}$ for a decreasing H_{m0}, while also having the highest absolute $q_{crit.}$ values in Figure 13. Thus, the weaker cross-sectional locations are less sensitive towards changes in wave height than the stronger locations.

The simulation results show that the $q_{crit.}$ values are largest for the high h–θ combination and lowest for the low h–θ combination, which is especially noticeable when looking at the lower H_{m0} values of locations 1 and 2. This is counterintuitive as one would initially expect the allowable overtopping discharge to decrease for increasing hydraulic conditions. However, that is only the case for a static dike design. The COM approach uses a dynamic dike design because the critical discharges, i.e. the tipping point values for failure of the grass cover, are found by changing the crest height. For a high water level the crest needs to be higher in order to find the same amount of grass cover damage as in a situation with a low water level. As a consequence, several characteristics of the outer dike design are altered, which eventually leads to different overtopping discharges. This is discussed in further detail in Section 5.5.1.

Notable anomalies in Figure 13 are the $q_{crit.}$ values of locations 1 and 2 for H_{m0} = 1.92 m in the simulation with the low h–θ conditions. Here, the two curves show an exception to the general trend by abruptly decreasing to one common $q_{crit.}$ value. Analysis of the intermediate simulations results showed that this can be attributed to a model limitation, which is further discussed in Section 5.2.

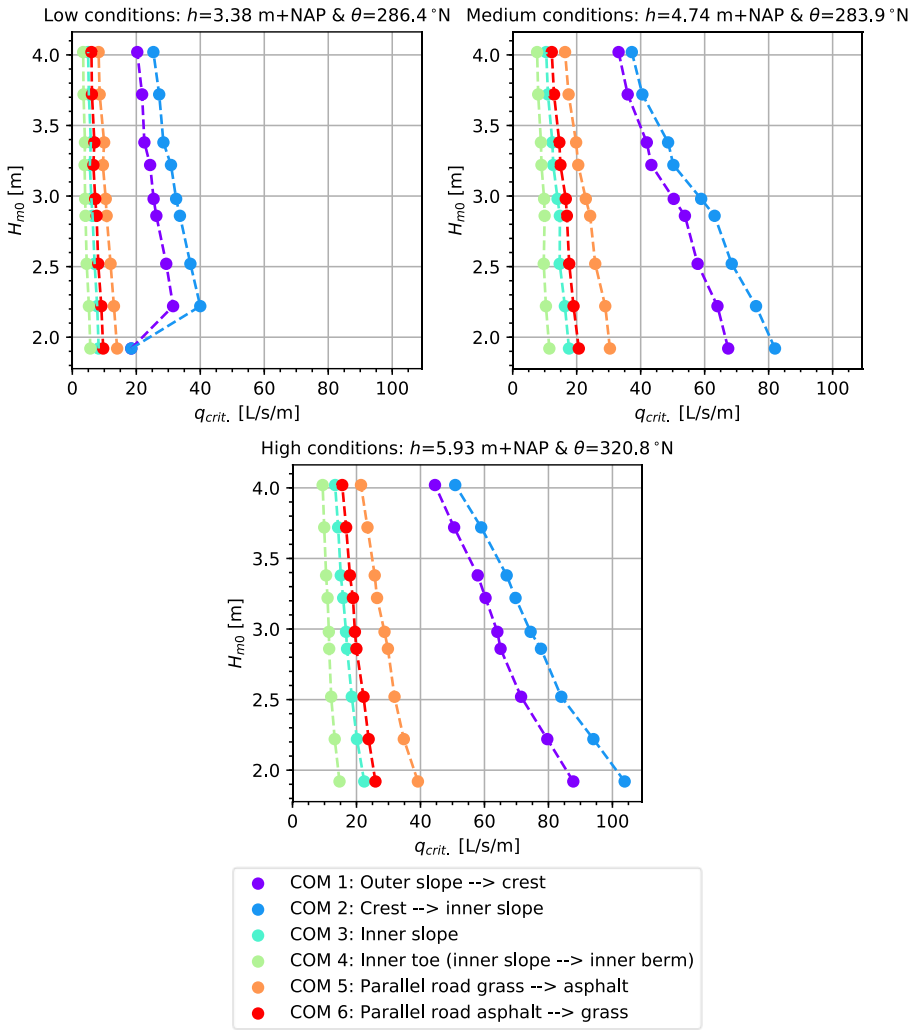

Figure 13: COM simulation results showing the relationship between the critical average overtopping discharge $q_{crit.}$ and the significant wave height H_{m0} using a critical flow velocity U_c = 6.5 m/s and low, medium and high conditions of normative water level h and angle of wave attack θ.

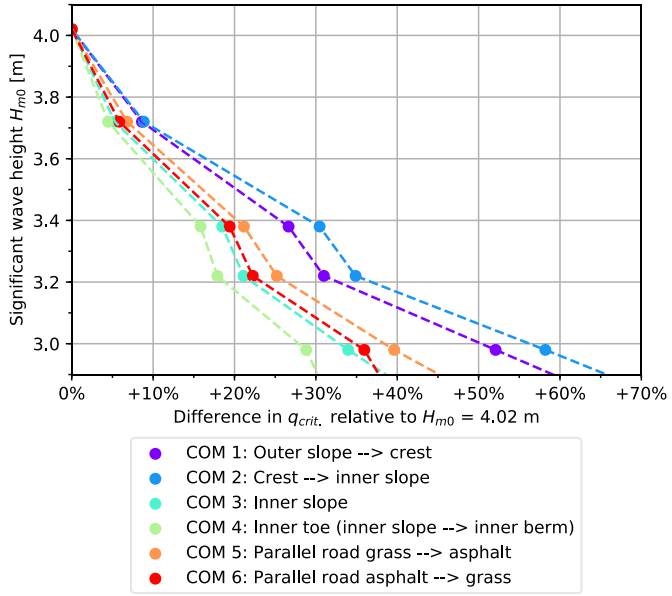

Figure 14: Differences in critical average overtopping discharge $q_{crit.}$ for significant wave heights H_{m0} ≥ 2.98 m, relative to the $q_{crit.}$ value at H_{m0} = 4.02 m. The results are obtained with the COM modelling approach using a critical flow velocity U_c = 6.5 m/s and medium h–θ conditions.

4.2 VE-TM

The relationships between the critical average overtopping discharge $q_{crit.}$ and the significant wave height H_{m0} that are predicted with the VE-TM modelling approach for the studied locations (Section 3.4.3) are presented in Figure 15. These relationships are found for the low, medium and high conditions of normative water level h and angle of wave attack θ (Section 3.2.1). Note that the curves of the locations on the crest partly overlap each other. Furthermore, the curves of locations 1 up to 6 are given the same color as in Section 4.1 for easy comparison. The additional locations A and B, which are only considered in the VE-TM modelling approach, are given distinct colors.

The simulation results show an increasing critical average overtopping discharge for a decreasing significant wave height. For all three h–θ combinations and all significant wave heights the inner toe (location 4) is the weakest cross-sectional location. In order of increasing critical average overtopping discharge, the inner toe is followed by the adjacent sections on the inner slope (location 3) and the inner berm (location B), the transitions at the parallel road (locations 5 and 6) and lastly locations 1, A and 2 on the crest. The critical discharges of the locations on the crest are approximately a factor 2.5 – 7.7 larger than those of the inner toe, with an overall maximum critical discharge of $q_{crit.}$ = 77.2 L/s/m at the transition from the crest to the inner slope for H_{m0} = 1.92 m and high h–θ conditions. Furthermore, for increasing h–θ conditions the critical discharges of all locations increase. For example, the overall lowest critical discharge is $q_{crit.}$ = 1.4 L/s/m at the inner toe for H_{m0} = 4.02 m and low conditions, while the same location and wave height result in $q_{crit.}$ = 3.7 L/s/m for high conditions. This is discussed in further detail in Section 5.5.1.

Figure 16 shows the differences in critical discharges for significant wave heights above 2.98 m relative to the $q_{crit.}$ value at H_{m0} = 4.02 m. Note that the curves of locations 1 and 2 overlap each other, as well as the curves of locations 5 and 6. The three locations on the crest (1, A and 2) show the lowest increase in $q_{crit.}$ for a decreasing H_{m0}. In other words: these locations are least sensitive towards a changing significant wave height. On the other hand, the two locations at the parallel road (5 and 6) show the largest increase. A small change in significant wave height therefore results in a relatively large change in critical discharge for these locations.

Lastly, the graph of the low h–θ conditions in Figure 15 shows a sudden decrease in critical discharges for locations 1, A, 2, 5 and 6 at H_{m0} = 2.98 m. This can be attributed to a model limitation, which is further discussed in Section 5.2.

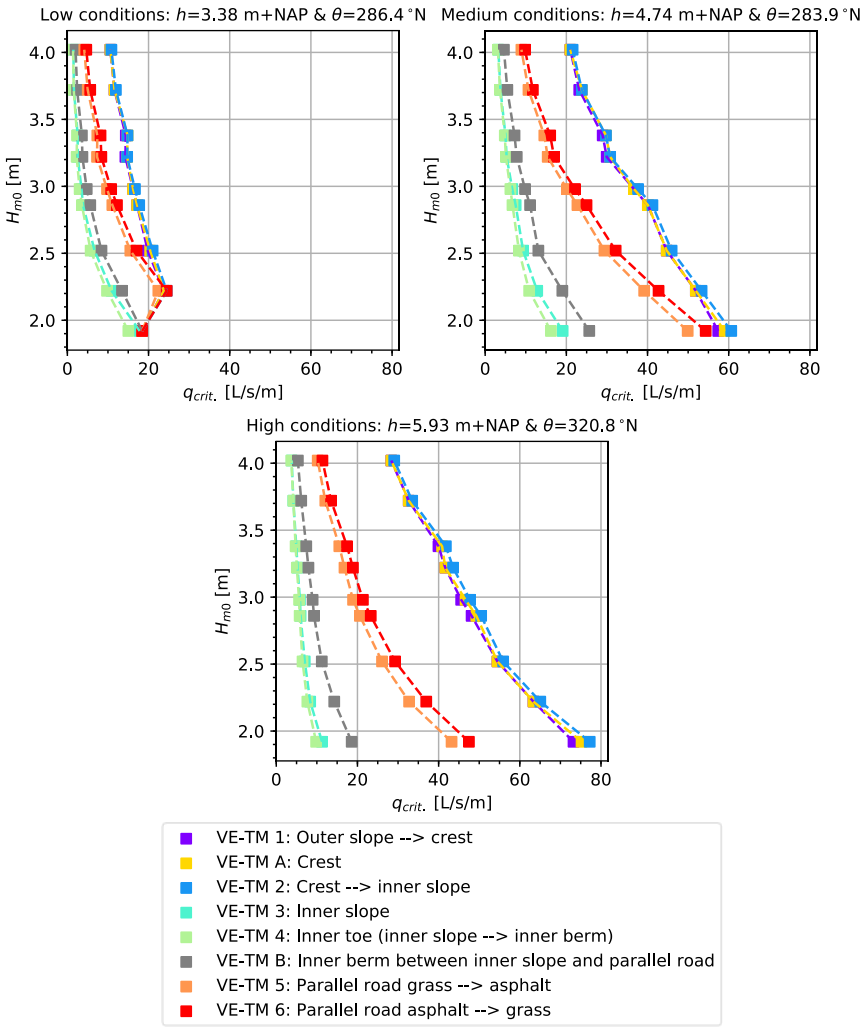

Figure 15: VE-TM simulation results showing the relationship between the critical average overtopping discharge $q_{crit.}$ and the significant wave height H_{m0} using a critical flow velocity U_c = 6.5 m/s and low, medium and high conditions of normative water level h and angle of wave attack θ.

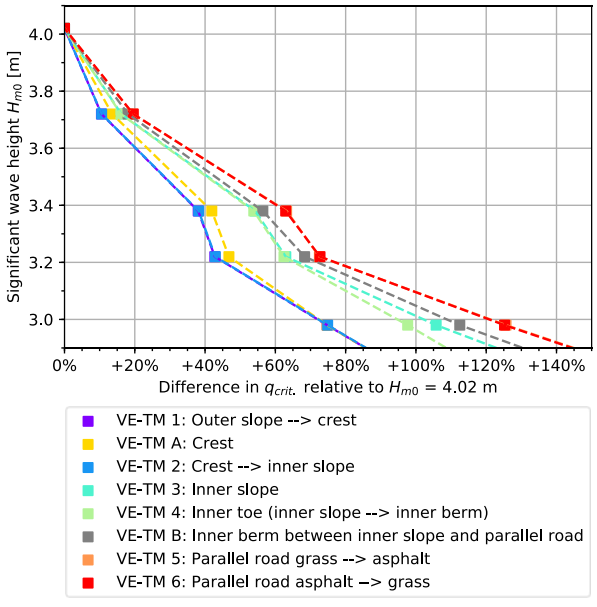

Figure 16: Differences in critical average overtopping discharge $q_{crit.}$ for significant wave heights H_{m0} ≥ 2.98 m, relative to the $q_{crit.}$ value at H_{m0} = 4.02 m. The results are obtained with the VE-TM modelling approach using a critical flow velocity U_c = 6.5 m/s and medium h–θ conditions.

4.3 Comparison COM & VE-TM

In Figure 17 the simulation results of the COM and VE-TM approaches for significant wave heights $H_{m0} \geq 2.98$ m are presented next to each other for easy comparison. These results are obtained using medium conditions of normative water level h and angle of wave attack θ (Section 3.2.1). The simulation results for all other significant wave heights and h–θ conditions can be found in Section 4.1 and Section 4.2. Note that VE-TM locations A and B are omitted in Figure 17 as these are not present in the COM approach. Furthermore, it should be noted that the curves of locations 3 and 4 in the graph with the VE-TM simulation results largely overlap each other.

Figure 17 shows that the COM generally predicts larger critical average overtopping discharges than the VE-TM for $H_{m0} \geq 2.98$ m. Furthermore, both approaches result in a similar order of locations based on the critical average overtopping discharges; the inner toe (location 4) is the weakest location while the transition from the crest to the inner slope (location 2) can withstand the highest overtopping discharges. However, the transitions at the parallel road (locations 5 and 6) are exceptions to this. The COM predicts that location 5 can withstand higher overtopping discharges than location 6, while the VE-TM predicts this the other way around. This is discussed in further detail in Section 5.5.3.

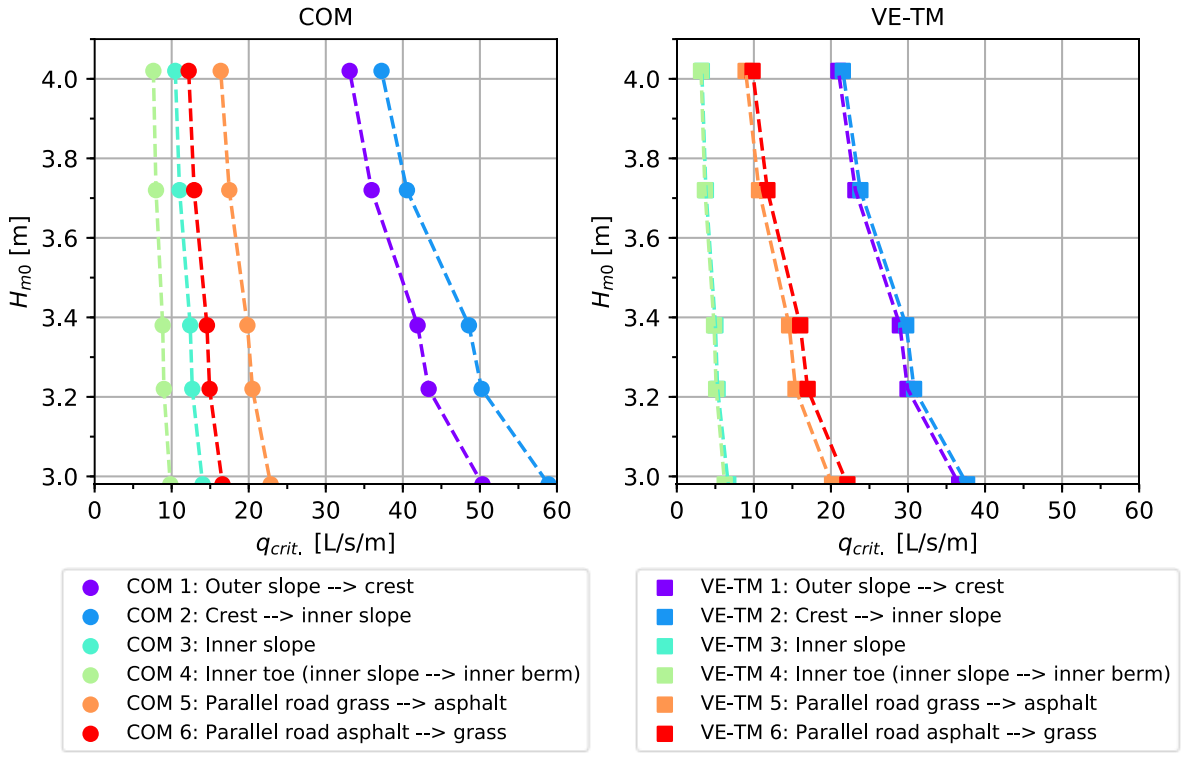

Figure 17: COM (left) and VE-TM simulation results (right) showing the relationship between the critical average overtopping discharge $q_{crit.}$ and the significant wave height H_{m0} for $H_{m0} \geq 2.98$ m. The results are obtained using critical flow velocities U_c = 6.5 m/s and medium h–θ conditions.

Figure 13 and Figure 15 show that for relatively low wave heights the VE-TM curves of locations 3 up to 6 (i.e. all locations that are not located on the crest) show higher critical discharges than in the COM approach, while this does not occur for locations 1 and 2. This is illustrated in more detail in Figure 18, which shows the critical discharges for locations 2, 4 and 6 for all significant wave heights. Note that the other locations are not include as this would decrease the readability of the figure. The COM and VE-TM curves of locations 4 and 6 cross each other, while those of location 2 appear to develop similarly. This is supported by Figure 19, which shows the differences of the predicted critical discharges for all simulated wave heights relative to the $q_{crit.}$ value at H_{m0} = 4.02. These curves show that, especially for higher wave heights, the critical discharges in the COM and the VE-TM for locations

on the crest develop similarly. For the other locations the VE-TM predicts a larger increase in critical discharge for a decreasing wave height than the COM. In other words: the effects of a changing wave height at these locations are larger in the VE-TM than in the COM. This can be attributed to the influence of the inner slope on the hydraulic load at these locations and is further elaborated in Section 5.5.2.

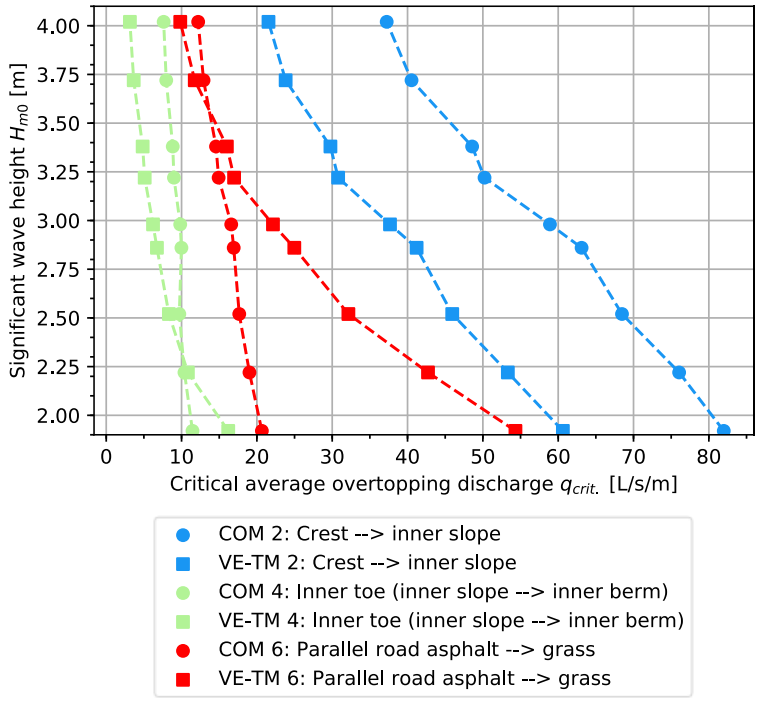

Figure 18: COM and VE-TM simulation results showing the relationship between the critical average overtopping discharge $q_{crit.}$ and the significant wave height H_{m0}. The results are obtained using critical flow velocities U_c = 6.5 m/s and medium h– θ conditions.

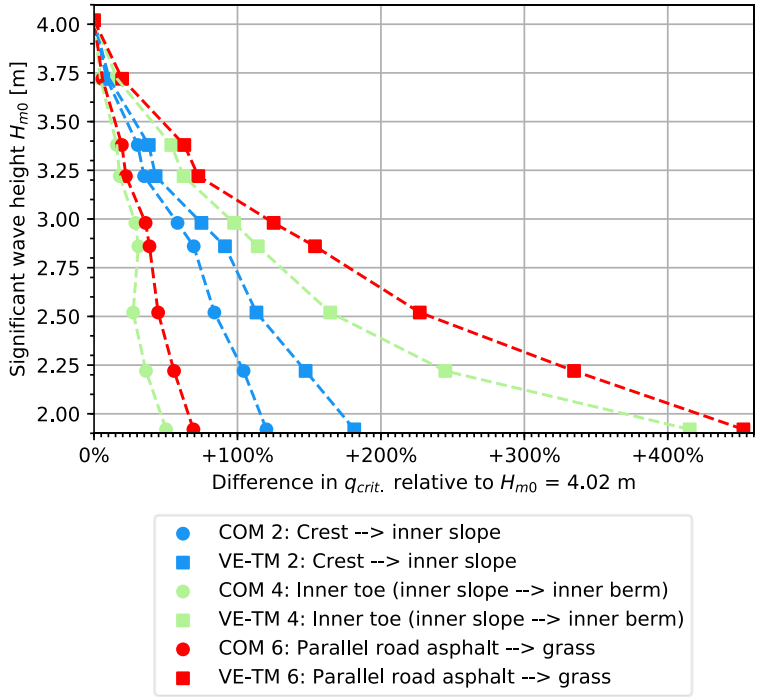

Figure 19: Differences in critical average overtopping discharge $q_{crit.}$ for locations 2, 4 and 6 for all simulated significant wave heights H_{m0}, relative to the $q_{crit.}$ value at H_{m0} = 4.02 m. The results are obtained with the COM and VE-TM modelling approach using critical flow velocities U_c = 6.5 m/s and medium h–θ conditions.

4.4 Sensitivity Analyses

In the sections below the results of varying several parameters in the COM and the VE-TM are presented. Simulations with modified values were carried out for all cross-sectional locations. These results can be found in Appendix C due to their size but are still discussed in this chapter. Furthermore, the simulation results at the inner toe (location 4) are given in more detail. Because both the COM and the VE-TM predicted that this is the location with the lowest critical average overtopping discharge, it is an important location to study in order to assess the safety of the Afsluitdijk.

4.4.1 Critical Flow Velocity (COM & VE-TM)

The simulation results for different critical flow velocities for both the COM and the VE-TM approaches are presented as Figure 34 and Figure 35, respectively, in Appendix C for all locations. In the default scenario the critical flow velocity is U_c = 6.5 m/s in both models. For the "default -12%" and "default +12%" scenarios the (depth-averaged) critical flow velocity for the cover layer is changed -12% and +12% respectively, as described in Section 3.6.1.

Table 7 shows the changes in critical discharge $\Delta q_{crit.}$ in the -12% and +12% scenarios relative to the default scenario at the inner toe (location 4) for both the COM and the VE-TM. It can be concluded that the COM is more sensitive towards changes in the critical flow velocity than the VE-TM as the changes relative to the default scenario are generally larger in the COM approach, especially in the +12% scenario. Furthermore, for both scenarios the $\Delta q_{crit.}$ ranges are significantly larger for the COM than the VE-TM approach. This indicates that a different U_c value has a less consistent effect on the critical discharges in the COM compared to the VE-TM. This means that the changes in $q_{crit.}$ for a known change in U_c can be approximated relatively well in the VE-TM approach as the effects of the changing U_c are relatively constant for all wave heights, while the $q_{crit.}$ values in the COM show a larger variation. This is also visible in Figure 20, which shows the H_{m0}–$q_{crit.}$ relationships at the inner toe for the different scenarios. These curves show that a changing U_c affects the critical discharges in the COM more than the VE-TM, especially for lower wave heights.

Table 7: Changes in critical average overtopping discharge $\Delta q_{crit.}$ at the inner toe (location 4) for the scenarios with a decrease of -12% and increase of +12% in the critical flow velocity U_c, relative to the default scenario in which U_c = 6.5 m/s.

	COM	VE-TM
Default U_c -12%	-31.3% ≤ $\Delta q_{crit.}$ ≤ -17.7%	-29.3% ≤ $\Delta q_{crit.}$ ≤ -22.3%
Default U_c +12%	+24.9% ≤ $\Delta q_{crit.}$ ≤ +47.4%	+16.6% ≤ $\Delta q_{crit.}$ ≤ +21.7%

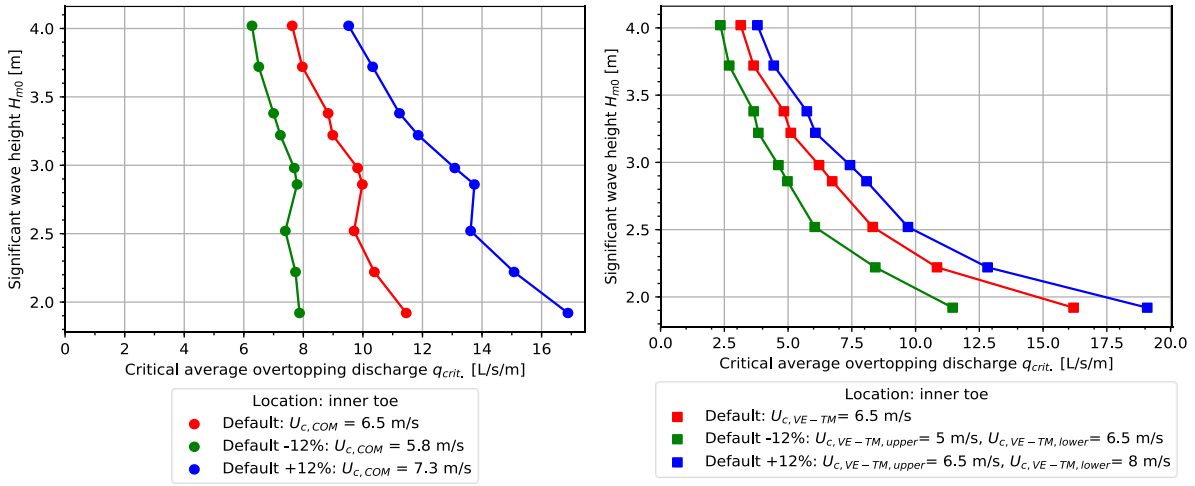

Figure 20: Simulation results showing the relationship between the critical average overtopping discharge $q_{crit.}$ and the significant wave height H_{m0} at the inner toe for the COM (left) and the VE-TM (right) using different critical flow velocities $U_{c,COM}$ and $U_{c,VE-TM}$. In the right graph, $U_{c,VE-TM,upper}$ and $U_{c,VE-TM,lower}$ indicate the critical flow velocity for the upper 10 cm and the lower 10 cm of the cover layer respectively. All simulations are carried out with medium h–θ conditions.

4.4.2 Flow Velocity at the Start of the Crest (COM & VE-TM)

The COM and VE-TM simulation results for a changing flow velocity at the start of the crest are presented as Figure 36 and Figure 37, respectively, in Appendix C. Note that the results of the COM show an unexpected decrease in critical average overtopping discharge for low wave heights for the low h–θ conditions, which is similar to the sudden decrease in critical discharge that is observed in the COM (Section 4.1) and the VE-TM (Section 4.2). This can be attributed to a model limitation and is further discussed in Section 5.2.

The graphs in Appendix C show that for both the COM and the VE-TM approach the scenario in which the $U_{i,crest}$ is decreased by 20% has a larger effect on the resulting critical discharges than an increase of 20%. This can also be observed in Figure 21, which shows the H_{m0}–$q_{crit.}$ relationships at the inner toe (location 4) for the different scenarios. Furthermore, the changes in critical discharge $\Delta q_{crit.}$ relative to the default scenario are presented for the inner toe in Table 8. This data shows that the changes in the critical discharge are significantly higher for the -20% scenario compared to the +20% scenario. In other words: overestimation of $U_{i,crest}$ has smaller effects on the calculated critical discharges than underestimation. Furthermore, the VE-TM approach shows larger $\Delta q_{crit.}$ ranges than the COM. This indicates that the VE-TM approach is more sensitive towards changes in the $U_{i,crest}$ values than the COM approach.

Table 8: Changes in critical average overtopping discharge $\Delta q_{crit.}$ at the inner toe (location 4) for the scenarios with a decrease of -20% and an increase of +20% in the flow velocity at the start of the crest $U_{i,crest}$, relative to the default scenario.

	COM	**VE-TM**
Default $U_{i,crest}$ -20%	+127.0% ≤ $\Delta q_{crit.}$ ≤ +196.5%	+28.6% ≤ $\Delta q_{crit.}$ ≤ +165.9%
Default $U_{i,crest}$ +20%	-55.5% ≤ $\Delta q_{crit.}$ ≤ -47.0%	-46.5% ≤ $\Delta q_{crit.}$ ≤ -17.6%

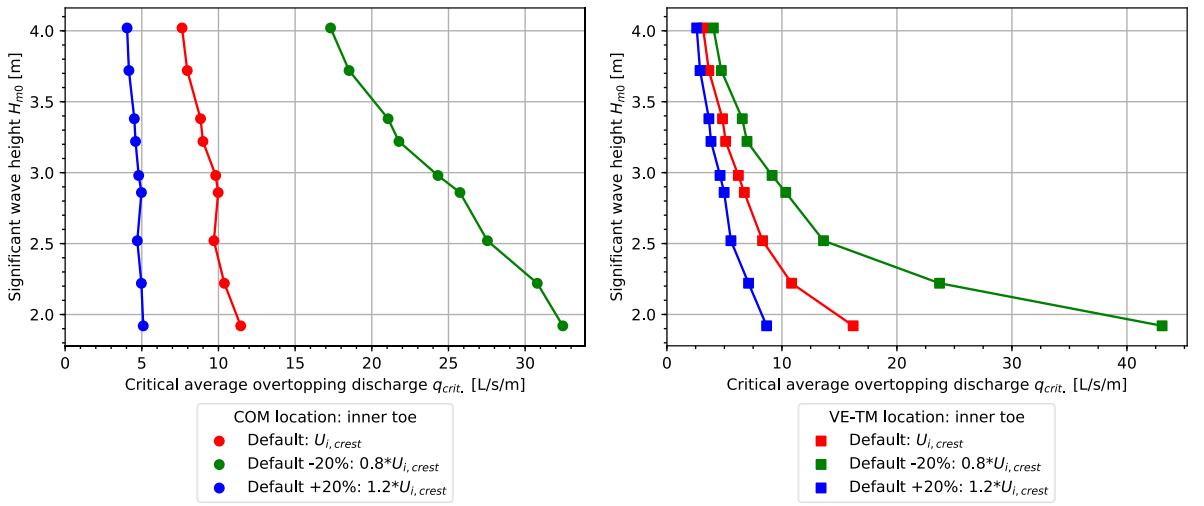

Figure 21: Simulation results showing the relationship between the critical average overtopping discharge $q_{crit.}$ and the significant wave height H_{m0} at the inner toe for the COM (left) and the VE-TM (right) using flow velocities at the start of the crest $U_{i,crest}$ as calculated with the equations in Section 3.2.3 (Default), a 20% decrease (Default -20%) and a 20% increase (Default +20%). All simulations are carried out using a critical flow velocity U_c= 6.5 m/s and medium h–θ conditions.

4.4.3 Load, Strength and Acceleration Factors (COM)

The COM simulation results for different combinations of load, strength and acceleration factor values α_m, α_s and α_a are presented as Figure 38 in Appendix C for all studied locations. Note that for the "low impact" combination of factor values the critical discharges of location 1 and 2 overlap each other, as well as the values for locations 3 and 4. This is logical when looking at the factor values for the low impact combination in Table 5, as these locations share the same factor values. Overlapping also occurs for locations 5 and 6 in the "high impact" combination, although the alpha-factors do not have the same values for these locations. However, the value that results from the product $\alpha_m * \alpha_a^2$, which is included in the part of the COM that describes the hydraulic load (Section 3.3.1), is approximately equal for the two locations. Because both locations also share the same α_s value, the resulting critical discharges are similar.

The results for the inner toe are presented in more detail in Figure 22, while Table 9 gives an overview of the changes in critical discharges $\Delta q_{crit.}$ for the low and high impact scenario (relative to the default scenario). The largest differences occur at the lower wave heights, indicating that the COM is more sensitive towards changes in the alpha-factors in these situations than for higher waves. Furthermore, the effects of the low impact scenario are significantly higher than those caused by the high impact scenario. Based on this it can be concluded that a small decrease in the severity of the alpha-factors can lead to a large increase in critical average overtopping discharges, while an increase in severity affects the critical discharges less.

Table 9: Changes in critical average overtopping discharge $\Delta q_{crit.}$ at the inner toe (location 4) for the scenarios with low impact and high impact alpha factors, relative to the default scenario.

Scenario	Changes in critical discharge relative to the default scenario
"Low impact" alpha-factors	$+146.8\% \leq \Delta q_{crit.} \leq +225.1\%$
"High impact" alpha-factors	$-61.7\% \leq \Delta q_{crit.} \leq -51.7\%$.

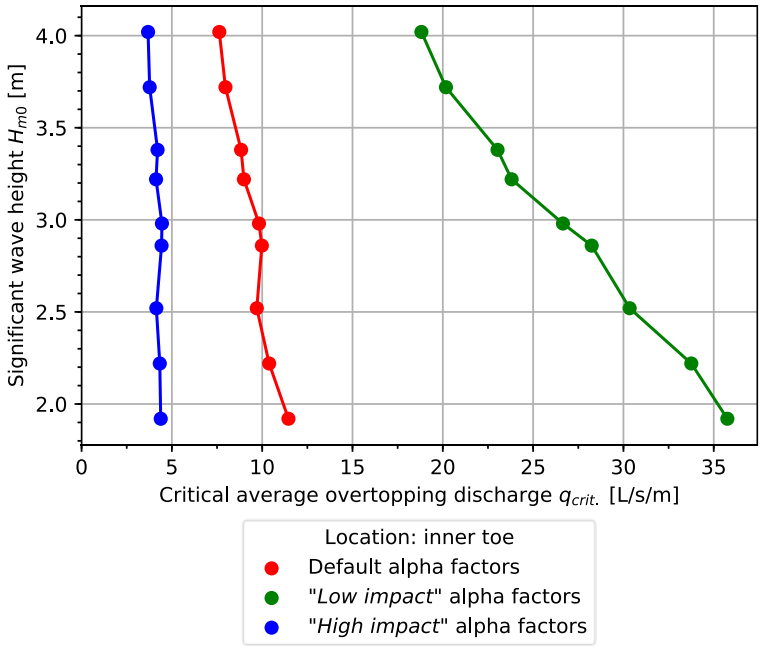

Figure 22: COM simulation results showing the relationship between the critical average overtopping discharge $q_{crit.}$ and the significant wave height H_{m0} at the inner toe for different combinations of load, strength and acceleration factor values α_m, α_s and α_a. All simulations are carried out using a critical flow velocity U_c = 6.5 m/s and medium h–θ conditions.

4.4.4 Relative Turbulence Intensity (VE-TM)

The VE-TM simulation results at all studied locations for a changing relative turbulence intensity r_0 are presented as Figure 39 in Appendix C. These graphs show that the simulations with the relative turbulence intensity values of Valk (2009) and Bomers et al. (2018) predict similar critical average overtopping discharges, which are 2 to 3 times smaller than those calculated using the equations of Hoffmans (2012). This indicates that, even though the values of Valk (2009) and Bomers et al. (2018) for the crest and inner berm $r_{0,hor.}$ and for the inner slope $r_{0,slope}$ are different, the average relative turbulence intensity $r_{0,avg}$ over the modelled cross-section as a whole are approximately equal for the two methods.

It is difficult to determine the exact $r_{0,avg}$ values for three methods, as each critical discharge corresponds to a different crest height and consequently in a different slope length. This changes the lengths of the sections where the $r_{0,hor.}$ and $r_{0,slope}$ values are applied, and results in difference average r_0 for each simulation. However, an average crest elevation of 7.67 m+NAP is found from the simulations results in Appendix C. From this it can be determined that, on average, approximately 80% of the modelled cross-section is horizontal (the crest and the inner berm) and 20% sloped (the inner slope). Furthermore, the equations of Hoffmans (2012) result in $r_{0,hor.} = 0.09$ and $0.08 \leq r_{0,slope} \leq 0.12$. Using this information, the following average relative turbulence intensities $r_{0,avg}$ are calculated:

- Hoffmans (2012): $r_{0,avg} = 0.09$ (default scenario).
- Valk (2009): $r_{0,avg} = 0.16$.
- Bomers et al. (2018): $r_{0,avg} = 0.16$.

As expected, the methods of Valk (2009) and Bomers et al. (2018) result in approximately equal average relative turbulence intensities (78% larger than the default $r_{0,avg}$ value), and therefore also in similar critical average overtopping discharges. Because of this, it is possible that the equations of Hoffmans (2012) underestimate the relative turbulence intensities.

However, it must be noted that the simulation results of the two methods in Appendix C still differ to a certain extent when looking at each cross-sectional locations as the $r_{0,avg}$ values are the average of all studied locations for all significant wave heights.

Figure 23 shows the simulation results for the inner toe, which illustrates the abovementioned conclusions more clearly. The critical discharges that are found with the methods of Valk (2009) and Bomers et al. (2018) are similar (Table 10), and their development for a changing significant wave height is almost identical. Thus, the choice between the constant relative turbulence intensities of these two methods only has a minimal effect on the calculated critical discharges. The main decision that therefore needs to be made when using the VE-TM is the implementation method for the relative turbulence intensity: as constant values from Valk (2009) and Bomers et al. (2018) or by calculating it using the equations of Hoffmans (2012).

Table 10: Changes in critical average overtopping discharge $\Delta q_{crit.}$ at the inner toe (location 4) for the scenarios with relative turbulence intensity values of Valk (2009) and Bomers et al. (2018), relative to the default scenario.

Scenario	Changes in critical discharge relative to the default scenario
Valk (2009) Default +78%	$-65.3\% \leq \Delta q_{crit.} \leq -40.5\%$
Bomers et al. (2018) Default +78%	$-71.5\% \leq \Delta q_{crit.} \leq -46.6\%$

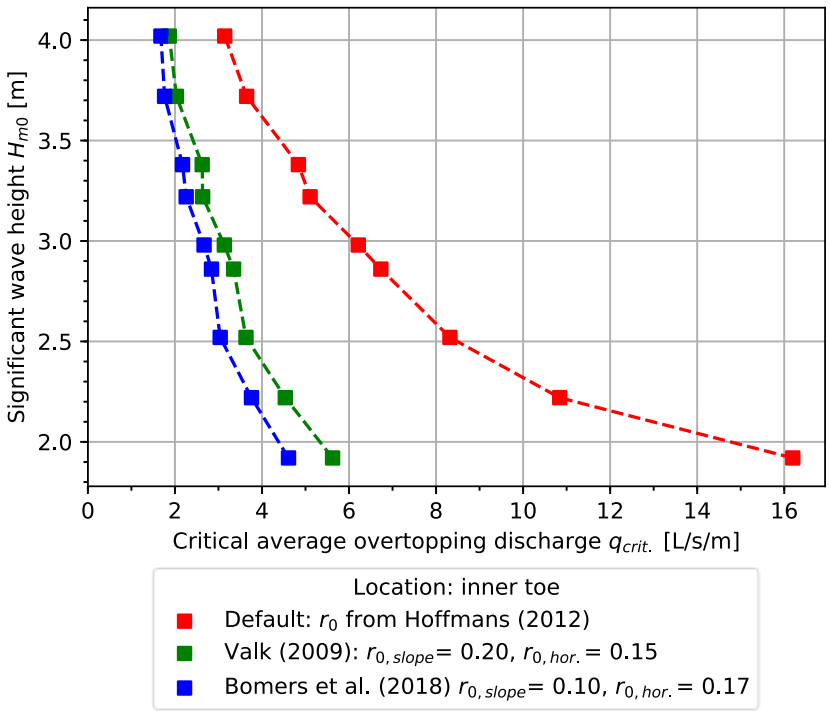

Figure 23: VE-TM simulation results showing the relationship between the critical average overtopping discharge $q_{crit.}$ and the significant wave height H_{m0} at the inner toe for different r_0 values using a critical flow velocity U_c = 6.5 m/s and medium h–θ conditions.

4.4.5 Overall Strength Parameter (VE-TM)

The simulation results for a changing overall strength parameter C_E of all studied locations are presented as Figure 40 in Appendix C. These graphs indicate that the three scenarios yield similar critical average overtopping discharges, especially for the higher wave heights, but that their values are lower than those of the default scenario. This is also the case for the inner toe (location 4), which is predicted as the weakest cross-sectional location in all scenarios. The H_{m0}–$q_{crit.}$ relationships at this location are presented in more detail in Figure 24 and show that the default scenario, in which the overall strength parameter is calculated using the critical flow velocity (Section 3.4.1), predicts significantly larger critical discharges than the three scenarios in which the overall strength parameter value is based on literature. This indicates that grass cover strength using the default method is higher than when using the literature value. Table 11 presents an overview of the changes in critical discharges $\Delta q_{crit.}$ for the three simulated scenarios, relative to the critical discharges of the default scenario. These values show that, compared to the results of the default scenario, the three different C_E values lead to similar changes in critical discharges. The main point of discussion regarding the implementation of the overall strength parameter in the VE-TM is therefore not necessarily what the exact C_E value should be based on literature, but rather which approach represents the strength of grass cover best: the literature values or calculation of C_E based on the critical flow velocity. For the Afsluitdijk, the most realistic approach is discussed in Section 5.6.

Table 11: Changes in critical average overtopping discharge $\Delta q_{crit.}$ at the inner toe (location 4) for the good, average and combined scenarios of the overall strength parameter C_E, relative to the default scenario.

Scenario	Changes in critical discharge relative to the default scenario
"Good" Default C_E +78%	-43.9% ≤ $\Delta q_{crit.}$ ≤ -40.0%
"Average" Default C_E +144%	-58.2% ≤ $\Delta q_{crit.}$ ≤ -52.2%
"Combined" Default C_E +111%	-52.3% ≤ $\Delta q_{crit.}$ ≤ -48.1%

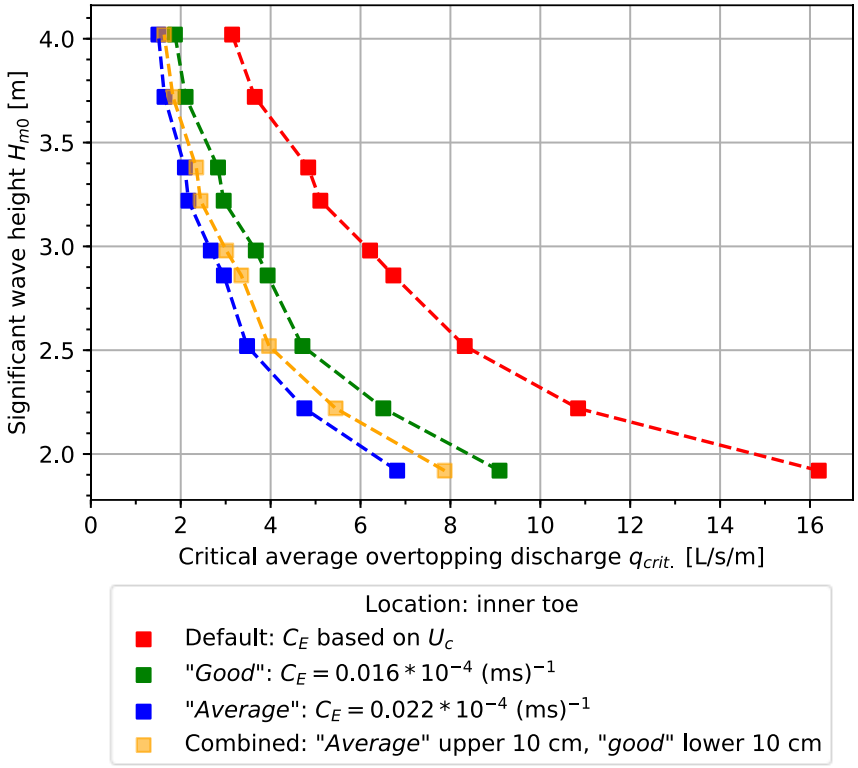

Figure 24: VE-TM simulation results showing the relationship between the critical average overtopping discharge $q_{crit.}$ and the significant wave height H_{m0} at the inner toe for different C_E values using a critical flow velocity U_c = 6.5 m/s and medium h–θ conditions.

5. DISCUSSION

5.1 HYDRAULIC BOUNDARY CONDITIONS

The simulation results from both the COM and the VE-TM are subject to several uncertainties that origin from determining the normative hydraulic characteristics in Table 2 and the development of these characteristics throughout a storm event (Section 3.2.1). First of all, Hydra-NL needs to extrapolate the values of the basic stochastic variables it uses, such as the wind and water level, for return periods larger than 20 000 years (Duits, 2017). For the Afsluitdijk this means that inaccuracies are introduced for significant wave heights larger than approximately 3.40 meter. Secondly, it is assumed that the schematization of the water level development throughout the storm event, described by Chbab and De Waal (2017) and Botterhuis et al. (2017), is correct. This schematization is based on measurements of storm conditions and is assumed to represent the majority of storms in the Wadden Sea accurately. However, storms may still deviate from these characteristics, especially as the timing of the tidal peak and the storm surge peak may not always be identical to the phase difference that is included. Thirdly, the development of the significant wave height throughout the storm is assumed to follow the development of the storm surge. This approach is used by Van Hoven (2015) but no argumentation is given regarding its correctness.

As mentioned in Section 3.2.1, Van Hoven and Van der Meer (2017) carry out calculations with the COM using a three-hour period of peak hydraulic conditions (i.e. the conditions stated in Table 2). When using this approach, it is assumed that the amount of grass cover erosion caused by the stationary peak conditions approximates the damage caused by an actual storm well (which has a longer duration and a build-up of hydraulic conditions towards the storm peak, followed by a decrease). In order to see to what extent the three-hour storm approach of Van Hoven and Van der Meer (2017) yields different results from the storm development approach (Section 3.2.1), simulations with the COM and the VE-TM are carried out for the three h–θ combinations.

The results at all studied cross-sectional locations using the three-hour storm approach are presented as Figure 41 (COM) and Figure 42 (VE-TM) in Appendix D. Furthermore, Figure 25 shows the COM and VE-TM simulation results for locations 2, 4 and 6 of both the three-hour storm approach and the storm development approach. It can be concluded that the COM simulation results of both storm approaches are similar to each other for all locations except locations 1 and 2 on the crest. Moreover, the smallest differences in predicted critical discharge occur for the situations with relatively low wave heights. The VE-TM simulations result in significantly larger differences, which are highest for the lower wave heights. At the inner toe (location 4) both approaches result in similar critical discharges for the higher wave heights, but for the other locations and different wave heights the differences are large. To conclude, for most cross-sectional locations the three-hour storm approach predicts similar H_{m0}–θ relationships as the storm development approach in the COM, while different relationships are predicted in the VE-TM. The three-hour storm approach consistently results in larger critical discharges, indicating that the total hydraulic load that is imposed by the storm event is lower than in the storm development approach. For design and safety assessment purposes it is therefore recommended to use the storm development approach in both the COM and the VE-TM, which results in more conservative critical average overtopping discharges. However, if the aim of the simulation is to get a rough estimate of the H_{m0}–θ relationships with the COM, one can decide to use the three-hour storm approach since this approach is easier to implement.

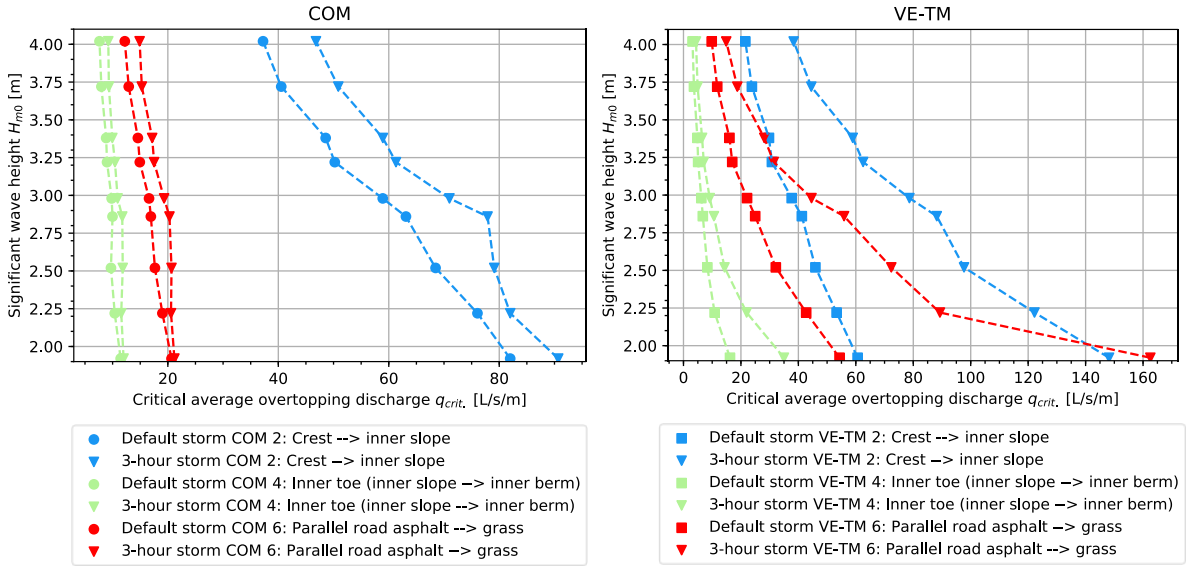

Figure 25: COM (left) and VE-TM simulation results (right) showing the relationship between the critical average overtopping discharge $q_{crit.}$ and the significant wave height H_{m0} at locations 2, 4 and 6 using the storm development approach (Section 3.2.1) and three-hour storm approach of Van Hoven and Van der Meer (2017). for low, medium and high conditions of normative water level h and angle of wave attack θ. All simulations are carried out using a critical flow velocity U_c = 6.5 m/s and medium h–θ conditions.

5.2 Modelling Approach

Simulations with the COM and VE-TM were carried out for three combinations of normative water level h and angle of wave attack θ. Figure 13, Figure 15 and Figure 36 (Appendix C) show that "low" conditions of h = 3.38 m+NAP and θ = 286.4 °N combined with a relatively low significant wave height of H_{m0} = 1.92 m result in a sudden decrease of critical average overtopping discharge for several studied locations. This does not match the general trend of the curves at higher wave heights or for different h and θ conditions, which shows a continuous increase of critical discharges for decreasing wave heights. A review of the intermediate simulation results shows that both models did not find any failure for these locations after the first iteration for the given combination of H_{m0}, h and θ. Therefore, the calculations are stopped and the critical discharge is calculated for a crest elevation that equals the outer berm elevation. As a result, the simulations yield one common (relatively low) critical discharge for these locations, which causes the unexpected decrease in the aforementioned figures. This is a model limitation, as the model is set-up in such a way that the crest elevation must always be above the outer berm elevation (Section 3.3.2), while the cover layer would be able to withstand a larger overtopping discharge. The correct critical average overtopping discharge would therefore be significantly higher than currently shown in the figures. Note that this limitation may also occur for significant wave heights larger than 1.92 m if, for example, the grass cover strength is increased or the hydraulic load at the studied locations is decreased. If these situations need to be simulated, a different modelling approach with a lower crest elevation in the first iteration should be considered.

Another limitation of both the COM and the VE-TM is that the effects of upstream erosion on the erosion rate at a certain cross-sectional location are not taken into account. For example, if an erosion hole is formed on the inner slope, the flow velocity and layer thickness of the overtopping water will be influenced due to local changes in slope angle and turbulence. Additionally, water from previous overtopping waves that is retained in the erosion hole can cause damping of the hydraulic load.

Lastly, both models assume a continuity of discharge. This means that infiltration of the overtopping water into the dike cover layer is not considered in the two modelling approaches. However, in reality

does occur (’t Hart et al., 2016), which decreases the overtopping discharge throughout the overtopping process. This causes the flow velocity and layer thickness to decrease, which in turn influences the amount of erosion that occurs. Infiltration of water into the dike may eventually lead to slipping of the cover layer, but since this is categorized as a different failure mechanism in the WBI 2017 (GABI) it is not considered in this study.

5.3 COM

In order to include transitions and the acceleration on the slope in the COM, the load, strength and acceleration factors α_m, α_s and α_a are included in the model. However, their values are not always well established, and it is therefore not always clear whether the resulting damage number for the studied locations is accurate. According to Van Hoven and Van der Meer (2017) the water quickly accelerates at the start of the inner slope, and after several meters it reaches a constant acceleration factor which is valid for the remaining part of the inner slope. This indicates that the found critical average overtopping discharges for the inner slope are not valid at the beginning of the slope; this part is likely described better by a higher critical discharge due to a lower acceleration factor. However, when considering the inner slope as a whole, the location on the slope with the lowest allowable overtopping discharge could be considered normative. Furthermore, the exact influence area of the acceleration factor is unknown. The acceleration factors presented in Table 3 are applied to the whole inner slope and to the transition from grass to asphalt. However, no information is given in the literature about the deceleration of the water after the inner toe transition. In the COM an acceleration factor of α_a = 1.2 was applied for the transition from grass to asphalt as it is expected that the flow velocity at this transition is still influence by the acceleration on the slope, but this value is an educated guess. It is possible that the water quickly decelerates after the inner toe and that an acceleration factor of α_a = 1.0 would be more suitable for the transition from grass to asphalt, but it could also be that the acceleration on the inner slope still influences the flow velocity at the transition from asphalt to grass or even farther on the inner berm.

A limitation of the COM is that it only includes the effects of roughness differences at transitions in the load factor α_m and not the effects of the roughness that the overtopping water experiences between the transitions. For example, when applying the load factor to a transition from grass to asphalt on the inner berm, the effects of the roughness from the grass between the inner toe and the grass to asphalt transition are not considered. It therefore does not matter for the COM simulation results whether the asphalt is located immediately after the inner toe or at the end of the inner berm. However, in reality the water at the transition at the end of the berm would have a lower flow velocity and a higher layer thickness compared to the transition close to the inner toe. It could therefore be argued that the COM needs to include an additional factor that accounts for these effects.

5.4 VE-TM

5.4.1 Spatial Considerations

There are several aspects regarding the implementation of the VE-TM that can affect the resulting critical discharges. Because the velocity equations depend on the cross-sectional location x, a choice needs to be made what the spatial step Δx should be. This is a trade-off between accuracy and computational time as a smaller step would result in more precise results, but also requires more computations. In Section 3.4.1 an arbitrary value of Δx = 0.1 m is chosen, while it could be argued that a smaller or larger value would be more suitable. One aspect on which this choice could be based is the expected size of erosion holes. According to Deltares (2015) failure occurs when the overtopping water creates an erosion hole that is deeper than 20 cm and is larger than 15 x 15 cm. Although it is not explicitly stated in the document, it appears as if this only applies to erosion holes that occur as a result of the overtopping water pulling out a grass sod at once, while the VE-TM simulates more gradual erosion. This could be a reason why the WBI 2017 does not define a specific size of the erosion

hole (’t Hart et al., 2016). Figure 26 shows the erosion profile for failure at the inner toe (location 4) for H_{m0} = 4.02 m. The curve is at its steepest at the inner slope, where it increases approximately 1.5 mm per spatial step of Δx = 0.1 m. Therefore, although a small spatial step is more accurate, a somewhat larger step will likely still yield realistic results. VE-TM simulations with a spatial step of Δx = 0.2 m confirm this. These simulation results are presented in Figure 27 next to the simulation results with the default value Δx = 0.1 m for easy comparison. Only small differences in critical discharges are observed, but overall the simulations predict approximately equal $H_{m0} - \theta$ relationships. The results of simulations in which larger spatial steps are used will differ more, but where the upper limit of this step size lies is open to debate.

Another aspect that influences the results is the choice of start and end points of the studied locations, which are shown in Figure 28. For example, there is no clear definition that states when the transition from grass to asphalt (location 5) starts. As the figure shows, its start is chosen immediately upstream of the asphalt, but one could argue that the influence of the transition is already noticeable further upstream. This would yield different critical discharges for the considered section and needs to be kept in mind when analyzing these results.

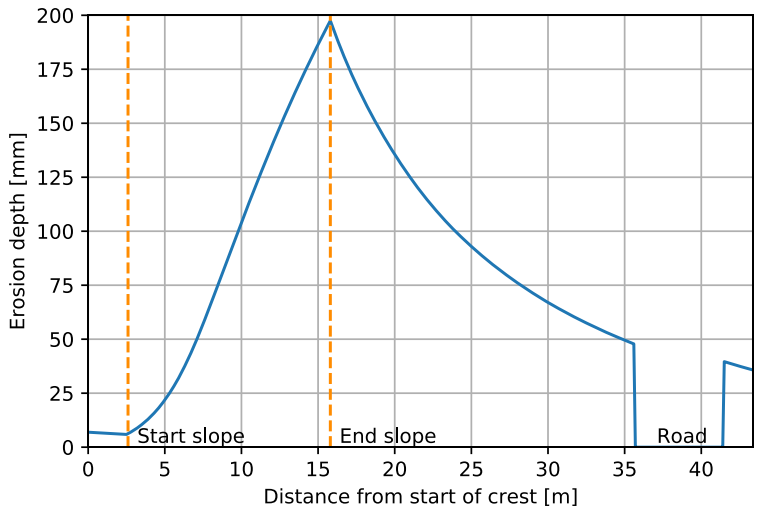

Figure 26: Erosion profile for the critical average overtopping discharge of the inner toe for H_{m0} = 4.02 m and medium h–θ conditions. The dashed orange lines indicate the start and end of the inner slope.

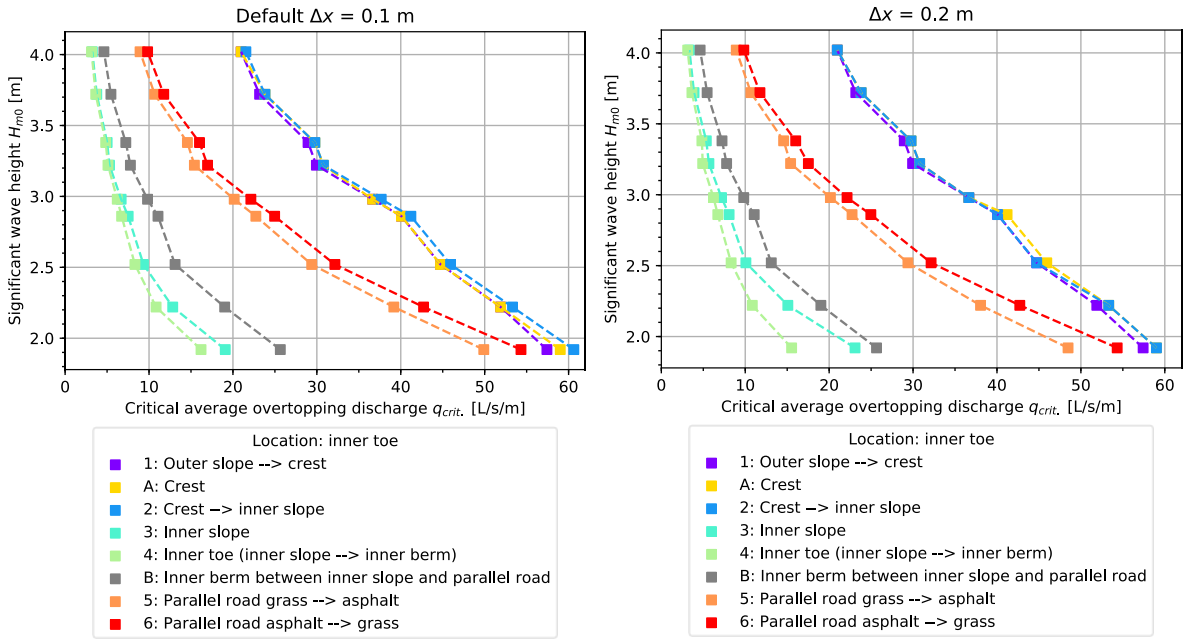

Figure 27: VE-TM simulation results showing the relationship between the critical average overtopping discharge $q_{crit.}$ and the significant wave height H_{m0} when using the default spatial step Δx = 0.1 m (left) and a spatial step of Δx = 0.2 m (right). All simulations are carried out using a critical flow velocity U_c = 6.5 m/s and medium h–θ conditions.

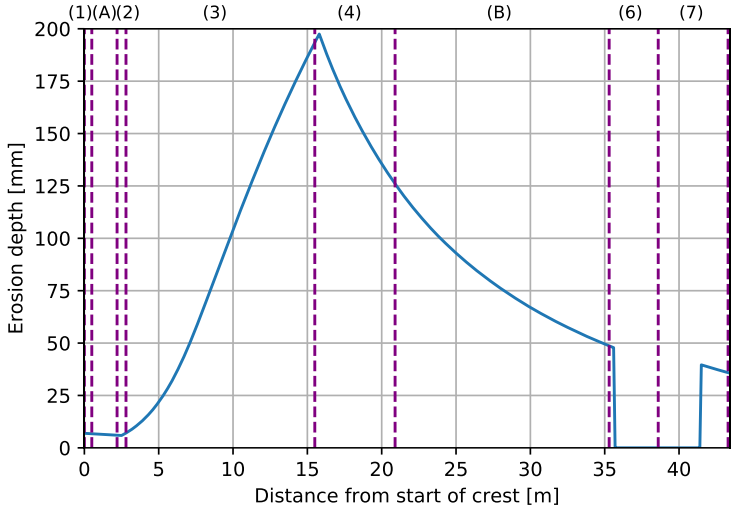

Figure 28: Erosion profile for the critical average overtopping discharge of the inner toe for H_{m0} = 4.02 m and medium h–θ conditions. The dashed purple lines indicate the start and end of the studied locations, the numbers and letters between brackets above the graph indicate the location number corresponding to Table 4.

5.4.2 Variables Throughout the Overtopping Event

According to Van Bergeijk et al. (2019b), that the maximum flow velocity and maximum layer thickness do not necessarily occur simultaneously. This indicates that using the maximum layer thickness in the VE (Section 3.4.1) is an overestimation and consequently that the discharge of the overtopping wave, which is calculated as the product of the maximum flow velocity and maximum layer thickness, is an overestimation. Hughes (2011) observed that both the flow velocity and layer thickness increase from zero to maximum values in a very short time span when a wave overtops the studied location, while the decrease to zero takes a long time relative to the initial jump. He therefore suggests that the flow velocity and layer thickness at a certain location can be represented for an idealized overtopping wave by a sawtooth-shape (Figure 29). In doing so, it is assumed that both the flow velocity and layer thickness reach their maximum values instantaneously when the overtopping wave reaches the studied location. In other words: the lag time between the occurrence of the maximum flow velocity

and maximum layer thickness is neglected. When considering the measurements presented by Van der Meer et al. (2010b) and Hughes et al. (2012), shown in Figure 29, this appears to be a rational simplification as the lag time in these measurements (approximately 0.5 – 1 second) is much smaller than the total overtopping duration (8 – 12 seconds). In conclusion: the found maximum overtopping discharge as the product of maximum flow velocity and maximum layer thickness is an overestimation which leads to more conservative values, but a justifiable simplification.

A related point of discussion is that the TM assumes that the bed shear stress that is exerted by overtopping wave i at location x (i.e. $\tau_{0,i}(x)$) is constant throughout the overtopping event. Because the bed shear stress is calculated using the VE, which describe the change in maximum flow velocity along the cross-section, the TM calculates the damage caused by a wave using the constant maximum load throughout the overtopping event. However, as the graphs of the flow velocity in Figure 29 show, the flow velocity at a certain location decreases throughout the overtopping duration. It would therefore be more accurate to let the bed shear stress depend on time as well, i.e. $\tau_{0,i}(x,t)$. Hughes (2011) presents an exponential function that describes this decrease in flow velocity, but it requires calibration using experimental data and can therefore not be applied in this case. Furthermore, the overtopping duration that is used in the TM (Section 3.4.1) is calculated using an equation of Bosman et al. (2008) and is assumed to be constant for the whole cross-section. However, the duration decreases as water flows over a horizontal surface because of the deceleration caused by the surface roughness. This decrease can be calculated using a different equation given by Bosman et al. (2008), but is only valid for the crest. For the inner slope, where the overtopping duration decreases due to the accelerating water, no equation exists. Additionally, Van Bergeijk et al. (2019b) assumed steady-state conditions for the VE, meaning that a constant overtopping duration throughout the overtopping event is considered. Using a constant value for the overtopping duration may therefore not be completely realistic, but it is the most suitable approach.

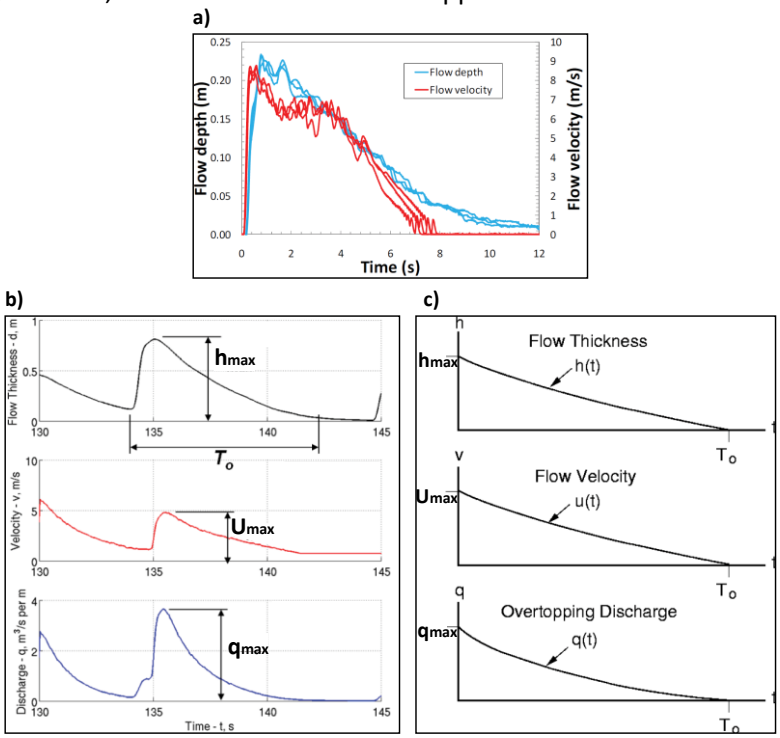

Figure 29: a) Measurements of the flow velocity and layer thickness (flow depth) at a fixed location throughout the overtopping event (Van der Meer et al., 2010b)*, b) Measurements of the flow velocity, layer thickness and overtopping discharge (product of the measured flow velocity and layer thickness) at a fixed location throughout the overtopping event* (Hughes et al., 2012)*. Note that the values at the start of the graph (t = 130 s) belong to a previous overtopping wave. In the figures, h_{max} indicates the maximum layer thickness, U_{max} the maximum flow velocity and q_{max} the maximum overtopping discharge, c) Schematization of an idealized overtopping wave, showing the sawtooth-shape simplification of the layer thickness $h(t)$, flow velocity $u(t)$ and overtopping discharge $q(t)$ with corresponding maximum values h_{max}, U_{max} and q_{max}* (Hughes, 2011)*. Furthermore, T_o indicates the overtopping duration.*

5.5 Comparison COM & VE-TM

5.5.1 Effects of Changing Water Levels and Angles of Wave Attack

Both COM and VE-TM simulations are carried out for the low, medium and high conditions of water level h and angle of wave attack θ. Intuitively, one would expect the low conditions to result in the largest critical average overtopping discharge and the high conditions in the lowest critical discharges. However, the simulations results show the opposite; the low conditions result in the lowest critical discharges while the medium and high conditions yield larger values. This can be explained by looking at the equations for the average overtopping discharge (Eq. 19a and Eq. 19b) and the parameter values that are presented in Table 12. The values in this table are the result of simulations with the three h–θ conditions for an arbitrarily chosen situation in which H_{m0} = 4.02 m and failure of the transition from the outer slope to the crest (location 1) occurs.

Table 12: Average values for the influence factors for the berm γ_b, roughness γ_f and oblique wave attack γ_β, breaker parameter $\xi_{m-1,0}$, tangent of the characteristic outer slope $\alpha_{outer,char.}$, run-up height and crest freeboard. The values were obtained from COM and VE-TM simulations with a crest elevation at which failure of the transition from the outer slope to the crest (location 1) occurs for a significant wave height H_{m0} = 4.02 m. These simulations are carried out for low, medium and high conditions of water level h and angle of wave attack θ with a critical flow velocity of U_c = 6.5 m/s.

H_{m0} = 4.02 m Outer slope --> crest (location 1)	Low conditions		Medium conditions		High conditions	
	COM	VE-TM	COM	VE-TM	COM	VE-TM
Average γ_b [-]	0.93	0.94	0.92	0.92	0.91	0.91
Average γ_f [-]	0.77	0.76	0.76	0.75	0.75	0.74
Average γ_β[-]	0.93	0.93	0.93	0.93	0.99	0.99
Average $\xi_{m-1,0}$ [-]	1.60	1.53	1.33	1.29	1.15	1.11
Average tan($\alpha_{outer,char.}$) [-]	0.37	0.35	0.30	0.29	0.26	0.25
Average run-up height [m]	2.89	2.75	2.26	2.15	2.01	1.91
Average crest freeboard [m]	5.79	6.04	5.18	5.36	5.06	5.25

A first observation from the data in Table 12 is that the influence factor for oblique wave attack γ_β is the same for the low and medium conditions, while a changing angle of wave attack should result in a different value. Despite this, the medium conditions result in higher critical discharges, which indicates that the increase can be mainly attributed to the increase in water level h. Figure 30 presents a schematized overview of the effects of an increasing water level on the parameters in the equations for the average overtopping discharge (Eq. 19a and Eq. 19b). These effects are each described in the paragraphs below.

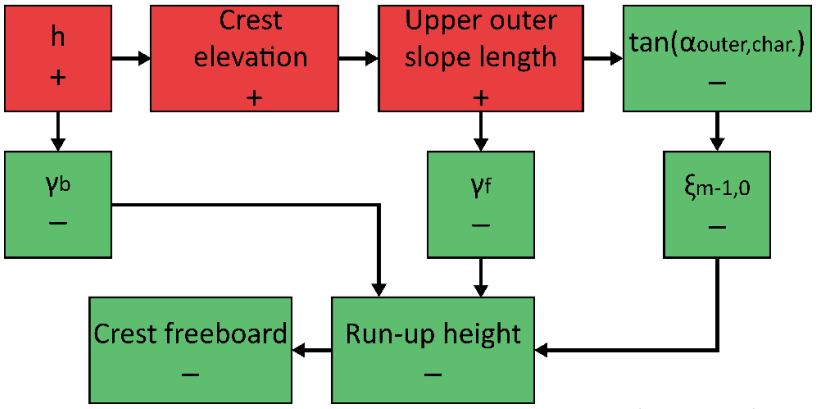

Figure 30: Schematization of the effects of an increasing water level h. Here, tan($\alpha_{outer,char.}$) is the tangent of the characteristic outer slope angle, γ_b and γ_f the influence factors for a berm and roughness respectively and $\xi_{m-1,0}$ the breaker parameter. Red indicates an increase of the parameter value (also indicated with a plus-sign) and green a decrease (also indicated with a minus-sign). Note that this overview is not generally applicable, as other hydraulic conditions and/or outer slope designs may yield different relationships between the parameters.

An increasing water level causes the vertical distance between the berm and the water level to decrease, meaning that the value for γ_b decreases (Table 12) because the influence of the berm increases (Section 3.2.2). It must be noted that when the berm is located below the still water level (SWL), an increased water level actually decreases the berm influence and therefore increases the γ_b value. For the high h–θ conditions the berm is located below the SWL, but because the water level is still located relatively close to the berm the simulations resulted in a decreased γ_b compared to the low and medium conditions.

When the water level is increased, the crest elevation must be increased as well in order to find the tipping point for failure of the grass cover layer. This is achieved by increasing the length of the upper outer slope, which is covered with a pattern of protruding blocks (Appendix A). This is the roughest cover material on the outer design of the Afsluitdijk, which increases the average roughness when the length of the upper outer slope is increased, resulting in a lower influence factor for roughness γ_f and a lower wave run-up height. Furthermore, a longer upper outer slope causes the characteristics outer slope $\alpha_{outer,char.}$ to decrease as it is the least steep slope in the outer design. As a result, the breaker parameter $\xi_{m-1,0}$ decreases.

According to the equations in Section 3.2.2, decreases in γ_b, γ_f and $\xi_{m-1,0}$ cause the wave run-up height to decrease. As a result, the crest freeboard can be lower for high water levels, which is in agreement with the data in Table 12. The crest freeboard is a major parameter for the calculation of the average overtopping discharges, and a decreasing freeboard causes a relatively large increase in average overtopping discharges (Eq. 19a and Eq. 19b). An increasing water level therefore results in higher critical average overtopping discharges.

5.5.2 Effects of Changing Wave Heights

Figure 13 and Figure 15 show the simulation results of the COM and the VE-TM approach, respectively. As concluded in the comparison of these results in Section 4.3, the VE-TM generally predicts lower critical average overtopping discharges than the COM. Furthermore, it was found that the $H_{m0} - q_{crit.}$ relationships of the COM and the VE-TM approach for the locations on the crest are similar. These observations can be explained by looking at the changes in flow velocity when the wave height is varied.

Figure 31 shows the average maximum flow velocity on the crest for varying significant wave heights. The left graph shows the velocity values on the crest for the iteration just before failure of location 2 occurs (i.e. the “critical iteration” of location 2), while the right shows the values for the critical iteration of location 5. The flow velocities of the critical iterations of location 2, which is located on the crest, develop similarly for the COM and the VE-TM. This causes the resulting damage and the critical average overtopping discharges to develop in a similar manner as well. However, the flow velocities of the critical iterations of location 5 that are predicted by the VE-TM differ from those of the COM approach. For the lower wave heights (up to approximately H_{m0} = 2.98 m), the velocity is higher in the VE-TM approach than in the COM approach, while the opposite is true for larger wave heights. This results in different developments of the critical average overtopping discharge for varying wave heights.

The different behavior of the two modelling approaches can be attributed to the way in which the effects of the inner slope are incorporated. In the COM, the acceleration of the overtopping water on the slope are included the calculations using a constant factor for acceleration α_a for all significant wave heights (Section 3.3.1). Because of this, the average maximum flow velocity at the crest increases approximately linearly for an increasing wave height for both locations. However, in the VE-TM approach the increase in flow velocity on the inner slope are directly related to its length (Section 3.4.1). For a certain slope length, the acceleration that is included in the COM approach using the α_a factor will equal the effects of flow acceleration that are included in the VE-TM. This means

that the flow velocity at the start of the slope is the same in both approaches. The right graph in Figure 31 shows that this situation occurs for location 5 around H_{m0} = 2.8 m. For higher waves the crest height needs to be increased in both the COM and the VE-TM approach. However, the acceleration of the flow on the inner slope in the COM does not change due to the constant α_a factor, while in the VE-TM the overtopping water can accelerate longer so that it arrives with a relatively higher velocity at location 5. To compensate for this, the crest elevation is increased in the VE-TM, which increases the crest freeboard and reduces the flow velocity on the crest (Eq. 17). Because the crest freeboard in the VE-TM approach is higher, the overtopping discharge decreases relative to those predicted by the COM for higher waves (Eq. 19a and Eq. 19b), while the opposite occurs for lower wave heights. This is in accordance with the findings in Section 4.3, and explains why the COM and the VE-TM show similar $H_{m0} - q_{crit.}$ relationships for locations 1 and 2 but not for the other locations.

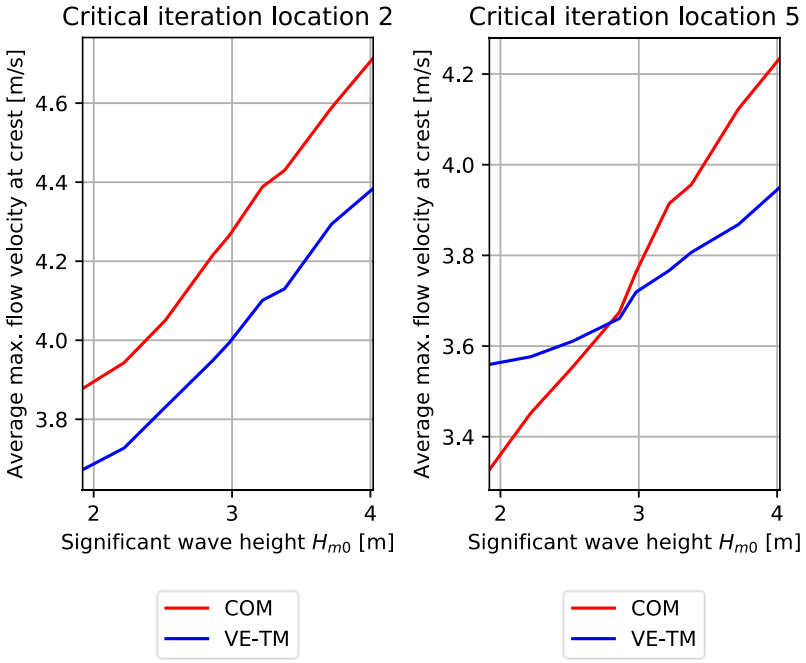

Figure 31: Average maximum flow velocity for changing significant wave heights in the COM and the VE-TM. The results are obtained from the iteration just before failure occurs at the transition from the crest to the inner slope (left) and the transition from grass to asphalt (right). All simulations are carried out with medium h-θ conditions.

5.5.3 Grass-Asphalt Transitions

The COM predicts that the transition from grass to asphalt is stronger than the transition from asphalt to grass, while this is the other way around in the VE-TM. This is because the load factor for the transition from asphalt to grass is α_m = 1.7 (Section 3.3.3), which is a relatively high value. The theory behind this load factor value is that the water flows faster over asphalt than grass due to a lower roughness, and that a local increase in turbulence increases the amount of erosion (Section 2.3). Figure 32 shows the cross-sectional average maximum flow velocities and average turbulence coefficients that are found with the VE-TM for H_{m0} = 1.92 m in the critical iteration of the transition from grass to asphalt (VE-TM location 5). The curve indicating the flow velocity shows that the deceleration of the water on the inner berm is slightly less on the parallel road than on grass, but the flow velocity at the transition from grass to asphalt is still higher than at the transition from asphalt to grass. As a result, a higher critical average overtopping discharge is found for the transition from asphalt to grass, and not for the transition from grass to asphalt as the COM results indicate. The turbulence of the overtopping water while it flows over the grass of the inner berm is constant because the bottom friction coefficient f is constant. However, since no validated bottom friction coefficient value is available for the asphalt, the bottom friction coefficient for the parallel road is calculated using Manning's roughness coefficient and the layer thickness at the moment of maximum flow velocity

(Section 3.4.1). Figure 32 shows that this does not cause a turbulence peak at the transition from asphalt to grass, which would be expected from information given by Bomers et al. (2018). It is likely that the turbulence at these transitions needs to be implemented using a different approach. This is in line with Warmink et al. (2018) who concluded that a detailed turbulence model is required for accurate calculations of the hydraulic load at these transitions.

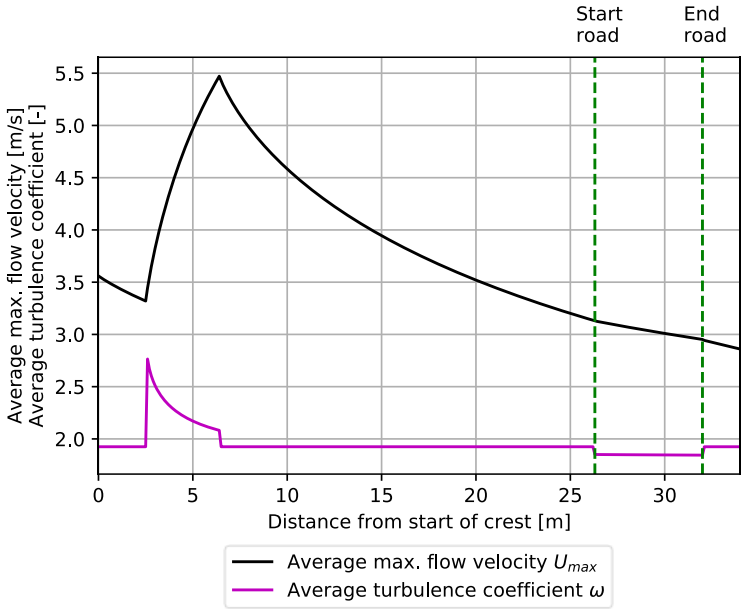

Figure 32: Cross-sectional values of the average maximum flow velocities U_{max} and average turbulence coefficient ω that are found with the VE-TM in the critical iteration of location 5. The simulation was carried out with U_c = 6.5 m/s, H_{m0} = 1.92 m and medium h-θ combination. The dashed green lines mark the location of the parallel road.

5.6 Sensitivity Analyses

Section 4.4 presents the results of the sensitivity analyses, in which the values of several selected parameters are varied. An overview of all analyses and the resulting changes in critical average overtopping discharges relative to the default simulations is given in Table 13.

Table 13: Overview of the results from the sensitivity analyses.

Parameter	**Change in parameter value relative to the default value**	**Modelling approach**	**Change in critical discharges relative to the default scenario $\Delta q_{crit.}$**
Critical flow velocity U_c	-12%	*COM*	-31.3% ≤ $\Delta q_{crit.}$ ≤ -17.7%
		VE-TM	-29.3% ≤ $\Delta q_{crit.}$ ≤ -22.3%
	+12%	*COM*	+24.9% ≤ $\Delta q_{crit.}$ ≤ +47.4%
		VE-TM	+16.6% ≤ $\Delta q_{crit.}$ ≤ +21.7%
Flow velocity at the start of the crest $U_{i,crest}$	-20%	*COM*	+127.0% ≤ $\Delta q_{crit.}$ ≤ +196.5%
		VE-TM	+28.6% ≤ $\Delta q_{crit.}$ ≤ +165.9%
	+20%	*COM*	-55.5% ≤ $\Delta q_{crit.}$ ≤ -47.0%
		VE-TM	-46.5% ≤ $\Delta q_{crit.}$ ≤ -17.6%
Factors for the load α_m,	"Low impact"	*COM*	+146.8% ≤ $\Delta q_{crit.}$ ≤ +225.1%

strength α_s and acceleration α_a	"High impact"	*COM*	-61.7% ≤ $\Delta q_{crit.}$ ≤ -51.7%
Relative turbulence intensity r_0	+78% (Valk, 2009)	*VE-TM*	-65.3% ≤ $\Delta q_{crit.}$ ≤ -40.5%
	+78% (Bomers et al., 2018)	*VE-TM*	-71.5% ≤ $\Delta q_{crit.}$ ≤ -46.6%
Overall strength parameter C_E	+78%	*VE-TM*	-43.9% ≤ $\Delta q_{crit.}$ ≤ -40.0%
	+111%	*VE-TM*	-52.3% ≤ $\Delta q_{crit.}$ ≤ -48.1%
	+144%	*VE-TM*	-58.2% ≤ $\Delta q_{crit.}$ ≤ -52.2%

The results of these analyses show that the COM is most sensitive towards changes in the load, strength and acceleration factors (α_m, α_s and α_a), but that the critical flow velocity U_c and the flow velocity at the start of the crest $U_{i,crest}$ can also cause significant changes in the resulting critical average overtopping discharge. As mentioned in Section 5.3 the appropriate values of the alpha-factors for certain cross-sectional locations are not always clear. This is especially true for the acceleration factor, as no values are given in literature for locations on the inner berm. Immediately downstream of the inner toe the flow still has a higher velocity than at the crest, meaning that $\alpha_a \geq 1$, while the flow velocity at locations that are located farther away on the inner berm is lower compared to the crest, i.e. $\alpha_a \leq 1$. It is therefore likely that the real flow velocity at these locations is calculated more accurately with different combinations of alpha-factors, thus increasing the likelihood of large changes in the predicted critical average flow velocities.

The VE-TM is most sensitive towards changes in the critical flow velocity U_c and the flow velocity at the start of the crest $U_{i,crest}$. However, the impact of changes in the relative turbulence intensity r_0 and the overall strength parameter C_E should not be underestimated. The main cause of uncertainty in these two parameters is the choice of calculation method. For the relative turbulence intensity either the equations of Hoffmans (2012) or the constant values from literature (Valk, 2009; Bomers et al., 2018) can be used, and the overall strength parameter can be determined based on either the critical flow velocity (Eq. 34) or from literature values (Hoffmans et al., 2009). Because only two calculation methods are available for each parameter, there are either no implications on the predicted critical discharges (if the used approaches are realistic) or large implications if one of the other calculation methods is more accurate. This is different for U_c or $U_{i,crest}$ as small changes in these parameter values are more likely to occur than large variations.

Regarding the overall strength parameter C_E in the VE-TM approach (Section 4.4.5), it can be argued that the results of both the default scenario and the "good" scenario in Figure 24 are conform the on-site grass cover tests that are described by Bakker et al. (2009). According to this study, the grass cover on the Afsluitdijk is classified as VTV 2006 grass type "good". Consequently, the results of the "good" scenario are realistic while the critical discharges that are predicted by the "average" and "combined" scenarios are less likely for the Afsluitdijk. However, the critical discharges that are predicted by the default scenario are realistic as well since this method results in the highest grass cover strength. Since the C_E literature value in the "good" scenario is an indicative value (Hoffmans et al., 2009) and the fact that "good quality" is the highest category that can be assigned to a grass cover in the VTV 2006 classification, the grass cover strength in the default method would also be classified as good quality (which follows the conclusions of Bakker et al. (2009)). To conclude, the most realistic results for the Afsluitdijk using the VE-TM approach are expected from simulations that use a C_E value based on the critical flow velocity or the C_E value of Hoffmans et al. (2009) corresponding to a good quality grass cover. However, for design and safety assessment purposes it is recommended to use the value of Hoffmans et al. (2009) as this results in lower, and therefore more conservative, critical average overtopping discharges.

6. CONCLUSIONS

The objective of this study is to find the relationship between the significant wave height and critical average overtopping discharge for wave heights up to 4 meter using the COM and the VE-TM, and to find towards which parameters this relationship is most sensitive. To answer this, four research questions were formulated which are answered in this chapter.

What is the relationship between the significant wave height and the critical average overtopping discharge that is found using the COM?

The COM predicts that the critical average overtopping discharge increases when the significant wave height decreases. For wave heights larger than 2.98 m this rate of decrease is smallest for the weakest cross-sectional locations and increases for locations that are able to withstand larger amounts of overtopping discharge. The simulation results show that the inner toe is the weakest cross-sectional location of the Afsluitdijk, with a minimum simulated critical average overtopping discharge of $q_{crit.}$ = 3.4 L/s/m for a significant wave height of H_{m0} = 4.02 m. Furthermore, the transition from the crest to the inner slope is able to resist the largest average overtopping discharges, with a maximum simulated critical average overtopping discharge of $q_{crit.}$ = 103.8 L/s/m for a significant wave height of H_{m0} = 1.92 m. Counterintuitively, an increasing water level results in a larger critical discharge for a constant significant wave height. This can be attributed to a decreasing crest freeboard, which is the result of an increasing overall roughness due to the protruding elements on the upper outer slope of the Afsluitdijk, a decreasing influence of the outer berm and a decreasing characteristic outer slope angle as the upper outer slope is the least steep slope of the outer design of the dam.

What is the relationship between the significant wave height and the critical average overtopping discharge that is found using the VE-TM?

The simulation results of the VE-TM show that the critical average overtopping discharge increases for a decreasing significant wave height. For wave heights above 2.98 m the locations on the crest are least sensitive towards a changing significant wave height, while the transitions at the parallel road show the largest increase in critical average overtopping discharge for a decreasing significant wave height. The inner toe is the location that is characterized by the lowest critical discharge, with a minimum of $q_{crit.}$ = 1.4 L/s/m for a significant wave height of H_{m0} = 4.02 m. The largest critical discharge, $q_{crit.}$ = 77.2 L/s/m for a significant wave height of H_{m0} = 1.92 m, is predicted to occur at the transition from the crest to the inner slope. Furthermore, higher critical average overtopping discharges are predicted for an increasing water level as a result of an increasing roughness, a decreasing effect of the outer berm and a decreasing characteristic outer slope angle.

How does the relationship between the significant wave height and the critical average overtopping discharge differ between the COM and VE-TM?

The VE-TM generally predicts three to four times lower critical average overtopping discharges than the COM. Despite these differences, the two modelling approaches predict approximately equal changes in critical average overtopping discharges for a changing significant wave height. This is due to the fact that the flow velocity on the crest develops similarly as a function of the wave height in both the COM and the VE-TM. For the other cross-sectional locations the two modelling approaches predict different relationships between the critical discharge and the significant wave height. This can be attributed to different hydraulic loads at these locations for a varying wave height as a result of a changing inner slope length. Furthermore, the COM and the VE-TM approaches both predict that the inner toe and the inner slope are the weakest cross-sectional locations, as these fail at the lowest critical average overtopping discharges, while the locations on the crest are able to withstand the highest critical discharges. The COM predicts that the transition from grass to asphalt would be able to withstand a higher critical discharge than the transition from asphalt to grass, while the VE-TM results showed the opposite. Based on literature, turbulence peaks are expected at these transitions

that increase the hydraulic load, which are not calculated by the VE-TM. The turbulence therefore needs to be calculated with a more detailed method in the VE-TM for these locations.

Towards which parameters in the COM and the VE-TM are the found relationships between the significant wave height and the critical average overtopping discharge most sensitive?

The sensitivity analyses showed that changes in the critical flow velocity and the flow velocity at the start of the crest have large influences on the simulation results in both the COM and the VE-TM approach. Especially the uncertainty in the flow velocity at the start of the crest is large because (1) the calculations that are needed to obtain a value for this variable contain many empirical coefficients for which the values are not well established and (2) because assumptions are required as hydraulic conditions may lie outside of the validation area of certain equations. Furthermore, a change in the load, strength and acceleration factor values in the COM approach results in large variations in the calculated critical average overtopping discharges. Especially the application of the acceleration factor for locations on the inner berm is uncertain as no area of influence is specified in the literature. The sensitivity analyses of the relative turbulence intensity and the overall strength parameter, which are both present in the VE-TM approach, showed that the resulting critical average overtopping discharges are mainly influenced by the method that is used to determine the values of these two variables. Constant values from the literature resulted in relatively similar critical discharges, while approaches in which equations were used to calculate the parameter values resulted in significantly larger critical discharges.

7. RECOMMENDATIONS

Based on the results of this study, several recommendations for future research are formulated. Firstly, it is recommended to carry out (scaled) wave overtopping experiments for wave heights that are larger than 3 meter, which include the inner slope and inner berm of the new design. The focus of these experiments should lie on finding the relationship between the significant wave height and the critical average overtopping discharge at these cross-sectional locations. These results can be used to validate the COM and VE-TM simulation results in this study, which was not possible due to the absence of data. Furthermore, it is suggested to carry out the same COM and VE-TM simulations for other dike sections of the Afsluitdijk or for a different dike or dam in order to assess whether this results in similar relationships between the significant wave height and critical average overtopping discharge, and to see if this yields the same differences between the COM and VE-TM results.

As input for the COM and the VE-TM modelling approaches a storm event was schematized. Following previous studies, it was assumed that the water level and wave height build up to their normative values at the peak of the storm, after which they decrease again. However, previous studies that applied the COM used a three-hour period in which constant peak storm conditions occur. Analysis of the differences between these two storm schematizations showed that the three-hour peak conditions can be used as a quick method to obtain a rough estimate of critical average overtopping discharges with the COM. However, for the VE-TM approach and for safety assessments using either the COM or the VE-TM simulation results it is recommended to use the storm schematization in which the hydraulic conditions develop over time, as this results in lower (more conservative) critical average overtopping discharges.

Both the COM and the VE-TM approach predict that the inner toe and the inner slope are the weakest cross-sectional locations of the Afsluitdijk, meaning that these are expected to fail first in the case of a storm event. The simulations have shown that the differences between the critical average overtopping discharges of these locations are small (0.1 – 3 L/s/m). Therefore, if it is decided that the inner toe requires reinforcement so that it can withstand larger average overtopping discharges, it is recommended to also reinforce the inner slope. The same could be considered for the part of the inner berm in between the inner toe and the parallel road, as several VE-TM simulations showed that the critical discharges at this location approximate those of the inner toe and the inner slope.

In this study, the results of the COM and the VE-TM approaches are presented as critical average overtopping discharges for a range of significant wave heights. However, in the WBI 2017 GEKB safety assessment a probability distribution of failure is used (Table 1). Therefore, in order to include significant wave heights larger than 3 meter in the WBI 2017, the modelling approaches that are presented in this study should be modified so that the probability distribution of failure is found.

From the sensitivity analyses it is concluded that both the results from the COM and the VE-TM are sensitive towards changes in the critical flow velocity and the flow velocity at the start of the crest. Calculation of the latter parameter is based on several assumptions and coefficients from the literature which are not well established. Future studies could focus on improving the accuracy of this flow velocity, which consequently increases the accuracy of the amount of erosion that is predicted by the COM and the VE-TM. Furthermore, it is concluded that the COM is sensitive to the load, strength and acceleration factors. For the acceleration factor it is unknown what the area of influence is. This should be studied more thoroughly in order to accurately estimate the erosion at locations on the inner berm. Lastly, the critical discharges that are found with the VE-TM approach differ significantly depending on which method is used to determine the value of the relative turbulence intensity and the overall strength parameter. It is therefore recommended to study these parameters in more detail in order to establish accurate values.

BIBLIOGRAPHY

't Hart, R., De Bruijn, H. and De Vries, G. (2016) *Fenomenologische beschrijving: Faalmechanismen WTI*, *Deltares Report 1220078-000-GEO-0010-gbh*. Delft, The Netherlands: Deltares.

Bakker, J. J., Mom, R. J. C. and Steendam, G. J. (2009) *Factual Report: Overslagproeven en afschuifproef Afsluitdijk*. Marknesse, The Netherlands: Infram.

Van Bergeijk, V. M., Warmink, J. J., Frankena, M. and Hulscher, S. J. M. H. (2019a) 'Modelling Dike Cover Erosion by Overtopping Waves: The Effects of Transitions', in *Conference Proceedings of Coastal Structures 2019 (submitted)*. Hannover, Germany.

Van Bergeijk, V. M., Warmink, J. J., Van Gent, M. R. A. and Hulscher, S. J. M. H. (2019b) 'An analytical model of wave overtopping flow velocities on dike crests and landward slopes', *Coastal Engineering*, 149, pp. 28–38. doi: 10.1016/j.coastaleng.2019.03.001.

Bomers, A., Aguilar Lopez, J. P., Warmink, J. J. and Hulscher, S. J. M. H. (2018) 'Modelling effects of an asphalt road at a dike crest on dike cover erosion onset during wave overtopping', *Natural Hazards*. Springer Netherlands, 93(1), pp. 1–30. doi: 10.1007/s11069-018-3287-y.

Van den Bos, W. (2006) *Erosiebestendigheid van grasbekleding tijdens golfoverslag (MSc thesis)*. Delft University of Technology. Available at: http://resolver.tudelft.nl/uuid:41fca8c5-ca13-4551-b112-0b6910b2f8d0.

Bosman, G., van der Meer, J., Hoffmans, G., Schüttrumpf, H. and Verhagen, H. J. (2008) 'Individual Overtopping Events at Dikes', in *Coastal Engineering 2008*. World Scientific Publishing Company, pp. 2944–2956. doi: 10.1142/9789814277426_0244.

Botterhuis, T., Waterman, R. and Geerse, C. (2017) *Gebruikershandleiding Waterstandsverloop: versie 3.0*, *Software Manual*. Lelystad, The Netherlands: HKV Lijn in Water.

Capel, A. (2015) 'Wave run-up and overtopping reduction by block revetments with enhanced roughness', *Coastal Engineering*. Elsevier B.V., 104, pp. 76–92. doi: 10.1016/j.coastaleng.2015.06.007.

Chbab, H. (2015) *Waterstandsverlopen kust: Wettelijk Toetsinstrumentarium WTI-2017*, *Deltares Report 1220082-002-HYE-0003*. Delft, The Netherlands: Deltares.

Chbab, H. and De Waal, H. (2017) *Achtergrondrapport Hydraulische Belastingen: Wettelijk Beoordelingsinstrumentarium 2017*, *Deltares Report 1230087-008-HYE-0001*. Delft, The Netherlands: Deltares.

Chen, W., Van Gent, M. R. A., Warmink, J. J. and Hulscher, S. J. M. H. (2019) 'The influence of a berm and roughness on the wave overtopping at dikes', (submitted to Coastal Engineering).

Deltares (2015) *Handreiking Dijkbekledingen - Deel 5: Grasbekledingen*. Delft, The Netherlands: Deltares.

Duits, M. (2017) *Gebruikershandleiding Hydra-NL: versie 2.0*, *Software Manual*. Lelystad, The Netherlands: HKV Lijn in Water.

Van Etten, R. (2009) *SBW-Golfoverslagproeven: Factual report grondonderzoek Afsluitdijk*, *Deltares Report 1001189-010-GEO-0001*. Delft, The Netherlands: Deltares.

Hoffmans, G., Akkerman, G. J., Verheij, H., van Hoven, A. and van der Meer, J. (2009) 'The erodibility of grassed inner dike slopes against wave overtopping', in *Coastal Engineering 2008*. World Scientific Publishing Company, pp. 3224–3236. doi: 10.1142/9789814277426_0267.

Hoffmans, G., Van Hoven, A., Steendam, G. J. and Van der Meer, J. (2018) 'Summary of research work about erodibility of grass revetments on dikes', in *Protections 2018 (3rd International Conference on Protection against Overtopping)*. Grange-over-Sands, UK. Available at: http://eprints.hrwallingford.co.uk/1503/.

Hoffmans, G. J. C. M. (2009) 'Closure problem to jet scour', *Journal of Hydraulic Research*, 47(1), pp. 100–109. doi: 10.3826/jhr.2009.3179.

Hoffmans, G. J. C. M. (2012) *The Influence of Turbulence on Soil Erosion*. Delft, The Netherlands: Eburon.

Hoffmans, G. J. C. M., van Hoven, A., Harderman, B. and Verheij, H. J. (2014) 'Erosion of grass covers

at transitions and objects on dikes', in *Scour and Erosion: Proceedings of the 7th International Conference on Scour and Erosion*. Perth, Australia: CRC Press / Balkema - Taylor & Francis Group, pp. 643–649. doi: 10.1201/b17703-84.

Van Hoven, A. (2015) *Memo Verdelingen kritisch overslagdebiet WTI2017*, *Deltares Memo 1220086-005-HYE-00003*. Delft, The Netherlands: Deltares.

Van Hoven, A. and Van der Meer, J. M. (2017) *Onderbouwing kansverdeling kritisch overslagdebiet ten behoeve van het OI2014v4*, *Deltares Report 1230090-011-GEO-0006-jvm*. Delft, The Netherlands: Deltares.

Hughes, S. A. (2011) *Adaptation of the Levee Erosional Equivalence Method for the Hurricane Storm Damage Risk Reduction System (HSDRRS)*, *ERDC/CHL TR-11-3*. U.S. Army Corps of Engineers - Engineer Research and Development Center.

Hughes, S. A., Thornton, C. I., Van der Meer, J. W. and Scholl, B. N. (2012) 'Improvements in Describing Wave Overtopping Processes', *Coastal Engineering Proceedings*, 1(33), p. 35. doi: 10.9753/icce.v33.waves.35.

Inspectie Verkeer en Waterstaat (2006) *Primaire Waterkeringen Getoetst: Landelijke Rapportage Toetsing 2006*. Lelystad, The Netherlands: Inspectie Verkeer en Waterstaat.

Inspectie Verkeer en Waterstaat (2011) *Derde Toets Primaire Waterkeringen: Landelijke Toets 2006-2011*. The Hague, The Netherlands: Inspectie Verkeer en Waterstaat.

Levvel (2018) 'Dwarsprofiel Dijkvak 17A Principeprofiel: Tekeningnummer ASD-TEK-WAT-DO-1.01.1.08B-DP-0263'. Gorinchem, The Netherlands: Levvel.

Van der Meer, J., Hoffmans, G. and Van Hoven, A. (2015) *WTI Onderzoek en ontwikkeling landelijk toetsinstrumentarium - Product 5.12 Analyses grass erosion in wave run-up and wave overtopping conditions*, *Deltares Report 1209437-005-HYE-0003*. Delft, The Netherlands: Deltares.

Van der Meer, J. and Van Hoven, A. (2014) *Analyse erosiebestendigheid Afsluitdijk*, *Deltares Report 1207410-000-HYE-0007*. Delft, The Netherlands: Deltares.

Van der Meer, J., Schrijver, R., Hardeman, B., Van Hoven, A., Verheij, H. and Steendam, G. J. (2010a) 'Guidance on erosion resistance of inner slopes of dikes from three years of testing with the Wave Overtopping Simulator', in *Coasts, marine structures and breakwaters: Adapting to change*. London, UK: Thomas Telford Ltd, pp. 2: 460-473. doi: 10.1680/cmsb.41318.0044.

Van der Meer, J. W., Allsop, N. W. H., Bruce, T., De Rouck, J., Kortenhaus, A., Pullen, T., Schüttrumpf, H., Troch, P. and Zanuttigh, B. (2018) *EurOtop - Manual on wave overtopping of sea defences and related structures*. www.overtopping-manual.com. Available at: www.overtopping-manual.com.

Van der Meer, J. W., Hardeman, B., Steendam, G.-J., Schüttrumpf, H. and Verheij, H. (2010b) 'Flow Depths and Velocities At Crest and Landward Slope of a Dike, in Theory and With the Wave Overtopping Simulator', *Coastal Engineering Proceedings*, 1(32). doi: 10.9753/icce.v32.structures.10.

Ministerie van Economische Zaken (2015) 'Kennisgeving terinzagelegging ontwerpRijksinpassingsplan, MER en overige ontwerpbesluiten project Afsluitdijk, ministerie van Infrastructuur en Milieu, ministerie van Economische Zaken', *Staatscourant*, (12782), pp. 1–3. Available at: https://zoek.officielebekendmakingen.nl/stcrt-2015-12782.html.

Ministerie van I&M and Ministerie van EZ (2015) *Nationaal Waterplan 2016 - 2021*. The Hague, The Netherlands: Ministerie van Infrastructuur en Milieu.

Ministerie van Verkeer en Waterstaat (2007) *Voorschrift Toetsen op Veiligheid Primaire Waterkeringen*. The Hague, The Netherlands: Ministerie van Verkeer en Waterstaat.

Mirtskhoulava, T. E. (1991) 'Scouring by flowing water of cohesive and noncohesive beds', *Journal of Hydraulic Research*, 29(3), pp. 341–354. doi: 10.1080/00221689109498438.

Morris, M., Escarameia, M., Hassan, M. and Van Hoven, A. (2012) *The Performance of Vegetation on Flood Embankments*, *FloodProBE Report WP03-01-10-06*. Wallingford, UK: FloodProBE.

Rijkswaterstaat (2009) *Legger Afsluitdijk*. Lelystad, The Netherlands: Ministerie van Verkeer en Waterstaat.

Rijkswaterstaat (2012) *Handreiking Toetsen Grasbekledingen op Dijken t.b.v. het opstellen van het beheerdersoordeel (BO) in de verlengde derde toetsronde*. Utrecht, The Netherlands: Ministerie van Infrastructuur en Milieu.

Rijkswaterstaat (2017) *Hydraulische Randvoorwaarden Afsluitdijk*. Utrecht, The Netherlands: Rijkswaterstaat.

Rijkswaterstaat (2018) *Schematiseringshandleiding grasbekleding*. The Hague, The Netherlands: Ministerie van Infrastructuur en Milieu.

Schüttrumpf, H. and Oumeraci, H. (2005) 'Layer thicknesses and velocities of wave overtopping flow at seadikes', *Coastal Engineering*, 52(6), pp. 473–495. doi: 10.1016/j.coastaleng.2005.02.002.

Sigurdarson, S. and Van der Meer, J. W. (2012) 'Wave Overtopping at Berm Breakwaters in Line with Eurotop', *Coastal Engineering Proceedings*, 1(33), p. 12. doi: 10.9753/icce.v33.structures.12.

Sprangers, J. T. C. M. (1999) *Vegetation dynamics and erosion resistance of sea dyke grassland (PhD thesis)*. Wageningen Agricultural University. Available at: http://library.wur.nl/WebQuery/wurpubs/63145.

Van Steeg, P. and Van Hoven, A. (2013) *Overgangen bij grasbekledingen in primaire waterkeringen: Aanzet tot oplossingsrichtingen*, *Deltares Report 1208394-000-HYE-0012*. Delft, The Netherlands: Deltares. Available at: http://resolver.tudelft.nl/uuid:93de0538-65a8-46ff-8a60-7a1f6df60889.

Van Steeg, P., Joosten, R. A. and Steendam, G. J. (2018) 'Physical model tests to determine the roughness of stair shaped revetments', in *3th International Conference on Protection against Overtopping, UK*, pp. 1–8.

Steendam, G. J., Hoffmans, G., Bakker, J., Van der Meer, J., Frissel, J., Paulissen, M. and Verheij, H. (2012) *SBW Wave overtopping and grass cover strength: Model development*, *Deltares Report 1206016-007*. Delft, The Netherlands: Deltares. Available at: https://www.researchgate.net/publication/254887769_SBW_Wave_overtopping_and_grass_cover_strength_Model_developement.

Steendam, G. J., Van der Meer, J. W., Hardeman, B. and Van Hoven, A. (2011) 'Destructive Wave Overtopping Tests on Grass Covered Landward Slopes of Dikes and Transitions to Berms', *Coastal Engineering Proceedings*, 1(32), p. 8. doi: 10.9753/icce.v32.structures.8.

TAW (1997) *Technical Report: Erosion Resistance of Grassland As Dike Covering*. Delft, The Netherlands: Technical Advisory Committee for Flood Defence in The Netherlands (TAW).

TAW (1999) *Grass cover as a dike revetment*. Translated by J. A. Muijs. Delft, The Netherlands: Technical Advisory Committee for Flood Defence in The Netherlands (TAW).

TAW (2002) *Technical Report: Wave Run-up and Wave Overtopping at Dikes*. Delft, The Netherlands: Technical Advisory Committee for Flood Defence in The Netherlands (TAW).

Trung, L. H. (2014) *Overtopping on grass covered dikes: Resistance and failure of the inner slopes (PhD thesis)*. Delft University of Technology. doi: 10.4233/uuid:8b33536e-fd2b-4d65-b493-410694b46131.

Valk, A. (2009) *Wave overtopping impact of water jets on grassed inner slope transitions (MSc thesis)*. Delft University of Technology. doi: 10.4121/uuid:a274f26d-0e77-4661-a7cb-fef63fb06493.

Verheij, H., Hoffmans, G., Steendam, G. J., Van der Meer, J. and Van Hoven, A. (2010) *SBW Golfoverslag en Sterkte Grasbekleding: Fase 3D Evaluatie Afsluitdijk*, *Deltares Report 1200259-010-GEO-0017*. Delft, The Netherlands: Deltares.

Verheij, H. J., Meijer, D. G., Kruse, G. A. M., Smith, G. M. and Vesseur, M. (1995) *Onderzoek naar de sterkte van graszoden van rivierdijken*. Delft, The Netherlands: WL | Delft Hydraulics. Available at: http://resolver.tudelft.nl/uuid:3693396e-2f38-414e-ba70-a2fa420e01a9.

Verruijt (2012) *Soil Mechanics*, *Soil Mechanics*. Delft, The Netherlands: Delft University of Technology. doi: 10.4324/9781315846484.

Warmink, J. J., Van Bergeijk, V. M., Chen, W., Van Gent, M. R. A. and Hulscher, S. J. M. H. (2018) 'Modelling Wave Overtopping for Grass Covers and Transitions in Dike Revetments', *Coastal Engineering Proceedings*, 1(36), p. 53. doi: 10.9753/icce.v36.papers.53.

Witteveen+Bos (2013) *Startdocument planuitwerking Afsluitdijk*. Utrecht, The Netherlands: Rijkswaterstaat Midden-Nederland.

Yuan, S., Li, L., Amini, F. and Tang, H. (2014) 'Numerical Study of Turbulence and Erosion of an HPTRM-Strengthened Levee under Combined Storm Surge Overflow and Wave Overtopping', *Journal of Coastal Research*, 30(1), p. 142. doi: 10.2112/JCOASTRES-D-12-00250.1.

LIST OF SYMBOLS

B	Width of the horizontal outer berm	[m]
B_c	Crest width	[m]
b_0	Empirical coefficient	[-]
$C_E(d)$	Depth-dependent overall strength parameter	[$m^{-1}s^{-1}$]
c_0	Empirical coefficient	[-]
$c_{h,2\%}$	Coefficient	[-]
$c_{U,2\%}$	Coefficient	[-]
D	Cumulative hydraulic overload (damage number)	[m^2/s^2]
d	Erosion depth	[m]
d_a	Diameter of the detaching aggregates	[m]
d_b	Vertical distance between the middle of the outer berm and the still water line	[m]
$E_{soil}(d)$	Depth-dependent soil erosion parameter	[m/s]
f	Bottom friction coefficient / Clay inhomogeneousity factor	[-] / [-]
g	Gravitational acceleration	[m/s^2]
H_{m0}	Significant wave height	[m]
$h_{i,discr.,crest}$	Maximum layer thickness at the start of the crest for wave i within the discretization period	[m]
$h_U(x)$	Location-dependent layer thickness at the moment of maximum flow velocity	[m]
L_1, L_2, L_3	Coverage length of the roughness elements on the upper outer slope, outer berm and lower outer slope	[m]
L_{berm}	Characteristic berm length	[m]
$L_{m-1,0}$	Spectral wavelength in deep water	[m]
L_{slope}	Horizontal length between the start and end point of the estimated characteristic slope	[m]
N	Total number of overtopping waves	[-]
$N_{discr.}$	Total number of incident waves within the discretization period	[-]
n	Manning's roughness coefficient	[$s/m^{1/3}$]
$P_{i,discr.}$	Probability of exceedance of wave i within the discretization period	[-]
q	Discharge of the overtopping wave	[$m^3/s/m$]
$q_{crit.}$	Critical average overtopping discharge	[L/s/m]
$RAR(d)$	Depth-dependent root area ratio	[-]
R_c	Crest freeboard	[m]
$R_{u2\%}$	Run-up height above the still water level that is exceeded by 2% of the incident waves (i.e. the 2% run-up height)	[m]
$R_{u2\%,discr.}$	Run-up height above the still water level that is exceeded by 2% of the incident waves within the discretization period	[m]
$R_{u,i,discr.}$	Run-up height above the still water line for wave i within the discretization period	[m]
r_0	Relative turbulence intensity	[-]
r_B	Influence of the outer berm width	[-]
r_{dh}	Influence of the berm level	[-]
$r_{i,discr.}$	Rank of wave i within the discretization period	[-]
s	Along-slope coordinate	[m]
$s_{m-1,0}$	Wave steepness	[-]
T_m	Mean wave period	[s]
$T_{m-1,0}$	Spectral wave period	[s]

$T_{m-1,0,discr.}$	Spectral wave period within the discretization period	[s]
$T_{ovt.}$	Overtopping duration at the studied cross-sectional location	[s]
$T_{ovt,i}$	Overtopping duration of wave i at the studied cross-sectional location	[s]
$T_{ovt.,2\% @ x=0}$	Overtopping duration that is exceeded by 2% of the incident waves at the start of the crest	[s]
$T_{ovt.,i,@ x=0}$	Overtopping duration for overtopping wave i at the start of the crest	[s]
T_p	Peak wave period	[s]
t_r	Root tensile strength	[N/m^2]
$t_{s,discr.}$	Duration of discretization period	[s]
U	Flow velocity of overtopping wave i	[m/s]
U_0	Maximum depth-averaged flow velocity at the start of the horizontal surface	[m/s]
$U_{2\%,crest}$	Flow velocity at the start of the crest exceeded by 2% of the incident waves	[m/s]
U_c	Critical flow velocity	[m/s]
$U_{i,crest}$	Maximum flow velocity at the start of the crest for overtopping wave i	[m/s]
$U_{max(s)}$	Maximum depth-averaged flow velocity of the wave at along-slope location s	[m/s]
$U_{max(x)}$	Maximum depth-averaged flow velocity of the wave at cross-sectional location x	[m/s]
$U_{s,0}$	Maximum depth-averaged flow velocity at the start of the slope	[m/s]
x:	Cross-dike coordinate	[m]
z_m	Maximum erosion depth	[m]
$z_{m,sum}$	Summed maximum erosion depth for all overtopping waves N	[m]
α	Velocity equation parameter	[m$^{1/3}$/s$^{2/3}$]
α_1, α_2, α_3	Location-weighting factor for the upper outer slope, outer berm and lower outer slope	[-]
α_a	Acceleration factor due to increase of flow velocity on slope	[-]
α_{cs}	Factor for clay cohesion increase over the depth	[m^{-1}]
α_E	Coefficient	[-]
α_m	Load factor indicating the influence of an obstacle/transition on the flow velocity U_i	[-]
$\alpha_{outer,char.}$	Characteristic outer slope angle	[°]
α_s	Strength factor indicating the influence of an obstacle/transition on the critical flow velocity U_c	[-]
α_{soil}	Coefficient	[m^2]
α_τ	Pressure fluctuation	[-]
β	Angle of wave attack / Velocity equation parameter	[°] / [s$^{1/3}$/m$^{2/3}$]
γ_b	Influence factor for a berm	[-]
γ_f	Influence factor for the roughness of the outer slope	[-]
$\gamma_{f,1}$, $\gamma_{f,2}$, $\gamma_{f,3}$	Roughness influence factors for the upper slope, berm and inner slope respectively	[-]
γ_v	Influence factor for a wall at the end of the outer slope	[-]
γ_β	Influence factor for oblique wave attack	[-]
$\Delta q_{crit.}$	Change in critical average overtopping discharge	[L/s/m]
θ	Angle of wave attack	[°]
μ	Velocity equation parameter	[m/s]
ν	Kinematic viscosity	[m^2/s]
$\xi_{m-1,0}$	Breaker parameter (/surf similarity parameter/Iribarren number)	[-]
ρ_s	Mass density of the soil	[kg/m^3]

ρ_w	Mass density of water	[kg/m^3]
$\tau_{0,i}$	Bed shear stress caused by overtopping wave i	[N/m^2]
$\tau_0(d)$	Depth-dependent bed shear stress caused by the overtopping wave	[N/m^2]
$\tau_c(d)$	Critical depth-dependent bed shear stress	[N/m^2]
$\tau_{clay,0}$	Cohesion of clay	[N/m^2]
$\tau_{total}(d)$	Depth-dependent total shear stress caused by the grass root tensile stress and clay cohesion	[N/m^2]
ϕ	Angle of the inner slope	[°]
ω	Turbulence coefficient	[-]

APPENDICES

APPENDIX A: NEW OUTER SLOPE DESIGN OF THE AFSLUITDIJK

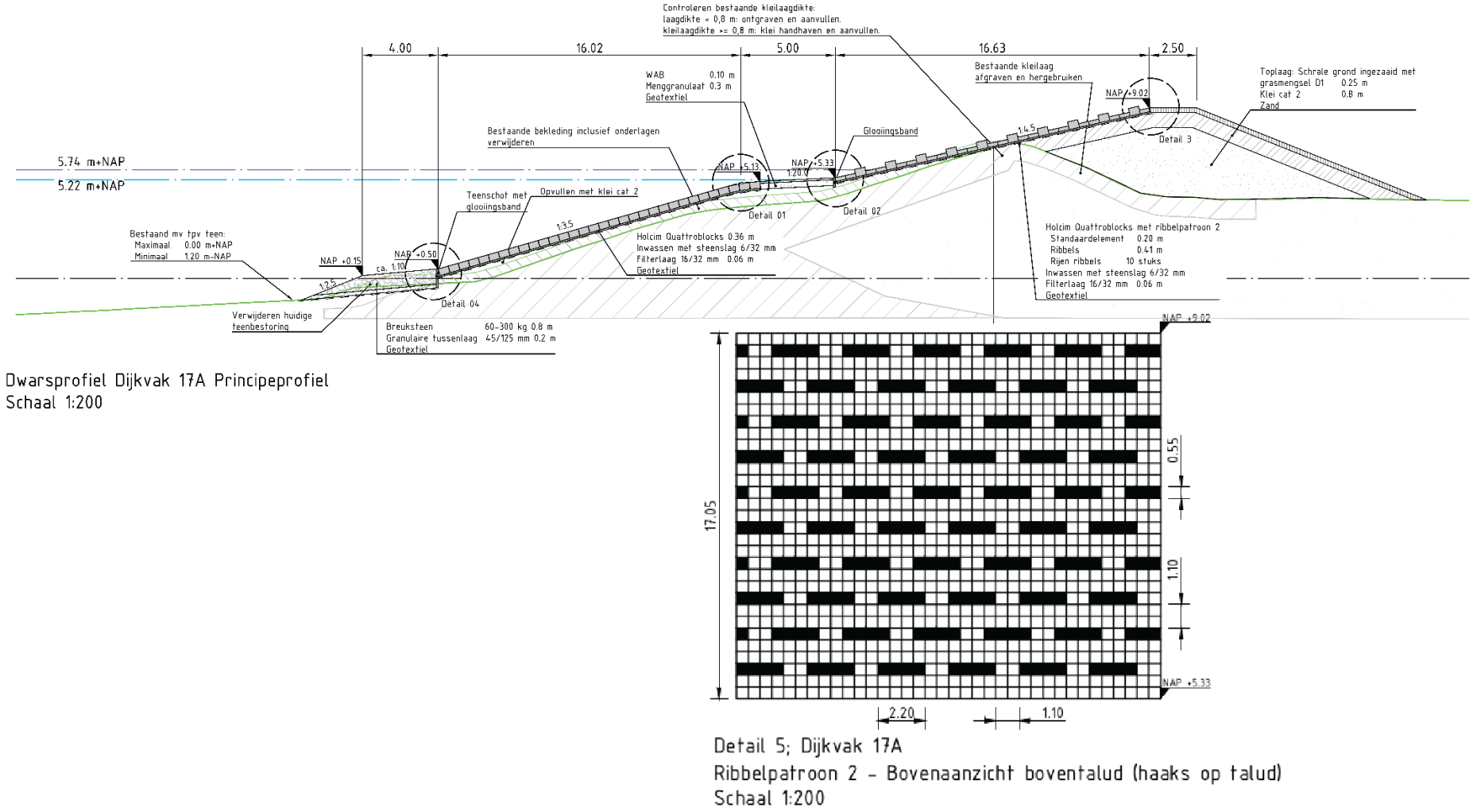

Figure 33: New outer slope design of the Afsluitdijk for dike section 17a, including a top view of the rib pattern of protruding elements on the upper outer slope. Scale: 1:200. Figure adapted from Levvel (2018).

APPENDIX B: AFSLUITDIJK TRANSITIONS AND COM FACTORS

Table 14: Overview of transitions and objects on the Afsluitdijk, including the corresponding load factor α_m and the strength factor α_s. Table adapted from Van der Meer and Van Hoven (2014).

Nr.	Transition/Objects			α_m	α_s
1	Hard cover material on the outer slope	→	Grass cover on the crest	1	0.9
2	Grass cover on the crest	→	Grass cover on the inner slope	1	1
3	Grass cover on the inner slope	→	Grass cover on the berm	1.2	1
4	Grass cover on the berm	→	Asphalt of the bicycle path	1	0.9
5	Asphalt on the bicycle path	→	Grass on the berm	1.7	0.9
6	Grass on the berm	→	Grass on the small slope between the berm and the A7 highway	1	1
7	Grass on the small slope between the berm and the highway	→	Guardrail next to the highway	1	1
8	Grass on the small slope between the berm and the highway	→	Asphalt of the highway	1.2	0.9
9	Asphalt on the highway	→	Grass cover between the two driving lanes of the highway	1.7	0.9
10	Grass cover between the two driving lanes of the highway	→	Guardrail next to the highway	1	1
11	Grass cover between the two driving lanes of the highway	→	Asphalt of the highway	1	0.9
12	*In the case of a road parallel to the highway:*			1.2	0.9
	Grass cover on slope besides parallel road	→	Asphalt cover of the parallel road		
13	*In the case of a road parallel to the highway:*			1.7	0.9
	Asphalt cover of the parallel road	→	Grass cover on slope besides parallel road		
14	Miscellaneous objects ≤ 15 centimeter			1	1
15	Miscellaneous round objects > 15 centimeter			1.4	0.9
16	Miscellaneous rectangular objects > 15 centimeter			1.5	0.9

APPENDIX C: SIMULATION RESULTS OF SENSITIVITY ANALYSES

Critical flow velocity U_c (COM & VE-TM)

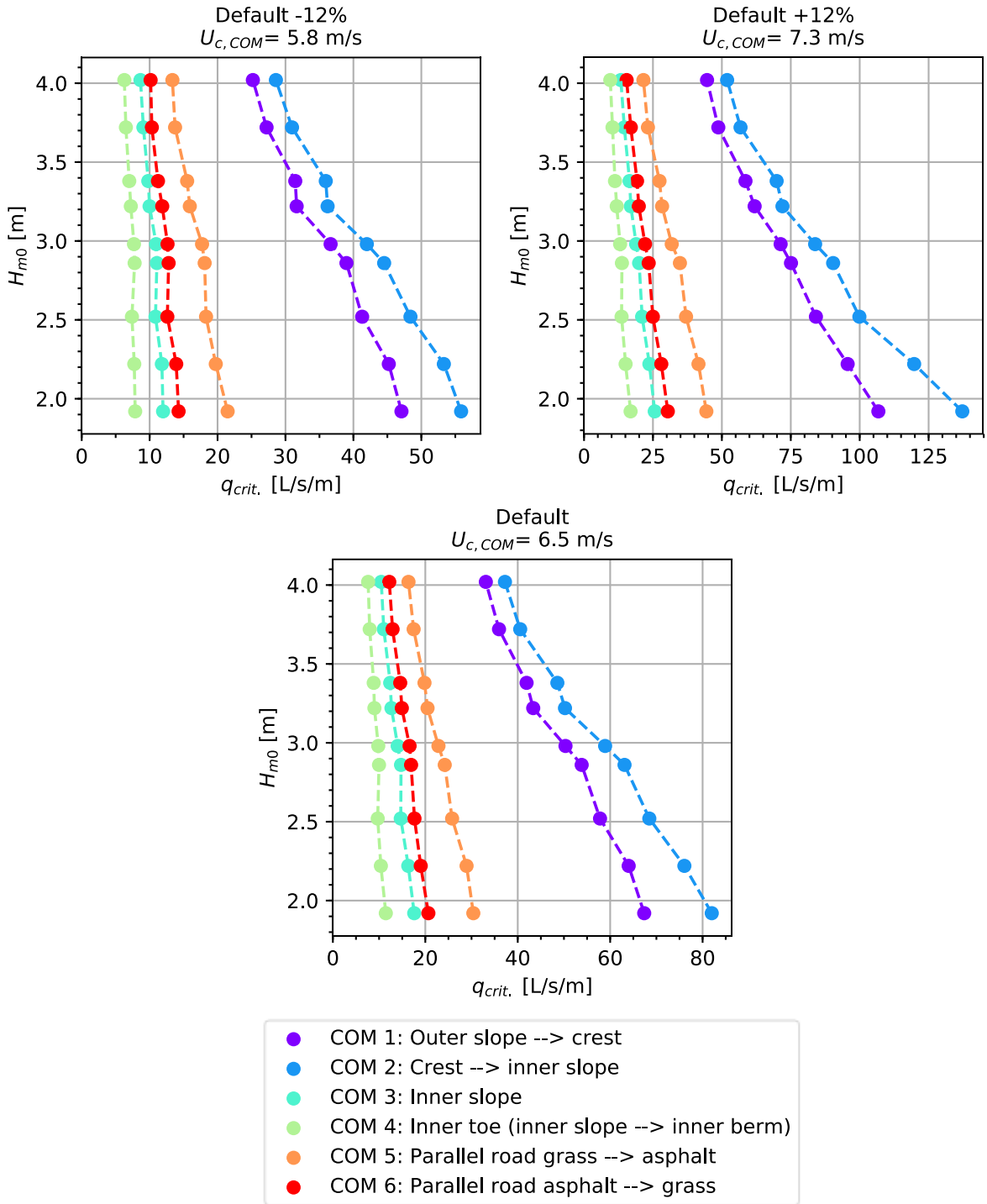

Figure 34: COM simulation results showing the relationship between the critical average overtopping discharge $q_{crit.}$ and the significant wave height H_{m0} for varying critical flow velocities $U_{c,COM}$. All simulations are carried out with medium $h-\theta$ conditions.

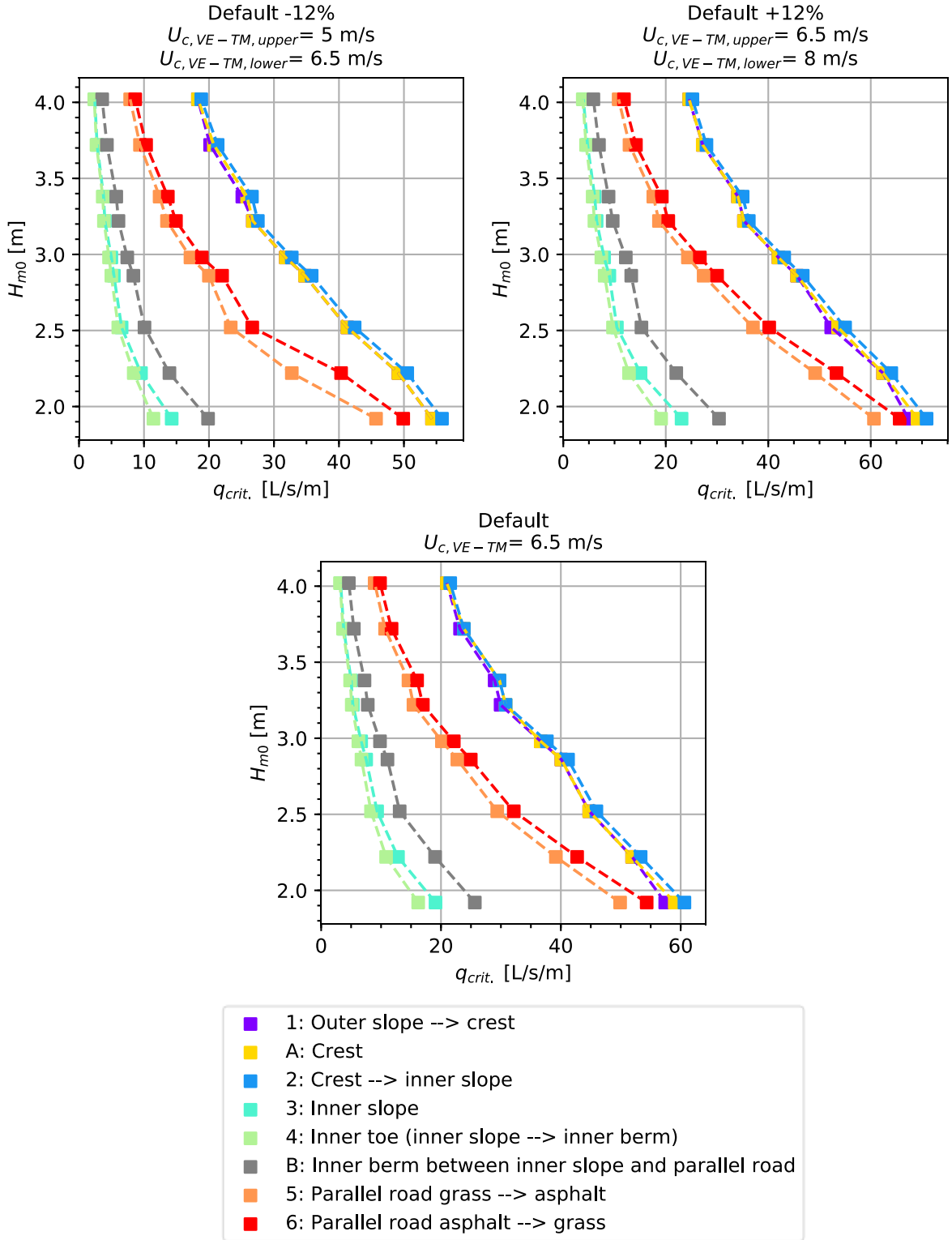

Figure 35: VE-TM simulation results showing the relationship between the critical average overtopping discharge $q_{crit.}$ and the significant wave height H_{m0} for varying critical flow velocities $U_{c,VE-TM}$. $U_{c,VE-TM,upper}$ and $U_{c,VE-TM,lower}$ indicate the critical flow velocity for the upper 10 cm and the lower 10 cm of the cover layer respectively. All simulations are carried out with medium h–θ conditions.

Flow velocity at the start of the crest $U_{i,crest}$ (COM & VE-TM)

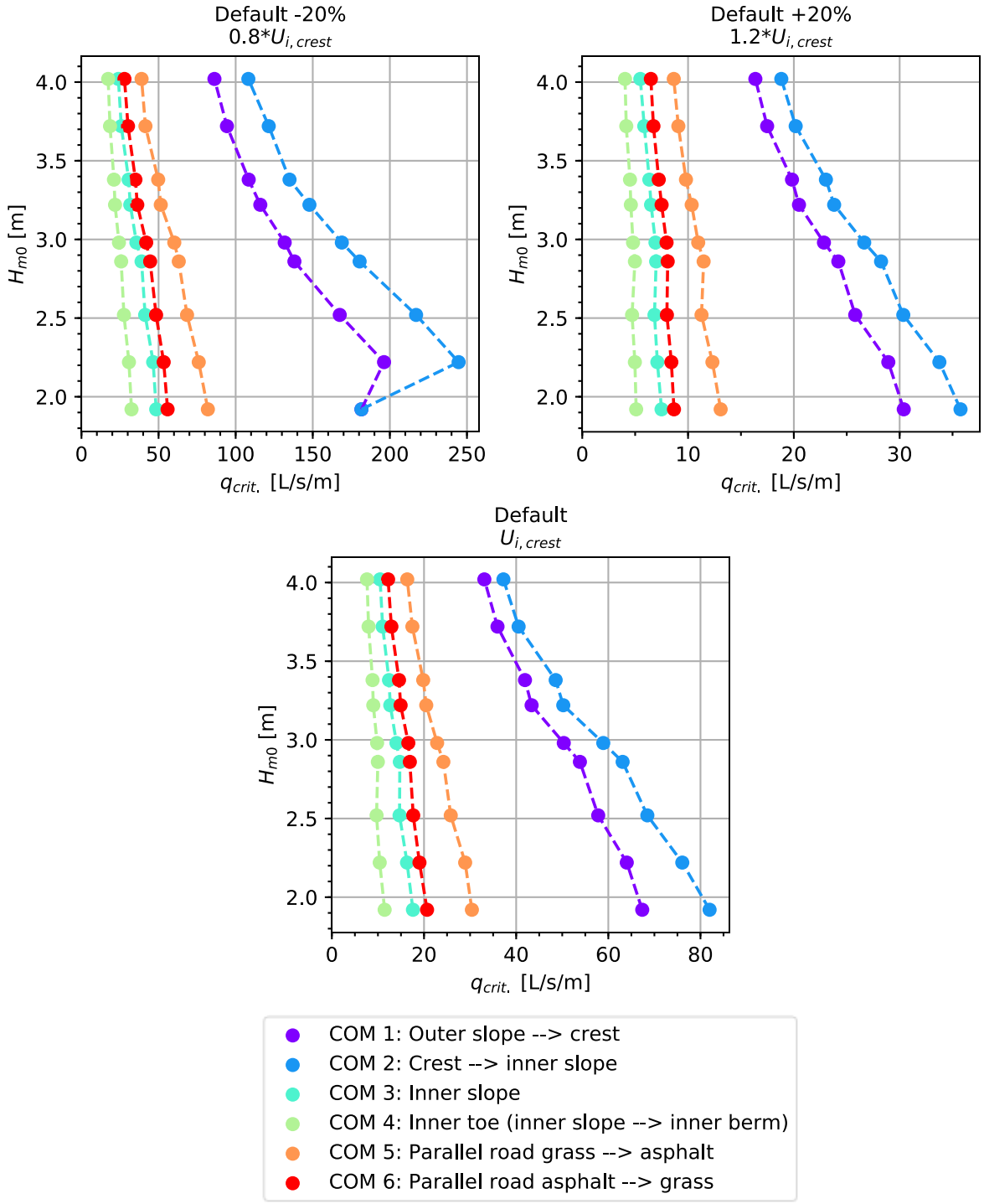

Figure 36: COM simulation results showing the relationship between the critical average overtopping discharge $q_{crit.}$ and the significant wave height H_{m0} for flow velocities at the start of the crest $U_{i,crest}$ as calculated with the equations in Section 3.2.3 (Default), a 20% decrease (Default -20%) and a 20% increase (Default +20%). All simulations are carried out using a critical flow velocity U_c = 6.5 m/s and medium h–θ conditions.

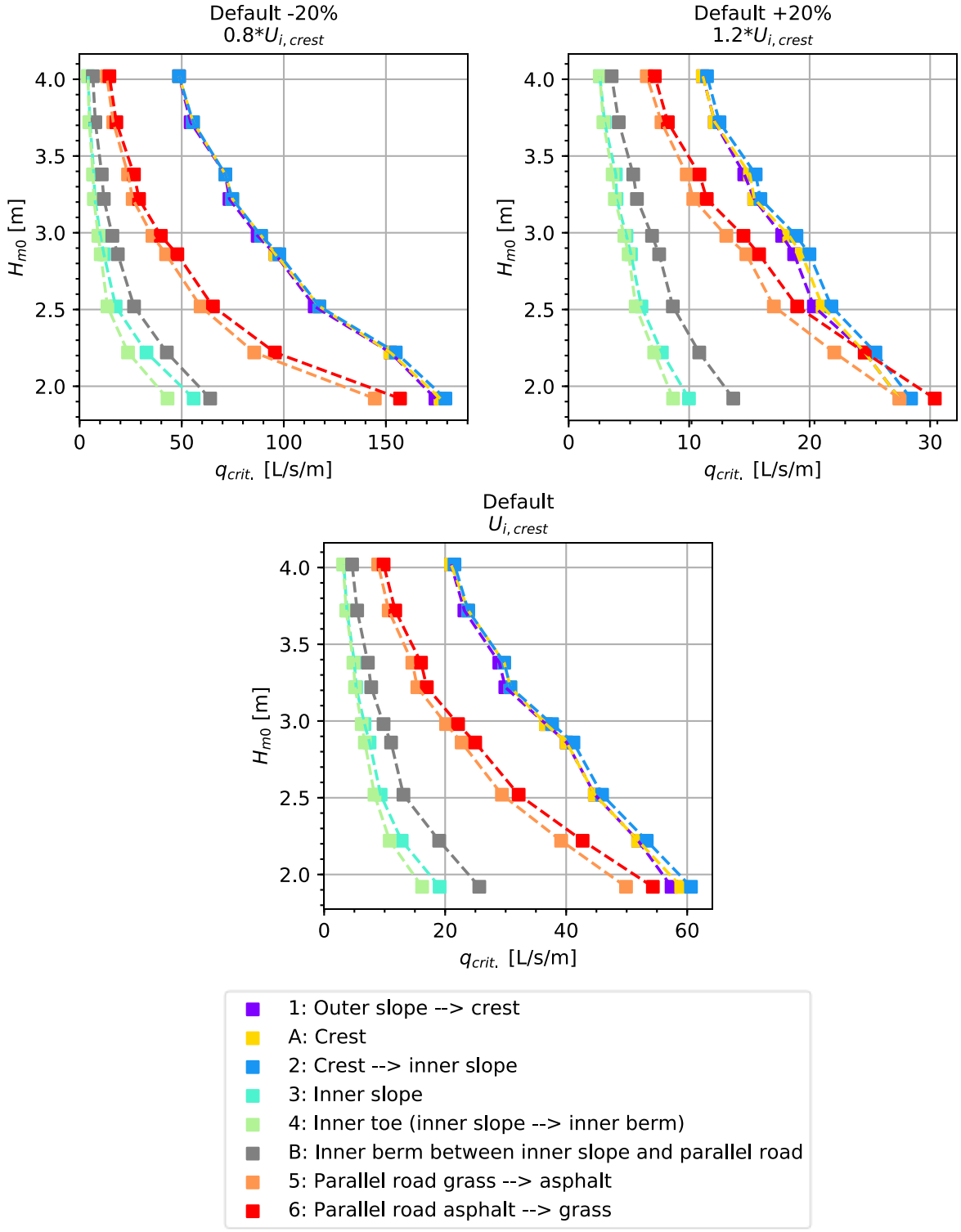

Figure 37: VE-TM simulation results showing the relationship between the critical average overtopping discharge $q_{crit.}$ and the significant wave height H_{m0} for flow velocities at the start of the crest $U_{i,crest}$ as calculated with the equations in Section 3.2.3 (Default), a 20% decrease (Default -20%) and a 20% increase (Default +20%). All simulations are carried out using a critical flow velocity U_c = 6.5 m/s and medium h–θ.

Load, strength and acceleration factors α_m, α_s and α_a (COM)

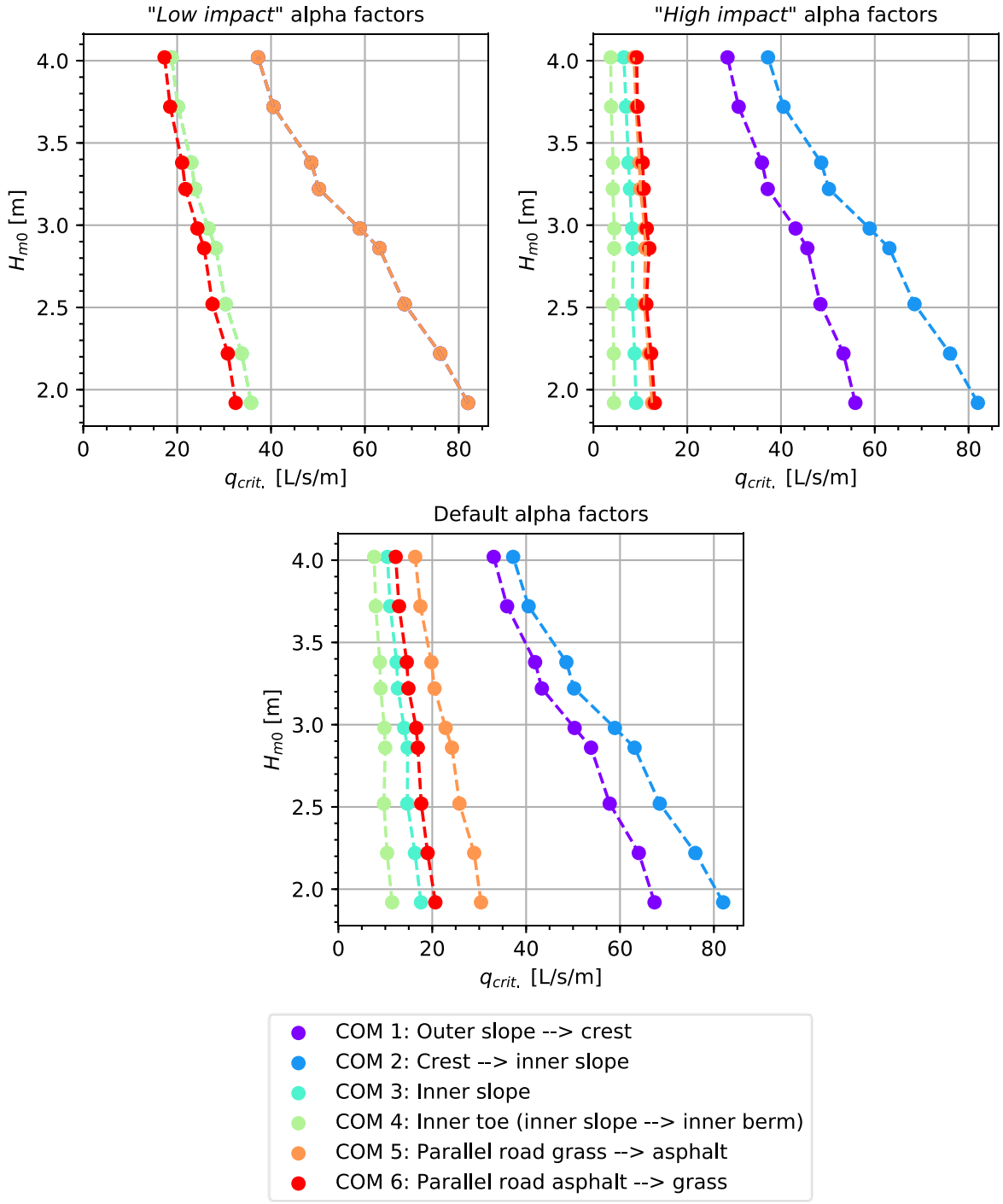

Figure 38: COM simulation results showing the relationship between the critical average overtopping discharge $q_{crit.}$ and the significant wave height H_{m0} for different combinations of load, strength and acceleration factor values α_m, α_s and α_a. All simulations are carried out using a critical flow velocity U_c = 6.5 m/s and medium h–θ conditions.

Relative turbulence intensity r_0 (VE-TM)

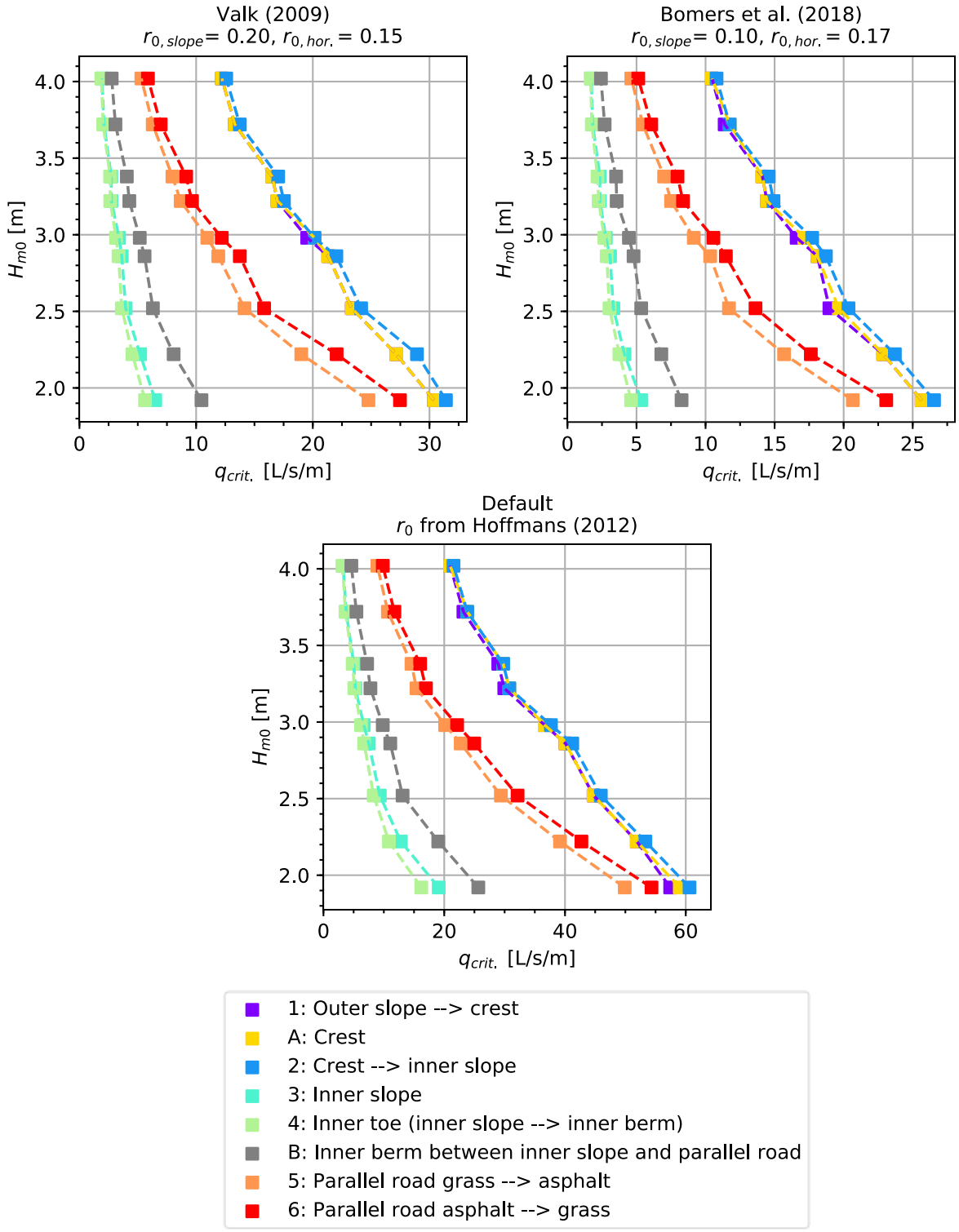

Figure 39: VE-TM simulation results showing the relationship between the critical average overtopping discharge $q_{crit.}$ and the significant wave height H_{m0} for different relative turbulence intensity values r_0, where $r_{0,slope}$ indicates a separate value for the inner slope and $r_{0,hor.}$ separate values for the horizontal surfaces (i.e. the crest and inner berm). All simulations are carried out using a critical flow velocity U_c = 6.5 m/s and medium h–θ.

Overall strength parameter C_E (VE-TM)

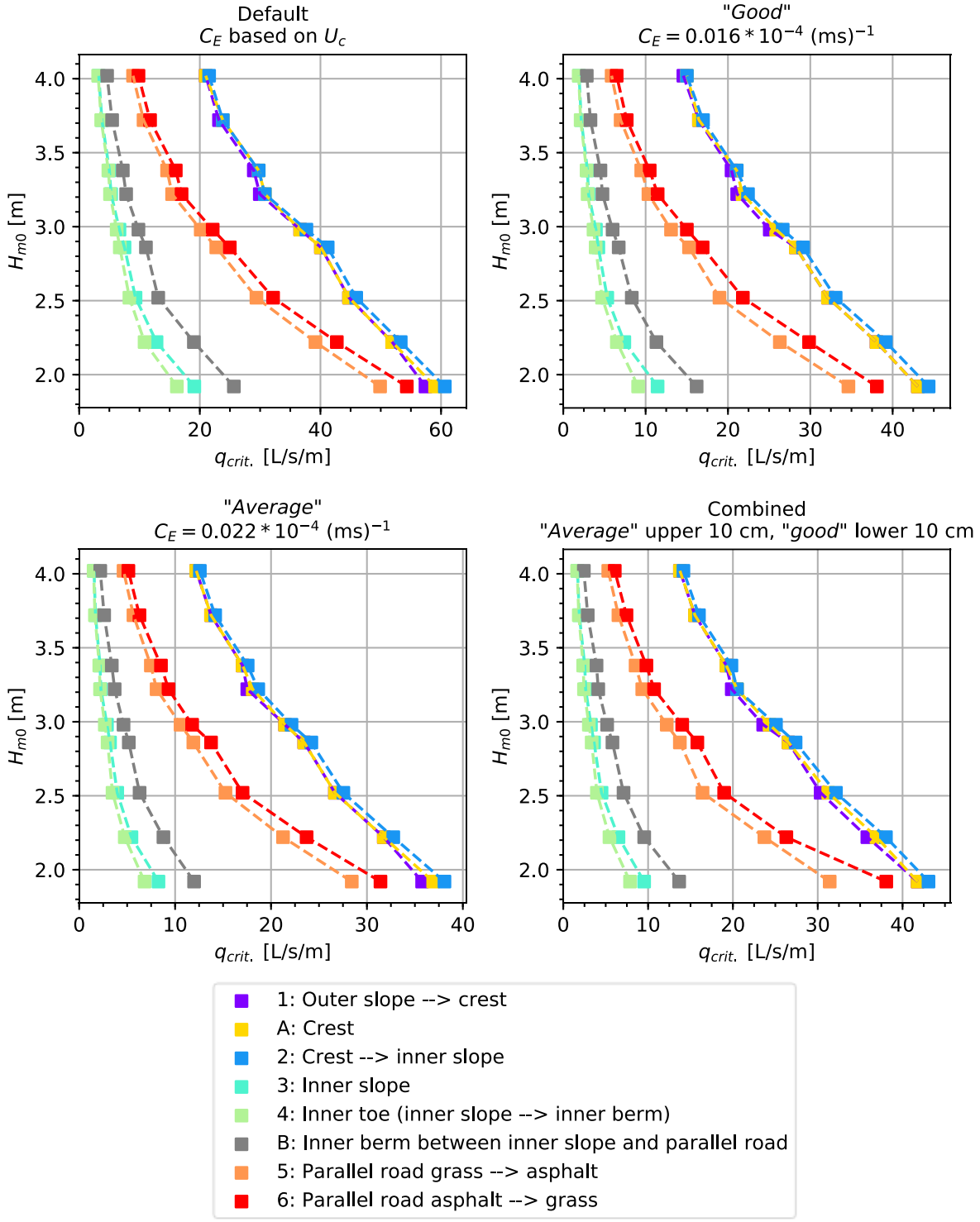

Figure 40: VE-TM simulation results showing the relationship between the critical average overtopping discharge $q_{crit.}$ and the significant wave height H_{m0} for different overall strength parameter values C_E. All simulations are carried out using a critical flow velocity U_c = 6.5 m/s and medium h–θ conditions.

APPENDIX D: SIMULATION RESULTS OF 3-HOUR STORM EVENT APPROACH

COM

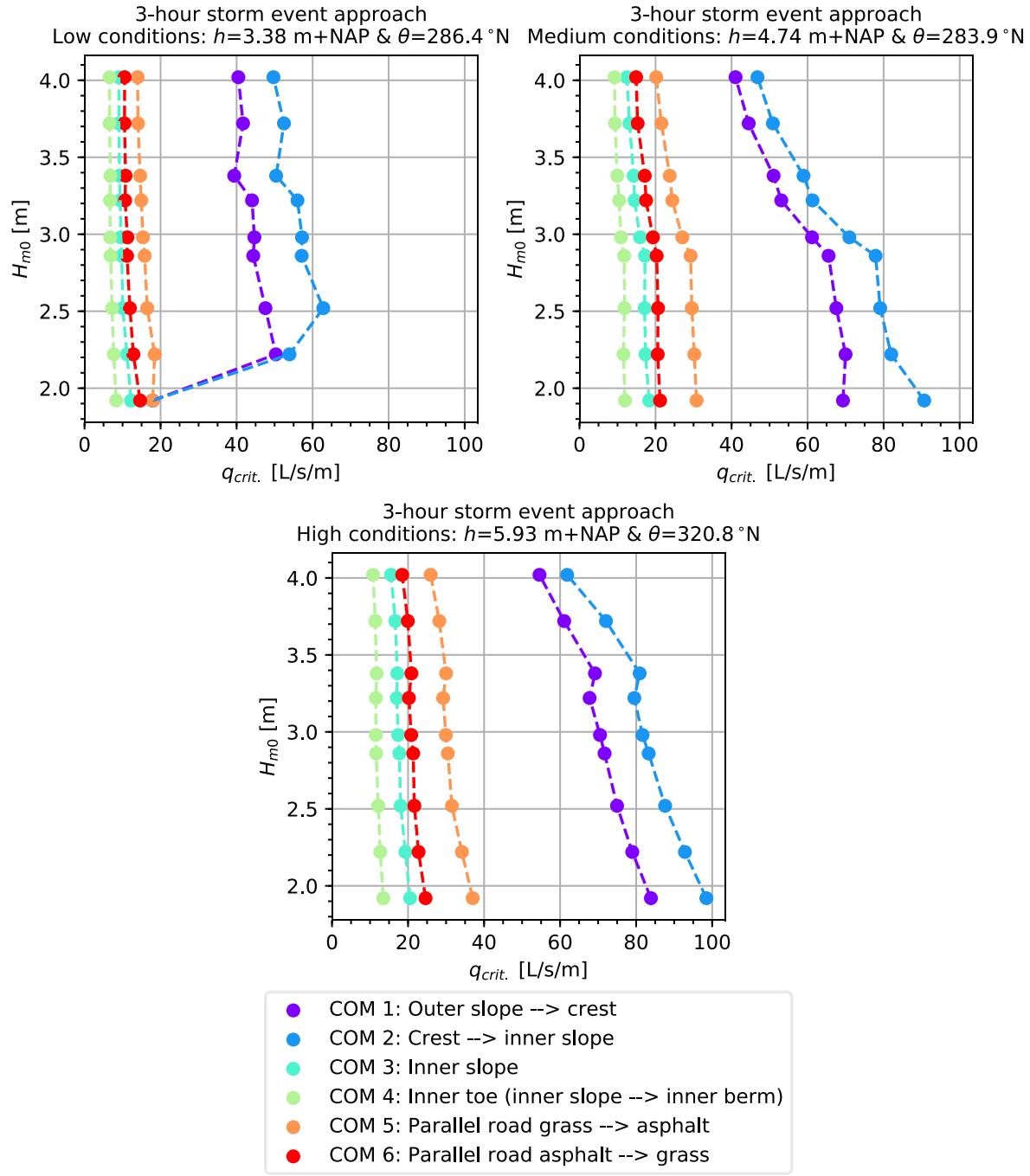

Figure 41: COM simulation results showing the relationship between the critical average overtopping discharge $q_{crit.}$ and the significant wave height H_{m0} using the 3-hour storm event approach of Van Hoven and Van der Meer (2017) for low, medium and high conditions of normative water level h and angle of wave attack θ. All simulations are carried out using a critical flow velocity U_c = 6.5 m/s.

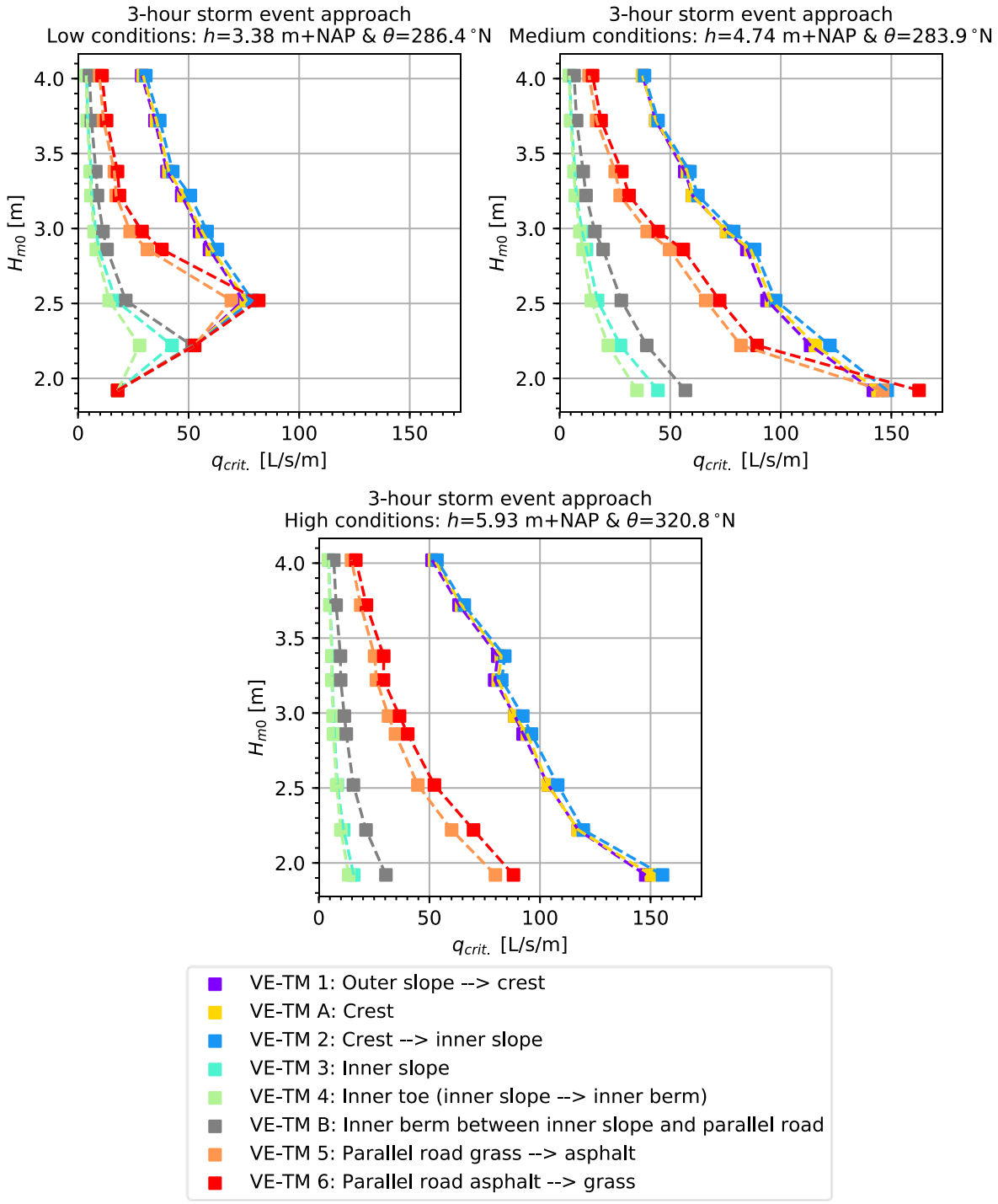

Figure 42: VE-TM simulation results showing the relationship between the critical average overtopping discharge $q_{crit.}$ and the significant wave height H_{m0} using the 3-hour storm event approach of Van Hoven and Van der Meer (2017) for low, medium and high conditions of normative water level h and angle of wave attack θ. All simulations are carried out using a critical flow velocity U_c = 6.5 m/s.